Modeling oxygen isotopes in ice sheets linked to Quaternary ice-volume variations

Dissertation zur Erlangung des Doktorgrades der Naturwissenschaften
am Fachbereich Geowissenschaften der Universität Bremen

vorgelegt von **Adriana SIMA**

Betreuung und 1. Gutachter: **Prof. Dr. Michael Schulz**

2. Gutachter: **Prof. Dr. Johannes Oerlemans**

Eingereicht am 21.03.2005

I want to know God's thoughts.
The rest are details.

Albert Einstein

Abstract

Climate change through the Quaternary was dominated by the repeated build-up and retreat of large ice sheets in North America, northern Europe and some further places on the globe. The best indicator for past variations of global ice volume is the isotopic composition $\delta^{18}O$ of seawater (δ_w) recorded in foraminiferal calcite in marine sediments. Especially the benthic foraminiferal $\delta^{18}O$ (δ_c) has been long recognized as a very good proxy for δ_w and, hence, for ice volume. But the interpretation of benthic δ_c records in terms of ice-volume variations is not at all straightforward, mainly because δ_c depends not only on δ_w, but also on seawater temperature. Furthermore, even if the contributions of δ_w and temperature could be accurately disentangled, other difficulties would arise. In common paleoceanographic practice the relationship between δ_w and ice volume is considered linear, but two main factors have the potential to induce considerable nonlinearity. One factor is the mean isotopic composition of ice, which varies during the course of a glacial-interglacial cycle and may introduce phase and amplitude differences between the ice-volume signal and the induced mean seawater isotopic enrichment. Another factor is the ocean circulation, which can induce phase differences between a freshwater signal due to ice-volume variations and the recording of that signal at different locations and depths in the ocean. In the present study, these two factors were investigated at glacial-interglacial timescale by means of numerical modeling. For this purpose, a 2.5-dimensional thermomechanical ice-sheet model including oxygen-isotope transport was developed. In a first step the ocean was treated in the simplest way, by assuming it well-mixed. The phase difference found between the ice-volume signal and the induced mean isotopic enrichment of seawater turned out to be negligible and the amplitude difference was generally less than 10 %. Hence, it was concluded that the effect of mean-ice $\delta^{18}O$ variations can be neglected in reconstructing ice volume from marine $\delta^{18}O$ records. Furthermore, the effect of ocean circulation on the relationship between ice-volume variations and the ocean isotopic response was investigated qualitatively, by forcing a climate model of reduced complexity with the freshwater flux simulated by the ice-sheet model. The North-Atlantic deep-water $\delta^{18}O$ variations were found to lead those in the South Atlantic Ocean, whereas the calcite-$\delta^{18}O$ anomalies showed an apparent lead of the South Atlantic over the North Atlantic Ocean during the deglaciation. It was concluded that (i) the ocean circulation is an important element to be taken into account in the climatic and stratigraphic interpretation of benthic $\delta^{18}O$ records and (ii) leads/lags inferred on the basis of proxies depending on more than one physical variable, such as benthic calcite-$\delta^{18}O$, can be misleading in interpreting causal relationships. Finally, using a simplified (1-dimensional) version of the ice-sheet model combined with a box-model of the North Atlantic Ocean, the interaction between climate variability at orbital and millennial timescales was investigated in order to gain further understanding of the origin of $\delta^{18}O$ variations recorded in marine sediments as well as in ice cores. It was found that YD-type events may occur during any deglaciation of the past 800 kyr, which means that YD is probably not a one-time event, but an intrinsic feature of the climate change at millennial timescales.

Aknowledgments

This work was carried out at the Geosciences Department of Bremen University, and was supported by the Deutsche Forschungsgemeinschaft within the European Graduate College „Proxies in Earth History“.

I would like to express my entire gratitude to Prof. Dr. Michael Schulz and Dr. André Paul. They are the ideal of a supervisor, by the talent and pleasure they have in sharing their knowledge. All the good things I have done from the scientifical point of view are due to their continuous support and guidance (for all the not too good things I have done, I take full responsability :-)).

Many thanks are due to Prof. Dr. Hans Oerlemans, for always being there when I needed his advice. And for the wonderful course on „Ice sheets and glaciers in the climate system“ he organised in 2004 in Karthaus, Italy, where I could meet and learn from experienced ice-sheet modelers as Dave Pollard and Tony Payne.

Thanks to all my colleagues from the „palmod“ group – it was a real joy to meet them every day during the past 3 years, and I will miss them a lot. Dr. Christian Schäfer-Neth (the best officemate), Dr. Andreas Manschke (the best network administrator), Prof. Dr. Gerrit Lohmann (who invited the first Romanians in the group), Dr. Norel Rimbu and Dr. Mihai Dima (their presence was priceless for me), Dr. Klaus Grosfeld, Dr. Matthias Prange, Dr. Martin Butzin, Dr. Xavier Giraud, Dr. Vanya Romanova, Lisa Könnecke, Svetlana Zech, Leslie Sütterlin (the best secretary), and, meteoric, Dr. Duane Thresher (maple syrup! :-)).

Many thanks to Prof. Dr. Helmut Willems, the speaker of EUROPROX, and to Maria Petrogiannis, the secretary, for their effort to make things smooth for the PhD students. Also, to Dr. Helena Filipsson and Dr. Mahyar Mohtadi (Marco), for support, and to all my colleagues from EUROPROX, for the interesting meetings and the funny coffee breaks.

Special thanks to Dr. Lev Tarasov, Dr. Claire Waelbroeck and Dr. Ulysses Ninnemann, who found the time to send me their data and other infomation I needed.

I must also mention here at least a few of the friends I found in Bremen: Gabriela Alexe, Elena Roventa, Alida Fodor, Gina Antonescu, Carmen Momeu, Liliana Wetjen, Mihaela Constantin - I cannot imagine the last 3 years without them. My gratitude to all the old friends from home and abroad, which, in spite of the distance, I’ve always felt close.

To all this people, to their families (!!) and to other I couldn't mention in only one page,

THANK YOU! :-)

This is dedicated to my parents,
to my brother Gabi
and my sister-in-law Cristina,
whose love and support,
even from a distance,
I could always feel and count on.

Contents

Chapter I

INTRODUCTION

I.1 The role of oxygen isotopes in paleoclimatology

The hydrological cycle is of greatest interest to scientists, because it links the different components of the physical climate system, and the processes redistributing moisture between these components are intimately linked to biogeochemical cycles. In particular, for paleoclimatologists, understanding why and how the hydrological cycle has changed in the past is vital in reconstructing Earth's climate history.

Prior to the instrumental period (i.e., the last 150 years), direct evidence about climate changes decreases in accuracy and resolution, and more emphasis is put on indirect climate signals recorded in so-called proxies. An invaluable resource of proxy information are the stable oxygen isotopes[1] contained in water molecules: ^{16}O (common) and ^{18}O (rare). They label individual components of the hydrological cycle (Figure I-1) and characterize the climatic and hydrological conditions prevailing at any given time.

Two major types of climate archives, offering long, continuous and detailed records of the isotopic ratio $^{16}O/^{18}O$ (expressed as the fractional deviation $\delta^{18}O$ from a standard; Appendix A), are of interest in the present study: ice cores and marine sediments.

Ice cores provide the most direct, high-resolution records of climate signals (especially atmospheric parameters: local temperature, precipitation rate, moisture-source conditions, wind strength). Also, they reveal information about forcing factors of global significance (greenhouse gases: CO_2, CH_4) and regional significance (aerosol fluxes of various origin: marine, volcanic, terrestrial, cosmogenic, anthropogenic). The two deep ice cores drilled in central Greenland in the beginning of 1990s, GRIP [1993] and GISP2 [*Grootes et al.*,

[1] Isotopes are variants of an element differing by the number of neutrons in the nucleus. In order of abundance, the stable oxygen isotopes are: ^{16}O (99.76%), ^{18}O (0.2%) and ^{17}O (0.04%). Paleoclimatic studies generally concentrate on the ratio of the first two isotopes.

1993], are source of reliable information back to 105 thousand years before present (kyr BP), whereas the new NGRIP core [*North Greenland Ice Core Project members*, 2004] extends back to 123 kyr BP. The corresponding ice-δ^{18}O records, which are highly detailed (time resolution frequently better than a year), largely reflect changes in local air temperature (Appendix A). In Antarctica, the longest cores were extracted from Vostok, covering the past 420 kyr [*Petit et al.*, 1999], and Dome C, going back to 740 kyr BP [*EPICA community members*, 2004]. For historical reasons, in Antarctic cores the hydrogen-isotopic composition of ice is measured, which basically contains the same information as δ^{18}O , namely, local air-temperature variations.

Marine sediments constitute a climate archive generally not as highly resolved as ice cores, but which goes much further back in time. A large amount of sediment cores have been recovered during the past few decades, especially within the framework of the Deep Sea Drilling Project (DSDP) and Ocean Drilling Program (ODP). These cores allowed retrieving long and relatively continuous calcite-δ^{18}O records from fossil shells of marine organisms, such as planktic and benthic foraminifera, containing information on the past ~65 million years (Myr) of Earth-climate history [e.g., *Zachos et al.*, 2001].

The oxygen-isotopic composition of foraminiferal calcite depends on the local temperature and the isotopic composition of the seawater in which the organisms develop. In turn, seawater δ^{18}O depends on the amount of water stored in ice sheets and the mean δ^{18}O of ice. As temperature and ice volume are two parameters critical in defining the mean climate state, foraminiferal δ^{18}O represents an important indicator of global climate change. In particular, for the past ~1 million years, the (especially benthic) foraminiferal-δ^{18}O signal measured in deep-sea sediments is a very good proxy for the global ice-volume history and the equivalent sea-level changes [e.g., *Imbrie et al.*, 1984; *Mix*, 1987; *Shackleton*, 1987; *Waelbroeck et al.*, 2002] (Appendix B). Hence, marine oxygen-isotope records provide not only climatic, but also stratigraphic information [e.g., *Shackleton and Opdyke*, 1976; *Imbrie et al.*, 1984] and form the basis for the marine isotope stage (MIS) stratigraphic system [*Imbrie et al.*, 1984; *Martinson et al.*, 1987].

I.2 The global oxygen-isotope cycle

Water moves through the hydrosphere mainly by evaporation, condensation and precipitation processes (Figure I-1). During these processes, the competing behaviour of water molecules containing different oxygen isotopes is determined by their different molecular mass. Molecules containing the oxygen isotope ^{16}O, lighter than those

containing ^{18}O, are preferentially evaporated and transported poleward, leaving the seawater enriched in the heavier isotope. On the way, condensation and precipitation occur, during which ^{18}O is preferentially removed from atmospheric moisture. As a consequence of this fractionation process[2], air masses reaching high latitudes contain water vapour significantly depleted in ^{18}O, and the snow falling on (and accumulating in) ice sheets mainly contains ^{16}O. At middle and high latitudes, the isotopic composition of precipitation was found to be linearly related to air temperature (Appendix A).

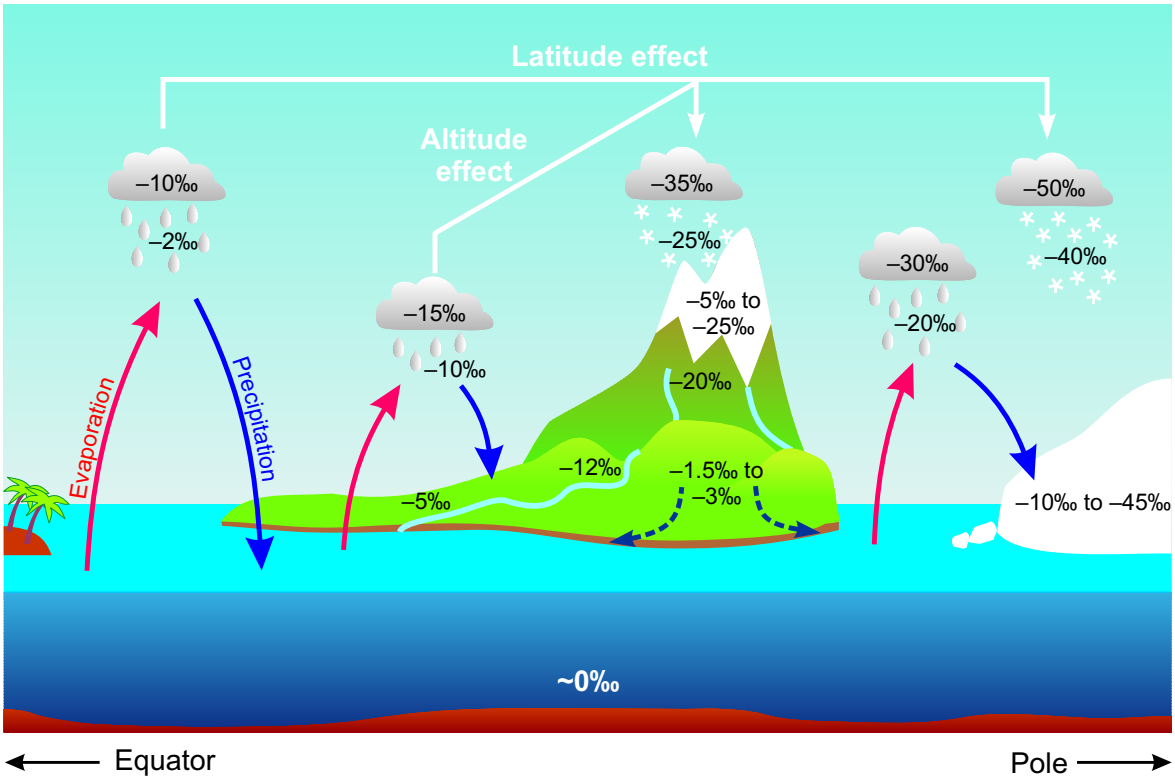

Figure I-1. *Oxygen isotopes in the hydrological cycle.* Schematically, the hydrological cycle consists of the following processes: water evaporation from the ocean at lower latitudes, moisture transport through atmosphere toward higher latitudes, condensation in clouds, and precipitation (i) back on the ocean, (ii) on land, followed by water returning to the ocean as river and underground runoff, or (iii) on ice sheets, where snow is accumulated and transformed in ice, then returns to the sea by melting and iceberg calving. Labelled isotope ratios $^{18}O/^{16}O$, expresed as $\delta^{18}O$ (‰)=[$(^{18}O/^{16}O)_{sample}/(^{18}O/^{16}O)_{standard}$– 1]×1000, indicate the individual components of the cycle, and can offer information about their origin and the environmental conditions they have experienced.

[2] Fractionation of oxygen isotopes occurs whenever a water mass undergoes a phase transition, and results in a difference in isotopic composition between the two phases. This process is temperature-dependent.

From a global perspective, the major water reservoirs are the global ocean and the ice sheets. Large ice sheets imply more ^{16}O isotope stored on land, which leaves the ocean enriched in ^{18}O, and vice versa; that is, a direct relationship exists between ocean isotopic enrichment and the global ice volume (Appendix B). The time it takes for water molecules after evaporation at ocean surface to return to the ocean ranges (i) from days to months if they are precipitated directly over the ocean, (ii) from one to a thousand years if they are precipitated over land and (iii) from tens to hundreds thousand years if they fall on ice sheets [e.g., *Peixoto and Oort*, 1992]. So, from a timescale point of view, returning of water to the ocean can be considered "instant" in cases (i) and (ii) in comparison with case (iii). Therefore, the large-scale (spatial and temporal) study of the hydrological cycle can be addressed by investigating variations in the distribution of water between the main reservoirs (the ocean and the ice sheets), best described by changes in their oxygen-isotopic composition.

I.3 Past climate changes reflected in marine and glacial $\delta^{18}O$ records

The applicability of foraminiferal $\delta^{18}O$ as a global index of climate change extends on a variety of timescales, from tectonic to millennial. An example of long and detailed marine $\delta^{18}O$ record is the one retrieved at the ODP site 659, in the eastern equatorial Atlantic [*Tiedemann et al.*, 1994], offering information on Earth-climate variations during the past 5 Myr (Figure I-2a).

Figure I-2. *Climate change at different timescales, reflected in* $\delta^{18}O$ *records*. (a) Benthic $\delta^{18}O$ record from site ODP-659, in the eastern equatorial Atlantic [*Tiedemann et al.*, 1994]. The shifts in $\delta^{18}O$ are obliquity-dominated (41-kyr periodicity). The trend towards heavier values after ~2.7 Myr BP is associated with intensification of the Northern Hemisphere glaciation. (b) Same record as in (a), but for the past 1 Myr. The Mid-Pleistocene Transition can be seen, with the two steps: the significant global ice-volume increase (at ~920 kyr BP) and the onset of the 100-kyr glacial cycles of the late Pleistocene (at ~640 kyr) [*Mudelsee and Schulz*, 1997]. (c) High-resolution planktonic record from core MD95-2042, from the Iberian Margin [*Shackleton et al.*, 2000], revealing millennial-timescale features which can be correlated with those from the Greenland ice-core records. (d) Sequence of the NGRIP $\delta^{18}O$ record, Greenland, showing key events of the last glacial-interglacial period: the Dansgaard-Oeschger (DO) oscillations, the Last Glacial Maximum (LGM) and the deglaciation steps: the Bølling/Allerød (BA), the Younger Dryas (YD) and the Preboreal (PB).

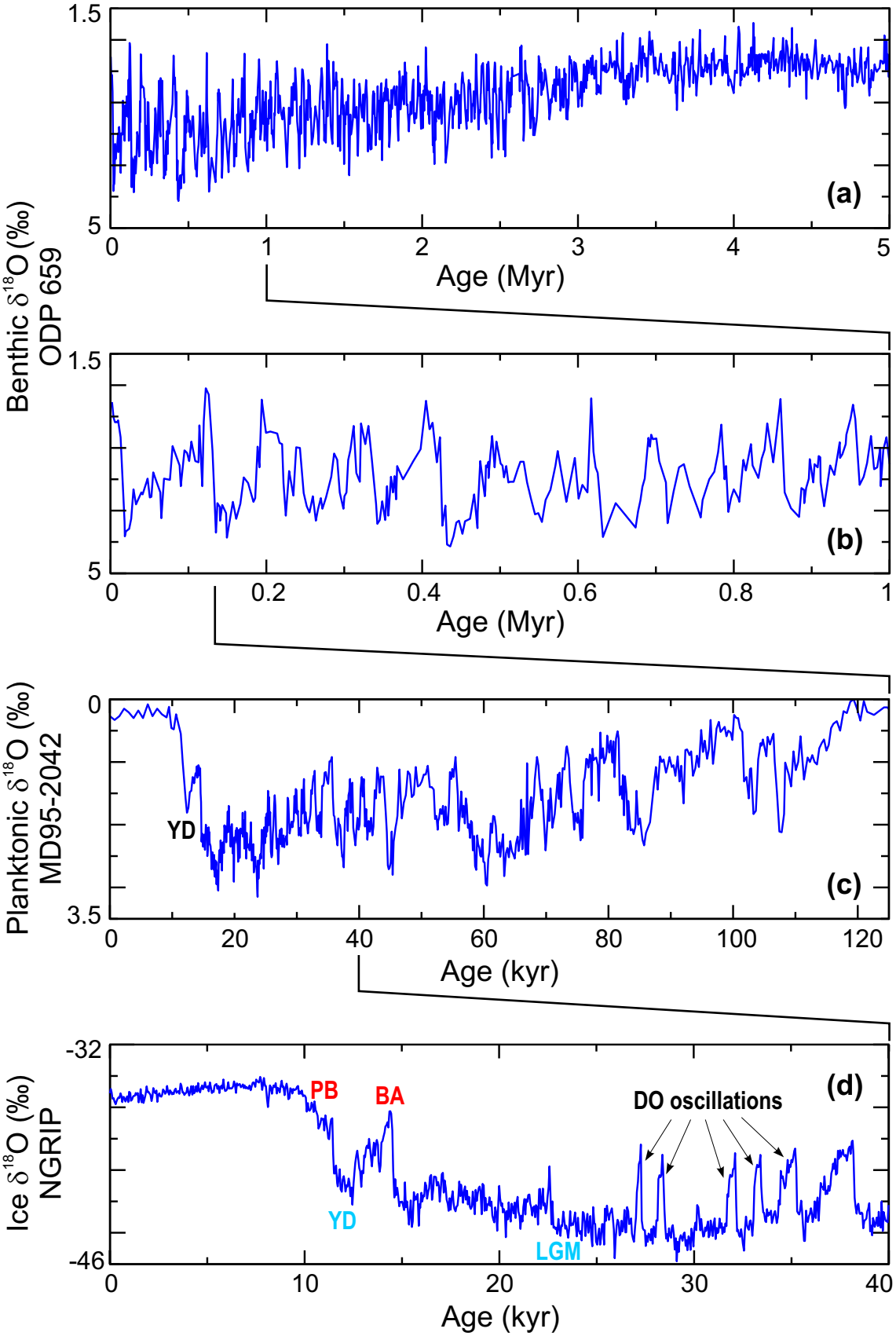
Benthic δ18O (‰)
ODP 659
1.5
5
0
1
2
3
4
5
Age (Myr)
(a)
1.5
5
0
0.2
0.4
0.6
0.8
1
Age (Myr)
(b)
Planktonic δ18O (‰)
MD95-2042
0
3.5
YD
0
20
40
60
80
100
120
Age (kyr)
(c)
Ice δ18O (‰)
NGRIP
-32
-46
PB
BA
YD
LGM
DO oscillations
0
10
20
30
40
Age (kyr)
(d)

The old part of the record, before ~2.7 Myr BP, is characterized by low $\delta^{18}O$ values, associated with a relatively warm climate. At that time little ice existed, locked up in polar caps, so the observed variations in the benthic data are thought to largely reflect temperature changes [cf. *Lea et al.*, 2000]. The main periodicity in the record is 41 kyr, corresponding to the obliquity component of the insolation forcing [*Milankovitch*, 1930].

After ~2.7 Myr BP, a major increase can be seen in the $\delta^{18}O$ record, related to the onset of the Northern Hemisphere glaciation [*Flesche Kleiven et al.*, 2002]. The amplitude of oscillations increases as well, indicating gradual intensification of the glacial episodes. The ice-volume component becomes more and more important in the foraminiferal-$\delta^{18}O$ signal. The rhythm of glaciations is still obliquity-dominated (41-kyr period).

The interval between approximately 950 and 650 kyr BP was one of complex climatic transformations. Known as the Mid-Pleistocene Transition, it involved two major steps [*Mudelsee and Schulz*, 1997]: the first, in the time domain, consisting of a significant increase in the global ice volume (centered at ~920 kyr BP), followed after ~280 kyr by the second, in the frequency domain, consisting in the onset of the 100-kyr glacial cycles which have dominated the late Pleistocene (i.e., the past ~640 kyr). Orbital-timescale variations in foraminiferal $\delta^{18}O$ during these last ~950 kyr were mainly induced by changes in the global ice volume (Figure I-2b).

Superimposed on the orbitally-driven climate changes, millennial-timescale variability occurs. This is particularly well documented during the last glacial cycle (i.e., the past ~120 kyr), for example in the highly-resolved $\delta^{18}O$ records from core MD95-2042, taken from the Iberian Margin. The rapid and large-amplitude transitions in the planktonic record (Figure I-2c), resembling those in Greenland ice-core data, largely reflect seawater-temperature variations [*Shackleton et al.*, 2000].

Millennial- and even finer-timescale climate variability features are revealed by Greenland ice cores. For example, the NGRIP $\delta^{18}O$ record, containing information about (mainly) air-temperature evolution above Greenland, shows in great detail key events of the last glacial-interglacial period: the Dansgaard-Oeschger (DO) oscillations, the Last Glacial Maximum (LGM) and the three main steps of the last deglaciation: the warm Bølling/Allerød (BA), the cold Younger Dryas (YD) and the warm Preboreal (PB) (Figure I-2d).

I.4 Foraminiferal $\delta^{18}O$ as proxy for Quaternary ice volume

Interpreting the Quaternary (past ~1.8 Myr) record of foraminiferal $\delta^{18}O$ as a proxy for global ice volume mainly relies on the work of *Shackleton* [1967]. He suggested that the individual contributions of seawater temperature and isotopic composition to the foraminiferal-$\delta^{18}O$ signal could be disentangled by analysing benthic instead of planktic species and assuming that in this case the changes in seawater temperature were minimal, limited by the freezing point of the deep ocean water. He concluded that in benthic foraminifera records the ice-volume signal prevails and the mean-ice $\delta^{18}O$ must have been about –30‰.

Subsequent work has shown that the simple use of benthic $\delta^{18}O$ data does not completely solve the ice-volume/temperature problem, as the high-amplitude variations in some records [e.g., *Shackleton*, 1977; *Duplessy et al.*, 1980; *Labeyrie et al.*, 1987; *McManus et al.*, 1999; *Shackleton et al.*, 2000] seem to require large changes in both parameters. Also, it was found [e.g., *Duplessy et al.*, 1981] that other processes may significantly influence the shape of particular $\delta^{18}O$ curves, for example vital and ecological effects of individual species, differential carbonate dissolution, bioturbation, sediment transport [e.g., *Mix*, 1987; *Mulitza et al.*, 2003 for reviews of the use of oxygen isotopes from foraminifera in paleoclimate studies].

One way to address such difficulties was to use records from regions where deep-water temperature changes were thought to be minimal [*Labeyrie et al.*, 1987]. Another approach was to stack more records from different locations [*Imbrie et al.*, 1984; *Martinson et al.*, 1987; *Bassinot et al.*, 1994], because in this way most of the other influences tended to cancel each other out, emphasizing the ice-volume component. The resulting curves have been considered to accurately (i.e., linearly) reflect ice-volume variations, and have been used as a reference in testing climate models of the Quaternary ice ages [e.g., *Pollard et al.*, 1980; *DeBlonde and Peltier*, 1991; *Saltzman and Verbitsky*, 1993; *Paul and Berger*, 1999].

I.5 Disagreement between δ^{18}O-derived sea level and independent sea-level data

For the late Quaternary, global ice-volume variations can be reconstructed from direct evidences for paleo-sea levels, such as shorelines and coral reefs. When compared to such direct sea-level estimates [e.g., *Lambeck and Chappell*, 2001; *Lambeck et al.*, 2002], the reconstructions based on foraminiferal-δ^{18}O do not match. This mismatch has been long recognised, and interpreted as mainly due to changes in deep-water temperature [*Chappell and Shackleton*, 1986; *Shackleton*, 1987]. However, in order to decide how much of the disagreement can be attributed to the temperature effect, two factors require careful investigation:

Factor 1: Isotopic composition of ice

The assumption of a linear relationship between seawater-δ^{18}O and ice volume is exactly true only if the mean ice-δ^{18}O remains constant through time. In reality, the mean isotopic composition of ice sheets changes during the course of glacial-interglacial cycles. This fact has been noted for a long time as a possible additional difficulty in interpreting foraminiferal δ^{18}O as a proxy for ice volume [e.g., *Shackleton*, 1967].

Mix and Ruddiman [1984] were the first to look closer into this problem. Based on a parameterization of snow δ^{18}O derived from observations on present-day Antarctic precipitation they showed qualitatively that (i) the mean δ^{18}O of an ice sheet can change largely from glacial inception to glacial maximum and (ii) there can be a lag of the isotopic equilibrium behind the mass-balance equilibrium which depends on the residence time of ice in the ice sheet (Figure I-3).

Furthermore, *Mix and Ruddiman* [1984] attempted to quantify the effect of nonequilibrium isotopic composition of ice sheets on the relationship between oceanic δ^{18}O and ice volume. Based on experiments with conceptual models simulating the ocean isotopic response to hypothetical transitions of ice growth and ice decay, they concluded that foraminiferal δ^{18}O may lag the ice volume by 1 to 3 kyr and misrepresent the amplitude of ice-volume variations by up to 30%.

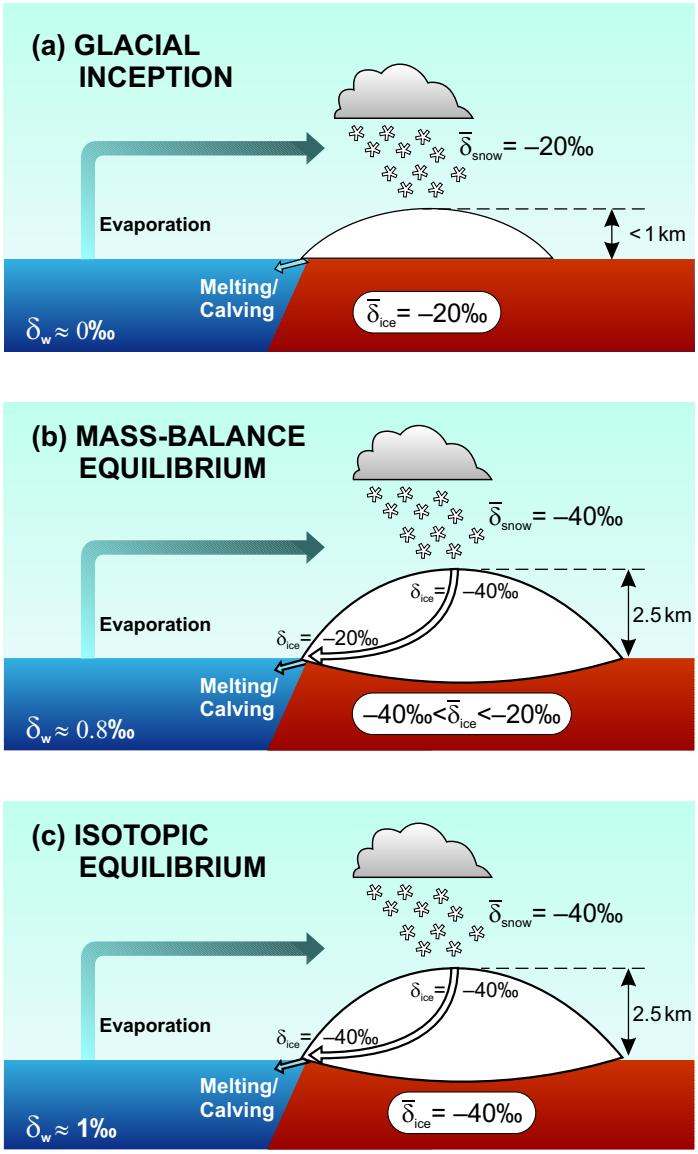

Figure I-3. *Scenario for the evolution of the mean-ice* $\delta^{18}O$ *during and after the growth phase of an ice sheet* [after *Mix and Ruddiman*, 1984]. Snow $\delta^{18}O$ is parameterized as a function of ice-surface altitude: –20‰ below 1000 m and linearly ramping to –40‰ at 2500 m, here considered the maximum ice-sheet elevation. (a) Snow accumulates and ice volume grows, but the mean ice $\delta^{18}O$ remains constant, –20‰, as long as the accumulation area is below 1000 m. (b) The ice sheet reaches the mass-balance equilibrium, corresponding to a surface elevation of 2500 m. The snow accumulated at the top is now –40‰, but most of the ice, formed during the transition and determining the mean for the ice sheet, is between –40‰ and –20‰. From now on the ice volume is constant, but the mean ice $\delta^{18}O$ keeps changing as new snow, with –40‰, is added and older ice, isotopically heavier, is ablated. (c) After all the ice formed during the growth phase has flown through the ice sheet and has been replaced by –40‰ snow, a new isotopic equilibrium is achieved. The lag between the two equilibria depends on the residence time of ice in the glacier.

Factor 2: Ocean circulation

The changes in $\delta^{18}O$ records from marine sediments were thought to be globally synchronous, implying (i) "instant" transmitting of the effect of freshwater input/ evaporative output in the ocean (i.e., with respect to the timescale of foraminiferal-$\delta^{18}O$ shifts) and (ii) in-phase variations of seawater temperature.

In reality, the effect of freshwater/evaporative fluxes associated with ice-volume changes is not instantly transmitted from source to the entire ocean. Between the water input/output signal and its recording in foraminifera at a specific location in the ocean, there must be a lag depending on the distance to the signal source and the ocean circulation. This lag might contribute to the mismatch between sea-level curves derived from calcite $\delta^{18}O$ and those inferred from direct evidences.

Another fact points also to the possible importance of the ocean circulation with respect to the mismatch between $\delta^{18}O$ - and coral-based sea level reconstructions. New data from the deep Atlantic and Pacific Oceans reveal that the benthic foraminiferal $\delta^{18}O$ variations are far from being simultaneous, and that a ~ 4,000-year lead of the Atlantic over the Pacific Ocean exists across the last deglaciation [*Skinner and Shackleton*, 2005]. Such a large discrepancy is interpreted as mainly resulting from a late increase in deep-water temperature at the Pacific site, but the delay in transmitting from one ocean to the other the $\delta^{18}O$ signal associated to ice-volume variations might also play a role.

I.6 Objectives

Separating the individual contributions of temperature and ice volume to the total change in foraminiferal $\delta^{18}O$ is an important problem in paleoceanography, which needs to be solved in order to correctly interpret the marine records in terms of climatic change. Also, from a stratigraphic point of view, accurate dating of climatic events is critical in developing and testing theories on mechanisms of past climate change, especially with respect to lead/lag relationships between various key parameters as ice volume, insolation, temperature, CO_2 etc.. Therefore, improving the understanding of the way that ice-volume variations are reflected in seawater-$\delta^{18}O$ changes, and, hence, in foraminiferal $\delta^{18}O$ records, is of great importance.

The theoretical result of *Mix and Ruddiman* [1984] shows that the isotopic disequilibrium of ice sheets has the potential to decouple the isotopic response of the ocean from the ice-

volume signal, and, therefore, may be partly responsible for the mismatch between ice-volume reconstructions from calcite-δ^{18}O records and those from direct evidence of past sea-level changes. The first objective of the present study is to re-assess this hypothesis using a more complex ice-sheet model and realistic glacial-interglacial ice-volume transitions.

The second objective is to test the effect of the ocean circulation on the way that ice-volume variations are reflected in changes of seawater isotopic composition at different geographical locations and depths, in order to evaluate the role of the ocean mixing time in the relationship between ice volume and seawater δ^{18}O .

Finally, the interaction between climate variability at orbital and millennial timescales is investigated, in order to gain further understanding of the origin of δ^{18}O variations recorded in ice cores and in fossil foraminiferas in deep-sea sediments. The objective is to test a hypothesis proposed by *Schulz et al.* [2002] regarding the origin and the supposed uniqueness [e.g., *Broecker*, 2003] of the YD event, the cold spell punctuating the last deglaciation in the Northern Hemisphere.

I.7 Testing tool: numerical climate models

Numerical models are tools which, together with the analysis of climate data, help to test hypotheses of climate change in a quantitative way. The best tool for an integrated interpretation of the climatic information contained in marine and ice-core δ^{18}O records would be a coupled model of the global geochemical cycle of water isotopes.

To test their idea, *Mix an Ruddiman* [1984] used simple, zero-dimensional ice-sheet models, along with the assumption of a well-mixed ocean and a parameterization of snow δ^{18}O based on data from Antarctica. At that time not enough was known about the history and dynamics of ice sheets as well as about the isotopic composition of precipitation and its glacial-interglacial changes.

Since then, complex two- and three-dimensional thermomechanical models have been developed for each of the large Pleistocene ice sheets: the still present Antarctic ice sheet (AnIS) [e.g., *Payne*, 1999; *Savvin et al.*, 2000; *Ritz et al.*, 2001; *Huybrechts*, 2002] and Greenland (GrIS) [e.g., *Huybrechts*, 1994; *Ritz et al.*, 1997; *Tarasov and Peltier*, 2002] as well as the now-vanished North-American ice-sheet complex [e.g., *Greve and MacAyeal*, 1996; *Marshall et al.*, 2002; *Tarasov and Peltier*, 2004] and Eurasian ice sheet (EIS) [e.g.,

Forsstrom and Greve, 2004; *Siegert and Dowdeswell*, 2004]. Such models still include many parameterizations, as some processes are not yet well understood (e.g., basal sliding, iceberg calving). Nevertheless, they keep improving in order to capture present and past features of the ice sheets (volume, general shape and extent, ice flow, thermal regime), as revealed by continuously updated reconstructions from geological evidences [e.g., *Dyke et al.*, 2002; *Svendsen et al.*, 2004].

Furthermore, water isotopes were successfully incorporated as passive tracers in thermomechanically-coupled models of GrIS [*Clarke and Marshall*, 2002; *Tarasov and Peltier*, 2003; *Lhomme et al.*, 2005a; *Lhomme et al.*, 2005b] and AnIS [*Lhomme*, 2004], using parameterizations for snow δ^{18}O based on its dependence on surface air temperature (Appendix A).

Atmospheric general circulation models including the transport of water isotopes in the atmosphere have been developed [e.g., *Joussaume et al.*, 1984; *Joussaume and Jouzel*, 1993; *Hoffmann et al.*, 1998]. They provide information on glacial-interglacial changes in the isotopic composition of precipitation on a global scale and allow deriving specific parameterizations of snow δ^{18}O for the domain of each large ice sheet. This is particularly interesting for the NAIS and EIS, from which, obviously, no ice-cores exist.

The transport of the water isotopes in the ocean has been also simulated, using oceanic general circulation models [*Schmidt*, 1998; *Paul et al.*, 1999].

Accordingly, many of the modeling tools needed for an integrated simulation of oxygen-isotope transport in the climatic system are now available. Two important components are still missing, namely, ice-sheet models including oxygen-isotope transport for the NAIS and the EIS.

I.8 Strategy

In order to achieve the objectives of the present study, a realistic and yet computationally-efficient ice-sheet model including oxygen-isotope transport is developed. This model is designed for the NAIS, as the largest contributor to ice-volume variations during the Quaternary [e.g., *CLIMAP Project members*, 1981; *Peltier*, 2004]

As a first step, the model is used to simulate the evolution of the volume and mean isotopic composition of the NAIS during the last glacial cycle and to study the isotopic response of

the ocean, assumed well-mixed, to the simulated ice-volume variations (Chapter II). This alows a re-examination of the possible phase and amplitude error in reconstructing ice-volume variations from changes in seawater $\delta^{18}O$ by neglecting the effect of changing ice $\delta^{18}O$ and employing a linear relationship (Chapter III).

Subsequently, the simplistic assumption of a well-mixed ocean (i.e., no spatial resolution) is replaced by an ocean model with explicit spatial resolution. This allows to test the hypothesis on the importance of the ocean circulation for the relationship between ice-volume variations and the changes induced in the $\delta^{18}O$ of the ocean water at different latitudes and depths (Chapter IV).

Finally, a simpler version of the ice-sheet model is used in connection with an ocean box-model to study the interaction of climate variability at Milankovitch and millennial timescale as a possible mechanism for DO- and YD-type events during the past 800 kyr (Chapter V).

References

Bassinot, F.C., L.D. Labeyrie, E. Vincent, X. Quidelleur, N.J. Shackleton, and Y. Lancelot (1994), The astronomical theory of climate and the age of the Brunhes-Matuyama magnetic reversal, *Earth Planet. Sci. Lett., 126*, 91-108.

Broecker, W.S. (2003), Does the trigger for abrupt climate change reside in the ocean or in the atmosphere?, *Science, 300* (5625), 1519-1522.

Chappell, J., and N.J. Shackleton (1986), Oxygen isotopes and sea level, *Nature, 324*, 137-140.

Clarke, G.K.C., and S.J. Marshall (2002), Isotopic balance of the Greenland Ice Sheet: modelled concentrations of water isotopes from 30,000 BP to present, *Quat. Sci. Rev., 21*, 419-430.

CLIMAP Project members (1981), Seasonal reconstructions of the Earth's surface at the last glacial maximum, Geological Society of America.

DeBlonde, G., and W.R. Peltier (1991), A one-dimensional model of continental ice volume fluctuations through the Pleistocene: Implications for the origin of the mid-Pleistocene climate transition, *J. Climate, 4*, 318-344.

Duplessy, J.C., G. Delibrias, J.L. Turon, C. Pujol, and J. Duprat (1981), Deglacial warming of the northeastern Atlantic Ocean; correlation with the paleoclimatic evolution of the European continent, *Palaeogeogr., Palaeoclimatol., Palaeoecol., 35*, 121-144.

Duplessy, J.C., J. Moyes, and C. Pujol (1980), Deep water formation in the North Atlantic Ocean during the last ice age, *Nature, 286*, 479-482.

Dyke, A.S., J.T. Andrews, P.U. Clark, J.H. England, G.H. Miller, J. Shaw, and J.J. Veillette (2002), The Laurentide and Innuitian ice sheets during the Last Glacial Maximum, *Quat. Sci. Rev., 21*, 9-31.

EPICA community members (2004), Eight glacial cycles from an Antarctic ice core, *Nature, 429*, 623-628.

Flesche Kleiven, H., E. Jansen, T. Fronval, and T.M. Smith (2002), Intensification of Northern Hemisphere glaciations in the circum Atlantic region (3.5-2.4 Ma) - ice-rafted detritus evidence, *Palaeogeogr., Palaeoclimatol., Palaeoecol., 184*, 213-223.

Forsstrom, P.L., and R. Greve (2004), Simulation of the Eurasian ice sheet dynamics during the last glaciation, *Global and Planetary Change, 42* (1-4), 59-81.

Greenland Ice-Core Project Members (1993), Climate instability during the last interglacial period recorded in the GRIP ice core, *Nature, 364*, 203-208.

Greve, R., and D.R. MacAyeal (1996), Dynamic/thermodynamic simulations of Laurentide ice-sheet instability, *Ann. Glaciol., 23*, 328-335.

Grootes, P.M., M. Stuiver, J.W.C. White, S. Johnsen, and J. Jouzel (1993), Comparison of oxygen isotope records from the GISP2 and GRIP Greenland ice cores, *Nature*, *366*, 552-554.

Hoffmann, G., M. Werner, and M. Heimann (1998), Water isotope module of the ECHAM atmospheric general circulation model: A study on timescales from days to several years, *J. Geophys. Res.*, *103* (D14), 16871-16896.

Huybrechts, P. (1994), The present evolution of the Greenland ice sheet - an assessment by modeling, *Glob. Plan. Change*, *9* (1-2), 39-51.

Huybrechts, P. (2002), Sea-level changes at the LGM from ice-dynamic reconstructions of the Greenland and Antarctic ice sheets during the glacial cycles, *Quat. Sci. Rev.*, *21*, 203-231.

Imbrie, J., J.D. Hays, D.G. Martinson, A. McIntyre, A.C. Mix, J.J. Morley, N.G. Pisias, W.L. Prell, and N.J. Shackleton (1984), The orbital theory of Pleistocene climate: Support from a revised chronology of the marine $\delta^{18}O$ record, in *Milankovitch and climate*, edited by A. Berger, J. Imbrie, J. Hays, G. Kukla, and B. Saltzman, pp. 269-305, D. Reidel Publ. Group, Dordrecht.

Joussaume, S., and J. Jouzel (1993), Paleoclimatic tracers: An investigation using an atmospheric general circulation model under ice age conditions. 2. Water isotopes, *J. Geophys. Res.*, *98* (D2), 2807-2830.

Joussaume, S., R. Sadourny, and J. Jouzel (1984), A general circulation of water isotope cycles in the atmosphere, *Nature*, *311* (D2), 24-29.

Labeyrie, L.D., J.C. Duplessy, and P.L. Blanc (1987), Variations in mode of formation and temperature of oceanic deep waters over the past 125,000 years, *Nature*, *327*, 477-482.

Lambeck, K., and J. Chappell (2001), Sea level change through the last glacial cycle, *Science*, *292*, 679-686.

Lambeck, K., Y. Yokoyama, and A. Purcell (2002), Into and out of the Last Glacial Maximum: sea-level change during Oxygen Isotope Stages 3 and 2, *Quat. Sci. Rev.*, *21*, 343-360.

Lea, D.W., D.K. Pak, and H.J. Spero (2000), Climate impact of late Quaternary equatorial Pacific sea surface temperature variations, *Science*, *289*, 1719-1724.

Lhomme, N. (2004), Modelling water isotopes in polar ice sheets, PhD thesis, Univ. of British Columbia, Vancouver.

Lhomme, N., G.K.C. Clarke, and S.J. Marshall (2005a), Tracer transport in the Greenland ice sheet: constraints on ice core and glacial history, *Quat. Sci. Rev.*, *24* (1-2), 173-194.

Lhomme, N., G.K.C. Clarke, and S.J. Marshall (2005b), Tracer transport in the Greenland Ice Sheet: constraints on ice cores and glacial history, *Quat. Sci. Rev., 24* (1-2), 173-194.

Marshall, S.J., T.S. James, and G.K.C. Clarke (2002), North American Ice Sheet reconstructions at the Last Glacial Maximum, *Quat. Sci. Rev., 21*, 175-192.

Martinson, D.G., N.G. Pisias, J.D. Hays, J. Imbrie, T.C. Moore, Jr., and N.J. Shackleton (1987), Age dating and the orbital theory of the icec ages: development of a high-resolution 0 to 300,000-year chronostratigraphy, *Quat. Res., 27*, 1-29.

McManus, J.F., D.W. Oppo, and J.L. Cullen (1999), A 0.5-million-year record of millennial-scale climate variability in the North Atlantic, *Science, 283*, 971-975.

Milankovitch, M. (1930), Mathematische Klimalehre und astronomische Theorie der Klimaschwankungen, in *Handbuch der Klimatologie*, edited by W. Köppen, and R. Geiger, pp. A1-A176, Verlag v. Gebr. Borntraeger, Berlin.

Mix, A.C. (1987), The oxygen-isotope record of glaciation, in *North America and adjacent oceans during the last deglaciation*, edited by W.F. Ruddiman, and H.E. Wright, Jr., pp. 111-135, Boulder, Geol. Soc. America.

Mix, A.C., and W.F. Ruddiman (1984), Oxygen-isotope analyses and Pleistocene ice volumes, *Quat. Res., 21*, 1-20.

Mudelsee, M., and M. Schulz (1997), The Mid-Pleistocene climate transition: onset of 100 ka cycle lags ice volume build-up by 280 ka, *Earth Planet. Sci. Lett., 151* (1-2), 117-123.

Mulitza, S., B. Donner, G. Fischer, A. Paul, J. Pätzold, and C. Rühlemann (2003), The South Atlantic oxygen isotope record of planktic foraminifera, in *The South Atlantic in the Late Quaternary: Reconstruction of Material Budgets and Current Systems*, edited by G. Wefer, S. Mulitza, and V. Ratmayer, pp. 121-142, Springer-Verlag Berlin Heidelberg New York Tokyo.

North Greenland Ice Core Project members (2004), High-resolution record of Northern Hemisphere climate extending into the last interglacial period, *Nature, 431*, 147-151.

Paul, A., and W.H. Berger (1999), Climate cycles and climate transitions as response to astronomical and CO_2 forcings, in *Computerized modeling of sedimentary systems*, edited by J. Harff, W. Lemke, and K. Stattegger, pp. 223-245, Springer Verlag, Berlin.

Paul, A., S. Mulitza, J. Pätzold, and T. Wolff (1999), Simulation of oxygen isotopes in a global ocean model, in *Use of proxies in paleoceanography: examples from the South Atlantic*, edited by G. Fischer, and G. Wefer, pp. 655-686, Springer Verlag, Berlin.

Payne, A.J. (1999), A thermomechanical model of ice flow in West Antarctica, *Clim. Dyn., 15*, 115-125.

Peixoto, J.P., and A.H. Oort (1992), *Physics of climate*, American Institute of Physics, New York, 520 pp.

Peltier, W.R. (2004), Global glacial isostasy and the surface of the ice-age Earth: the ICE-5G (VM2) model and GRACE, *Ann. Rev. Earth Plan. Sci., 32*, 111-149.

Petit, J.R., J. Jouzel, D. Raynaud, N.I. Barkov, J.-M. Barnola, I. Basile, M. Bender, J. Chappellaz, M. Davis, G. Delaygue, M. Delmotte, V.M. Kotlyakov, M. Legrand, V.Y. Lipenkov, C. Lorius, L. P,pin, C. Ritz, E. Saltzman, and M. Stievenard (1999), Climate and atmospheric history of the past 420,000 years from the Vostok ice core, Antarctica, *Nature, 399*, 429-436.

Pollard, D., A.P. Ingersoll, and J.G. Lockwood (1980), Response of a zonal climate–ice sheet model to the orbital perturbations during the Quaternary ice ages, *Tellus, 32*, 301-319.

Ritz, C., A. Fabre, and A. Letreguilly (1997), Sensitivity of a Greenland ice sheet model to ice flow and ablation parameters: consequences for the evolution through the last climatic cycle, *Clim. Dyn., 13*, 11-24.

Ritz, C., V. Rommelaere, and C. Dumas (2001), Modeling the evolution of Antarctic ice sheet over the last 420,000 years: Implications for altitude changes in the Vostok region, *J. Geophys. Res., 106* (D23), 31943-31964.

Saltzman, B., and M.Y. Verbitsky (1993), Multiple instabilities and modes of glacial rhythmicity in the Plio-Pleistocene: A general theory of late Cenozoic climate change, *Clim. Dyn., 9*, 1-15.

Savvin, A., R. Greve, R. Calov, B. Mugge, and K. Hutter (2000), Simulation of the Antarctic ice sheet with a three-dimensional polythermal ice-sheet model, in support of the EPICA project. II. Nested high-resolution treatment of Dronning Maud Land, Antarctica, *Ann. Glaciol., 30* (1-4), 69-75.

Schmidt, G.A. (1998), Oxygen-18 variations in a global ocean model, *Geophys. Res. Lett., 25*, 1201-1204.

Schulz, M., A. Paul, and A. Timmermann (2002), Relaxation oscillators in concert: A framework for climate change at millennial timescales during the late Pleistocene, *Geophys. Res. Lett., 29* (24), 10.1029/2002GL016144.

Shackleton, N.J. (1967), Oxygen isotope analyses and Pleistocene temperatures, re-assessed, *Nature, 215*, 15-17.

Shackleton, N.J. (1977), The oxygen isotope stratigraphic record of the late Pleistocene, *Phil. Trans. Roy. Soc. London, B 280*, 169-182.

Shackleton, N.J. (1987), Oxygen isotopes, ice volume and sea-level, *Quat. Sci. Rev., 6*, 183-190.

Shackleton, N.J., M.A. Hall, and E. Vincent (2000), Phase relationships between millennial-scale events 64,000-24,000 years ago, *Paleoceanography, 15*, 565-569.

Shackleton, N.J., and N.D. Opdyke (1976), Oxygen isotope and paleomagnetic stratigraphy of Pacific core V28-239, late Pliocene to latest Pleistocene, in *Investigation of late Quaternary paleoceanography and paleoclimatology*, edited by R.M. Cline, and J.D. Hays, pp. 449-464, Geol. Soc. Amer., Boulder.

Siegert, M.J., and J.A. Dowdeswell (2004), North American Ice Sheet reconstructions at the Last Glacial Maximum, *Quat. Sci. Rev.*, *23* (11-13), 1273-1283.

Skinner, L.C., and N.J. Shackleton (2005), An Atlantic lead over Pacific deep-water change across Termination I: implications for the application of the marine isotope stage stratigraphy, *Quat. Sci. Rev.*, *24* (5-6), 571-580.

Svendsen, J.I., H. Alexanderson, V.I. Astakhov, I. Demidov, J.A. Dowdeswell, S. Funder, V. Gataullin, M. Henriksen, C. Hjort, M. Houmark-Nielsen, H. Hubberten, O. Ingolfsson, M. Jakobsson, K. Kjaer, E. Larsen, H. Lokrantz, J. Lunkka, A. Lysa, J. Mangerud, A. Matiouchkov, A. Murray, P. Moller, F. Niessen, O. Nikolskaya, L. Polyak, M. Saarnisto, C. Siegert, M. Siegert, R. Spielhagen, and R. Stein (2004), Late quaternary ice sheet history of northern Eurasia, *Quat. Sci. Rev.*, *23* (11-13), 1229-1271.

Tarasov, L., and W.R. Peltier (2002), Greenland glacial history and local geodynamic consequences, *Geophys. J. Int.*, *150* (1), 198-229.

Tarasov, L., and W.R. Peltier (2003), Greenland glacial history, borehole constraints, and Eemian extent, *J. Geophys. Res.*, *108* (B3), Art. No. 2143.

Tarasov, L., and W.R. Peltier (2004), A geophysically constrained large ensemble analysis of the deglacial history of the North American ice-sheet complex, *Quat. Sci. Rev.*, *23* (3-4), 359-388.

Tiedemann, R., M. Sarnthein, and N.J. Shackleton (1994), Astronomic timescale for the Pliocene Atlantic $\delta^{18}O$ and dust flux records of Ocean Drilling Program Site 659, *Paleoceanography*, *9*, 619-638.

Waelbroeck, C., L. Labeyrie, E. Michel, J.-C. Duplessy, J.F. McManus, K. Lambeck, E. Balbon, and M. Labracherie (2002), Sea-level and deep water temperature changes derived from benthic foraminifera isotopic records, *Quat. Sci. Rev.*, *21*, 295-305.

Zachos, J., M. Pagani, L. Sloan, E. Thomas, and K. Billups (2001), Trends, rhythms, and aberrations in global climate 65 Ma to present, *Science*, *292*, 686-693.

Chapter II

THE ICE SHEET MODEL

II.1 Development and partial validation procedures

A 2.5-dimensional thermomechanical ice-sheet model has been developed on the basis of lower-complexity 1- and 2-dimensional models, by combining their most interesting characteristics from the point of view of this study. A stepwise implementation approach offered the possibility to test key features of the model at different stages of the development.

II.1.1 One-dimensional (ice-sheet height) model

II.1.1.1 Description

As a first step, a simple, one-dimensional thermodynamical ice sheet model was constructed for the Laurentide ice sheet. In this model, the dimension considered is the ice-sheet height (H). The approximation of perfect plasticity is employed. The model allows for a slab, but also for a (more realistic) parabolic profile. The bedrock elevation is considered to be constant. Mass conservation relates ice-volume rate of change to accumulation and ablation rates. The thermodynamic equation contains only vertical advection and vertical diffusion terms. The oxygen-isotopic composition of ice is introduced as a passive tracer, using the snow δ^{18}O parameterization of *Mix and Ruddiman* [1984]: –20‰ for $H < 1000$ m and ramping linearly to –40‰ for $H = 2500$ m. Computation is done using a streched coordinate [cf. *Payne and Dongelmans,* 1997]: $\sigma = 1 - z / H$. The stretched vertical grid contains 12 layers.

I.1.1.2 Validation of vertical diffussion and advection schemes: comparison to the analytical solution

At this stage, the numerical schemes for the vertical advection and diffusion in the model were validated by comparing the simulated steady-state temperature profile at the ice-sheet divide to the analytical solution of *Robin* [1955]. The numerically-computed temperature distributions reproduce the analytically-derived profiles fairly accurately. Results based on accumulation rates (b) and ice thickness (H) typical for central Greenland and East Antarctica are presented (Figure II-1) in terms of dimensionless variables, as in *Paterson* [1994, Figure 10.4 therein]. These variables are the normalized distance above the bed $\xi = \frac{z}{H}$ and the dimensionless temperature $\theta = -\frac{k(T - T_a)}{GH}$, where k is the thermal conductivity of ice, G the geothermal heat flux and T_a the near-surface air temperature (see Table II.1 for parameter values).

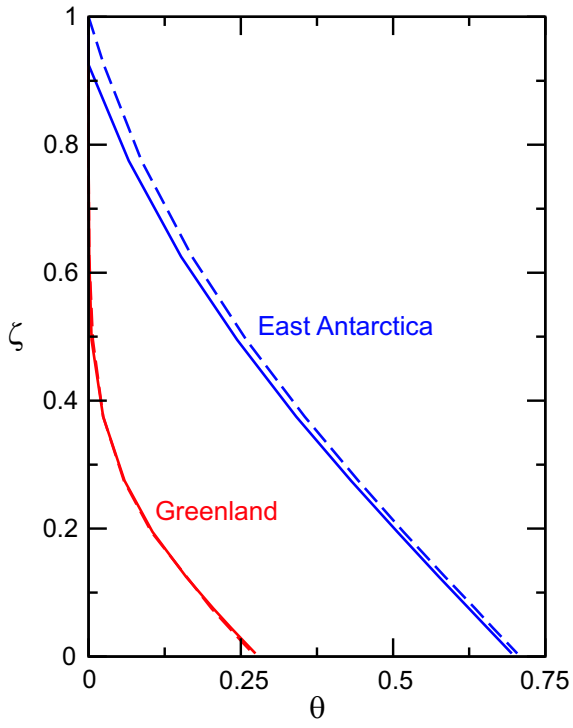

Figure II-1. *Numerically-computed temperature distributions (solid lines) versus analytically-derived profiles (dashed lines).* Typical parameters were used for present-day central Greenland (accumulation rate b = 0.25 m yr^{-1} and ice thickness H = 3000 m) and East Antarctica (b = 0.025 m yr^{-1} and H = 3500 m). Dimensionless variables on the axes are the normalized distance above the bed ξ and the dimensionless temperature θ [cf. *Paterson*, 1994, Figure 10.4 therein].

II.1.1.3 Validation of tracer treatment: comparison to book-keeping

This simple version of the model also allowed testing the accuracy of the treatment of δ^{18}O transport.

In reality, every new parcel of snow deposed at ice-sheet surface and transformed in ice keeps its oxygen-isotopic composition while being transported through the ice sheet. The most accurate approach for the tracer transport would be to label every ice particle and track it on its way until it leaves the ice-sheet by melting or calving.

Using a stretched coordinate in the vertical, with a fixed number of layers, implies that, whenever the ice sheet grows or shrinks, there is an artificial mixing between layers, just by re-arranging the grid levels at every timestep and recomputing the mean δ^{18}O for each layer. At a given time step, the mixing of the internal layers does not affect the mean δ^{18}O of the ice sheet as a whole. However, the situation is different for the top and bottom layers, where mass exchange between the system and the environment occurs. For example, if at a time step a certain amount of ice is added to at ice-sheet top, the δ^{18}O of the new ice is instantly mixed with the δ^{18}O of the topmost σ-layer, forming a new and homogenous σ-layer. If at the next time step the same amount of ice is melted at ice-sheet surface, the δ^{18}O of the ice leaving the system is not that of ice deposed at the previus moment (as it would be in reality), but that of the entire top σ-layer. In a similar way, when melting occurs at the ice-sheet bottom, the ice removed has not the original δ^{18}O with which it was deposed, but the δ^{18}O of the bottom σ-layer, resulted from repeated mixing with upper layers.

Hence, simulating the time evolution of the mean δ^{18}O of the ice sheet by using a stretched cordinate in the vertical induces a conservation error, which for integrations over long intervals might be important. In order to estimate this error, the aproach was to compare the model output to results from a perfectly accurate method, i.e., a book-keeping algorithm. This algorithm was constructed on the basis of the idealised settings employed by *Mix and Ruddiman* [1984] in their age-dependent model.

The age-dependent model imagined by *Mix and Ruddiman* [1984] is the simplest possible model that can incorporate isotopic disequilibrium. It assumes that ablation is age-dependent: all new snow falling on the ice sheet is preserved and the oldest ice is preferentially melted. A slab profile is assumed for the ice sheet (i.e., the ice-sheet height and volume are linearly related). Hypothetical evolutions are imposed for the ice volume, consisting in sinusoidal transitions normalized to 100 units amplitude in 10 kyr, followed by 10 kyr of constant volume. Ablation rate is prescribed, constant in each experiment.

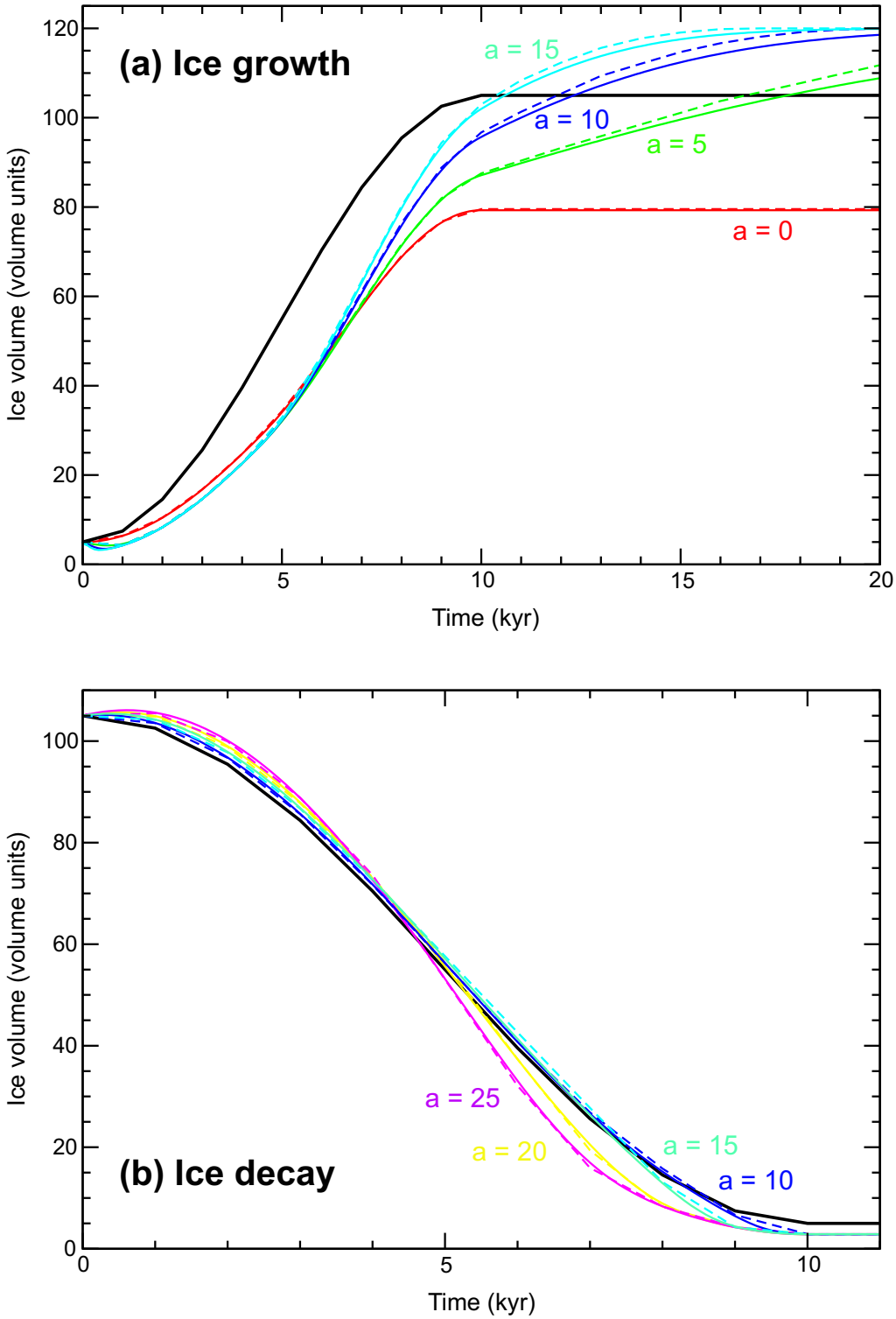

Figure II-2. *Comparison of book-keeping and sigma-layer model results.* Experiments were performed for ice growth and decay, with different ablation rates *a* (volume units/kyr), using the (exact) book-keeping algorithm (dashed lines) and the sigma-coordinate method (solid lines). The values for isotopic volume obtained from book-keeping are the same as those derived by *Mix and Ruddiman* [1984, Figure 3 therein]. The values from sigma-coordinate treatment are also quite similar, especially in the ice-decay experiments. The black lines represent the true ice-volume evolution.

Accumulation rate is computed at each time step from mass-conservation considerations. An "isotopic ice volume" is calculated, i.e., the $\delta^{18}O$ record scaled to ice-volume units by assuming a constant isotopic composition of ice of –35‰:

$$V_{iso} = V_{ice} \frac{\overline{\delta_{ice}}}{-35‰}.$$

Our book-keeping algorithm takes into account at every time step the new ice accumulated and the ice ablated, with the corresponding $\delta^{18}O$ values. Ice layers preserve their original $\delta^{18}O$ from the moment they are added to the ice sheet until they are ablated, as it happens in reality. The mean $\delta^{18}O$ computed for the ice sheet by this method is, therefore, exact, and it is used to derive the reference values for V_{iso}, to which the sigma-coordinate model results are compared.

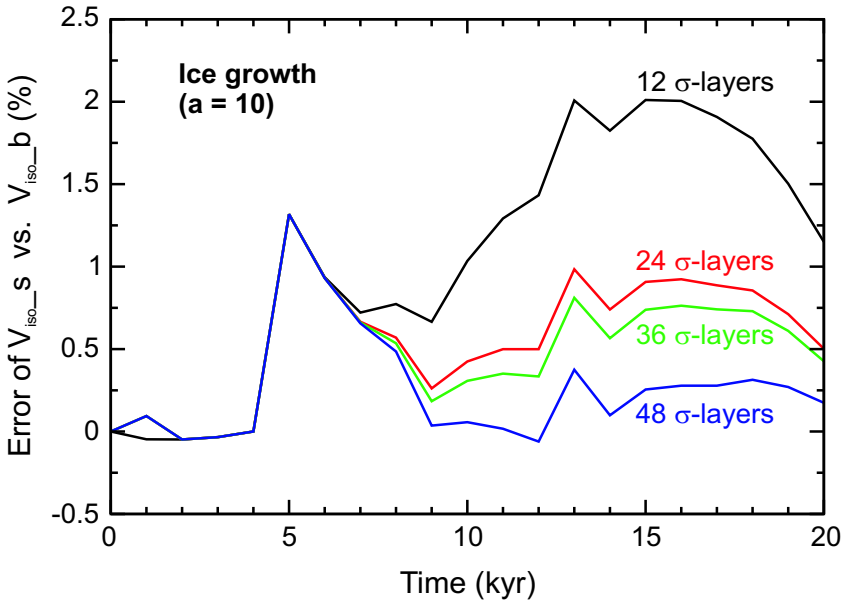

Figure II-3. *Sensitivity of the sigma-coordinate model to the number of layers*. Results are presented from experiments for ice-growth, with an ablation rate a = 10 volume units/kyr. Differences between isotopic-volume values computed with the (approximate) sigma-coordinate method (V_{iso}_s) and those given by the (exact) book-keeping algorithm (V_{iso}_b) are computed for vertical grids with 12, 24, 36 and 48 sigma-layers, and are represented as relative error: (V_{iso}_s – V_{iso}_b)/ V_{iso}_b × 100 %. The error decreases with increasing number of sigma-layers.

Numerical experiments for ice growth and decay, for different ablation rates, were made with the book-keeping and the sigma-coordinate models (Figure II-2). The V_{iso} values from book-keeping were precisely the same as those of *Mix and Ruddiman* [1984, Figure 3 therein]. The sigma-coordinate treatment gave also very similar results, especially in the ice-decay experiments. The departure of V_{iso} values provided by the sigma-coordinate treatment from those given by book-keeping was computed for ice-growth transition, for sigma-grids with different number of layers (Figure II-3). As it was to expect, the larger the number of levels, the smaller the error. However, even in the case of using only 12 levels, the error was less than 2%.

Based on these results, the sigma-coordinate treatment was considered reasonably accurate even when using a relatively small number of layers. Therefore, for computational efficiency, in further developing of the ice-sheet model a vertical grid with 12 sigma layers was used.

II.1.2 Two-dimensional (latitude-height) model

The next important step was to combine the 1-dimensional model, allowing computation in the vertical, with another 1-dimensional model [after *Pollard*, 1983; *Clark and Pollard*, 1998], designed to represent the Laurentide ice sheet, and having as dimension the latitude (described in detail in Section 5.2.1).

II.1.2.1 Description

In the 2-dimensional (latitude-height) ice sheet-bedrock model, the computation is done along a typical north-south flow-line through the Laurentide ice sheet. The ice-dynamics computation follows *Payne* [1995], but without thermomechanical coupling (i.e., the flow-law parameter is set to a constant value, corresponding to an ice temperature of ~ –10ºC). Bedrock deflection under the ice load is computed from a local lithosphere–relaxed asthenosphere model [*Le Meur and Huybrechts*, 1996], with a relaxation time of 5000 years. A calving mechanism as in *Pollard* [1983] helps to simulate complete deglaciations. Temperature and $\delta^{18}O$ distributions in the ice sheet along the flow line are computed. The thermodynamic equation contains vertical diffusion, horizontal and vertical advection, and frictional heat terms. For $\delta^{18}O$ there is no diffusion, but only advection, based on the same numerical scheme (first-order upwind) as temperature. As boundary conditions, the parameterization of *Huybrechts* [1986] is used for ice-surface temperature, and that of *Mix*

and Ruddiman [1984] for snow $\delta^{18}O$. The equations for temporal evolution of ice thickness and bedrock deflection along the flow line are solved on a latitudinal grid with 0.5° resolution. In order to derive the ice-sheet volume from the computed cross-sectional area, a perfectly plastic (parabolic) profile symmetric to ice-sheet crest is assumed in direction perpendicular to the flow line. The model is forced with insolation variations [*Milankovitch*, 1930] through the snow-line elevation [*Oerlemans*, 1980].

II.1.2.2 Validation: EISMINT benchmarks for testing ice-sheet models

In order to test how well the 2-dimensional model solves the continuity, flow and temperature equations, the EISMINT [European Ice Sheet Modelling INiTiative, *Huybrechts et al.*, 1996] benchmarks were used. This allowed to check the accuracy of the numerical schemes employed in both vertical and horizontal directions.

The EISMINT comparison at level I tests steady-state as well as time-dependent model behavior, and implies experiments under fixed and moving-margin conditions. Vertically-integrated isothermal ice flow is considered. Temperature is computed, but it does not affect ice flow (no thermomechanical coupling). An idealized geometry is used, wich for flow-line models consists in an equidistant grid with 1500 km resolution. The bedrock is assumed flat, at zero elevation.

According to the EISMINT classification, our model falls into the "2d/type I" category [*Huybrechts et al.*, 1996]. Results from steady-state experiments under fixed and moving-margin conditions are presented (Figure II-4). Due to axial symmetry (implied by the constant climatic forcing imposed), it is sufficient to show only half of the entire grid domain.

In the fixed-margin experiment, when the vertically-averaged horizontal velocity is computed using the EISMINT pre-exponential flow-law parameter (A), the computed ice thickness at divide is 3601m (upper-left panel), very well in the range of the EISMINT "2d/type I" models (3601.6 ± 2.1 m). When A is computed by vertical integration over the 12 sigma-layers, the computed thickness is 0.6% smaller, 3578.5 m, which indicates the diffusivity of the first-order upwind scheme we use. Interestingly, this value is closer to the analytical solution (3575.1 m). In the moving-margin experiment, the tickness is 2973 m (upper-right panel), 0.8% smaller than EISMINT reference value (2997.2 ± 6.4 m).
The spatial distributions of the quantities describing the horizontal mass transport, i.e., the mass flux per unit width and the vertically-averaged horizontal velocity (Figure II-4, middle panels), are quite similar to the EISMINT distributions for the same type of models [*Huybrechts et al.*, 1996, Figures 2 and 5 therein].

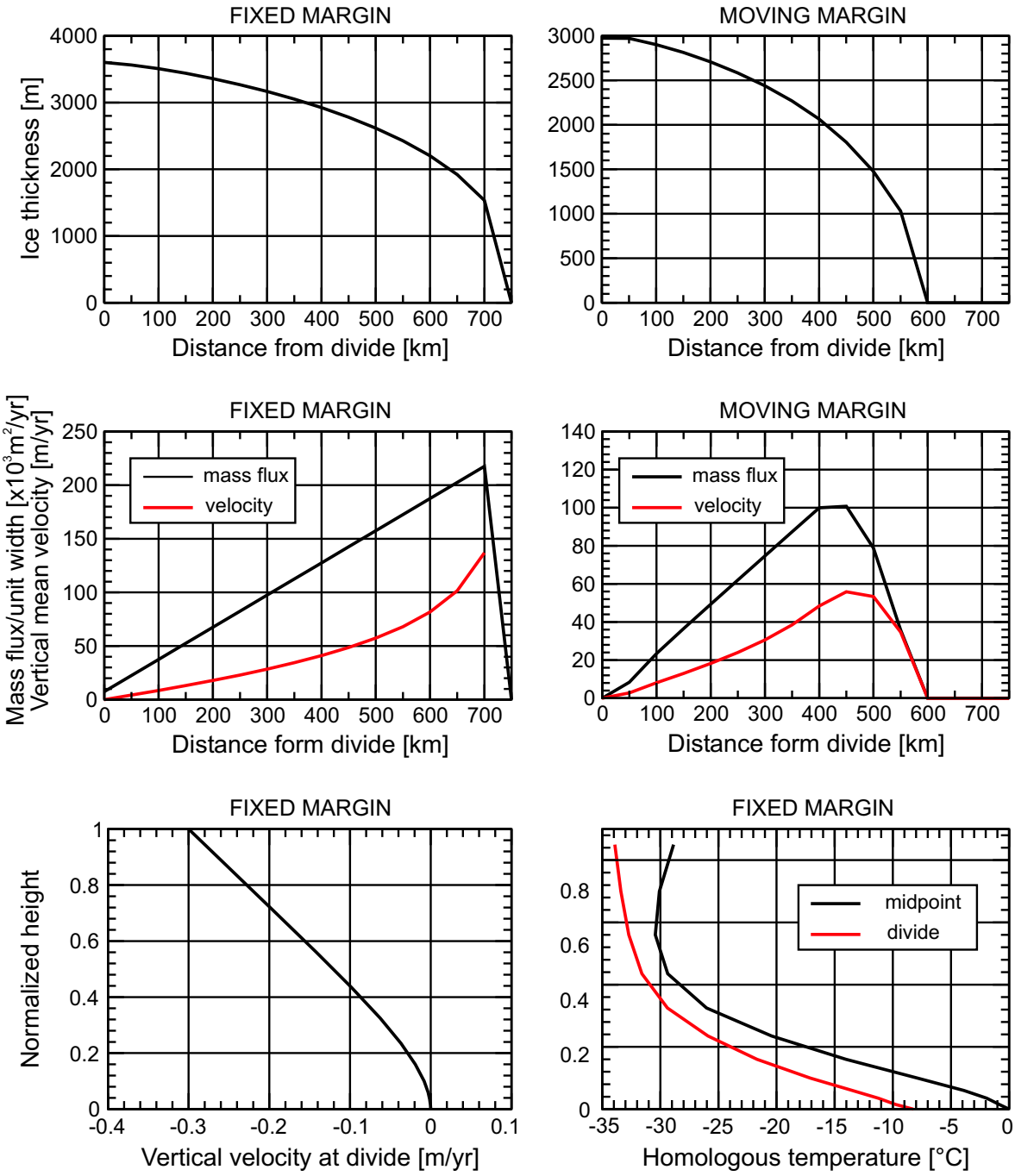

Figure II-4. *Response of the 2-dimensional ice-sheet model to steady-state EISMINT I tests* [*Huybrechts et al.*, 1996]. Upper panel: ice thickness in fixed and moving-margin experiments. Middle panel: quantities characterizing the horizontal transport: the mass flux per unit width and the vertically-averaged horizontal velocity, also under fixed and moving-margin conditions. Lower panel: for a fixed-margin experiment only, the profile of (left) vertical velocity at divide and (right) homologous temperature at divide and at the midpoint. To make easier the comparison to the results of EISMINT I project, the graphs have the same format as the corresponding figures (2, 3 and 5) in *Huybrechts et al.* [1996]. According to the EISMINT classification, our model is "2d/type I".

The vertical velocity at the ice divide and the temperature (relative to the pressure-melting point) at the divide and at the midpoint are also presented, from the fixed-margin experiment only (Figure II-4, lower panel). The simulated vertical velocity at the divide (left) is in very good agreement with the EISMINT solution (Figure 3 therein). No plots are shown in *Huybrechts et al.* [1996] for temperature distributions from 2-dimensional models. However, the temperature profile computed with our model (Figure II-4, lower-right panel) is similar to the mean profile from 3-dimensional EISMINT models (Figure 3 therein). The simulated basal temperature (not shown) is lower at ice divide (–8.2° versus –6.72°C, EISMINT, Table 2), and higher around the midpoint (pressure-melting point is reached at 300 km distance from divide, compared to 400 km in the 3-dimensional EISMINT models). This could be mainly due to the dissipation-heat treatment (see Section II.2.1, equation (14) and the vertical resolution. The numerical scheme (first-order upwind) for horizontal and vertical advection might also play a role, even though it produced satisfactory results in the EISMINT tests. It must be noted that also between the EISMINT models there are relatively large differences in the simulated thermal regime. In the moving-margin experiment, temperature computation could not be done in due to numerical instability problems. These were solved in the next model version.

II.2 The 2.5-dimensional (latitude-height) thermomechanical ice-sheet model

Two important requirements for a more realistic simulation of the ice-sheet volume and oxygen-isotopic composition imposed further development of the 2-dimensional model to a 2.5-dimensional thermomechanical model.

First, the ice-sheet volume must be derived from the computed 2-dimensional cross-section along the flow line. A flow line with constant width, as in the 2-dimensional model, implies a slab profile in direction normal to the flow, and the only criterium for choosing the longitudinal dimension of that profile is to provide a reasonable ice-sheet volume at the Last Glacial Maximum. A more realistic approach is to assume a parabolic profile in East-West direction and to take into account the real longitudinal extent of the continent.

Second, in reality the thermal regime influences the ice dynamics. Only a thermo-mechanical model can realistically simulate ice flow (also including processes as basal melting and sliding) and, hence, tracer transport through ice. This is critical in estimating the mean-ice $\delta^{18}\mathrm{O}$, as well as the magnitude, isotopic composition and latitudinal distribution of the freshwater flux from the ice sheet to the ocean.

II.2.1 Model description

The 2.5-dimensional thermomechanical ice-sheet model combines the computation along a north-south flow line after *Payne* [1995] with an equilibrium profile in the zonal direction following *Gallée et al.* [1992] and *Crucifix and Berger* [2002]. Our model simulates the North-American Ice Sheet (NAIS), which dominated ice-volume variations during the late Pleistocene.

The ice-surface elevation is denoted by $s = H + h$, where H is the ice thickness and h the bedrock elevation with respect to present-day sea level.

The evolution of ice-sheet thickness at the divide as a function of latitude φ is given by the continuity equation [cf. *Gallée et al.*, 1992, equation 1 therein]:

$$\frac{\partial H}{\partial t} = M - \frac{1}{a\cos\varphi}\frac{\partial}{\partial\varphi}\left(\overline{u_y} H \cos\varphi\right) - D_\lambda - S, \tag{1}$$

where M is the local annual mass balance at ice surface, a the radius of the Earth, $\bar{u}$ is the vertically-averaged horizontal velocity, D_λ represents the lateral discharge of ice mass and S the melt rate at the ice-sheet base (see Table II-1 for parameter values).

In the east-west direction a perfectly-plastic profile symmetric to the ice-sheet crest is assumed [*Gallée et al.*, 1992; *Crucifix and Berger*, 2002]. For the zonal ice-mass discharge we employ a parameterization similar to *Gallée et al.* [1992]:

$$D_\lambda = -\frac{1}{(a\cos\varphi)^2} DH \frac{\partial^2 s}{\partial\lambda^2} = DH\frac{s}{L^2} \tag{2}$$

with $D = 8\bar{A}\frac{(\rho g)^n}{a^2}\left|\frac{\partial s}{\partial\varphi}\right|^{n-1}$, where $\bar{A}$ is the vertically integrated (in our case temperature-dependent) flow parameter and L is the longitudinal extent of the ice sheet. The parameter L is related to the ice surface elevation as follows:

$$L = s^2 / \mu \tag{3}$$

with $\mu = \frac{2\tau_0}{\rho g}$, where ρ is the ice density, g the gravitational acceleration and τ_0 the prescribed, constant bottom stress, derived from the *CLIMAP* [1981] reconstruction [*Crucifix and Berger*, 2002].

A vertical distribution of the lateral discharge, consistent with the perfect-plasticity assumption, is:

$$d_\lambda(z) = \frac{1}{H} D_\lambda , \tag{4}$$

with $\int_h^s d_\lambda(z)dz = D_\lambda$.

In the north-south direction, ice deformation is assumed to be driven by horizontal shear stress (τ_{yz}), approximated by:

$$\tau_{yz}(z) = -\rho g(s-z)\frac{\partial s}{\partial y}. \tag{5}$$

Assuming a nonlinear Glen flow law for ice, the meridional velocity is derived as:

$$u_y(z) = -2\frac{(\rho g)^n}{a^2}\left|\frac{\partial s}{\partial \varphi}\right|^{n-1}\frac{1}{a}\frac{\partial s}{\partial \varphi}\int_h^z A(T^*)(s-z)^n dz + u_y(h), \tag{6}$$

where $u_y(h)$ is the meridional component of the sliding velocity.

The parameter A introduces the temperature dependence of ice deformation. It is assumed to be an Arrhenius-type function of the absolute temperature of the ice, corrected for the dependence of the melting point on pressure (T^*):

$$A(T^*) = EA_0 \exp\left(\frac{-Q}{RT^*}\right), \tag{7}$$

with:

$$T^* = T - T_{pmp} + T_0 , \tag{8}$$

$$T_{pmp} = T_0 - \rho_i g \Phi(s-z), \tag{9}$$

where T is ice temperature, T_{pmp} the pressure melting point temperature, T_0 the triple point temperature of water and Φ the rate of change of melting point temperature with pressure. Furthermore, in eq.(7), Q is the creep activation energy, R is the universal gas constant, A_0 is a constant coefficient and E an empirical flow enhancement factor introduced into Glen's flow law to account for the effects of crystal anisotropy and impurities on bulk ice

deformation [*Marshall et al.*, 2000]. The values for A_0 and Q are those indicated in the EISMINT II model intercomparison project [*Payne et al.*, 2000]. The vertically integrated flow coefficient used in the calculation of lateral discharge is obtained by numerically integrating:

$$\bar{A} = \int_h^s \left(\int_h^z A(T^*)(s - z')^n dz' \right) dz .$$

The sliding velocity is assumed to be directly related to basal shear stress:

$$\begin{cases} u_y(h) = -B\rho g H \dfrac{\partial s}{\partial y} & \text{if } T_{base} = T_{pmp} \\ u_y(h) = 0 & \text{if } T_{base} < T_{pmp} \end{cases} \tag{10}$$

where T_{base} is the basal ice temperature and B a free parameter. A numerical integration of equation (6) provides the vertically averaged horizontal velocity employed in (1).

The distribution of vertical velocity can be found from the meridional velocities calculated in (6) and the lateral discharge profile (4), using the incompressibility condition:

$$w(z) = -\int_h^z \frac{\partial u_y}{\partial y} dz - \int_h^z d_\lambda dz + w(h), \tag{11}$$

with the velocity at ice-sheet base:

$$w(h) = \frac{\partial h}{\partial t} + u_y(h)\frac{\partial h}{\partial y} - S \ , \tag{12}$$

where S is the basal melt rate.

Bedrock adjustment is computed from a local lithosphere–relaxed asthenosphere model [*Le Meur and Huybrechts*, 1996] with a characteristic time constant τ_b:

$$\frac{\partial h}{\partial t} = \frac{1}{\tau_b}\left[h_{eq} - h - \frac{\rho H}{\rho_b} \right], \tag{13}$$

where h_{eq} is the equilibrium bedrock elevation with respect to present-day sea level and ρ_b the bedrock density. The initial topography along the flow line is taken from *Clark and Pollard* [1998]: 500 m above sea level southward of 70ºN, -500 m northward of 74ºN and a linear ramp between 70º and 74ºN.

The ice temperature T influences the model dynamics in two ways: it determines the flow parameter A used in computing horizontal velocity and lateral discharge, and it determines whether or not sliding occurs. The equation for temperature evolution contains vertical diffusion, horizontal and vertical advection and frictional heat generation terms:

$$\frac{\partial T}{\partial t} = \frac{k}{\rho c}\frac{\partial^2 T}{\partial z^2} - u_y \frac{\partial T}{\partial y} - d_\lambda T - w\frac{\partial T}{\partial z} + \frac{\tau_{yz}}{\rho c}\frac{\partial u_y}{\partial z}, \tag{14}$$

where k is ice thermal conductivity and c ice specific heat capacity.

When the temperature computed for the basal layer (T_{base}) exceeds the pressure melting point, a melt rate is calculated:

$$S = \frac{c}{\lambda}\left(T_{base} - T_{pmp}\right)\frac{\Delta z_{base}}{\Delta t}, \tag{15}$$

where λ is the latent heat capacity of ice, Δz_{base} the thickness of the basal layer, and Δt the timestep (see section "Numerical Solution" for details of the discretization). After computing the melt rate, T_{base} is reset to T_{pmp}.

Enhanced flow in the zonal direction during periods when the basal temperature is at the melting point is represented by a gradual decrease of the bottom stress τ_0 with a rate $d\tau/dt = 0.2$ Pa/yr. This parameterization is based on the treatment of Heinrich events by *Crucifix and Berger* [2002] and results in increasing the lateral discharge by an additional term [cf. *Crucifix and Berger*, 2002, Appendix B therein]:

$$\frac{\partial s}{\partial t} = -\frac{1}{\tau}\frac{d\tau}{dt}\frac{s^2 - sh}{3s - 2h} \tag{16}$$

The decrease of τ_0 is limited to a minimum value of 10,000 Pa.

Ice-volume computation also follows *Crucifix and Berger* [2002, Appendix A therein]. The volume of an ice-sheet slice comprised in a latitude band of width $\Delta\varphi$ is:

$$V_{\Delta\varphi} = \begin{cases} \frac{2}{3}\frac{2s^2(s-h)}{\mu}a\Delta\varphi & \text{if } 2L \le x_p(\varphi) \\ \frac{4}{3}\left[L^{3/2} - \left(L - \frac{x_p}{2}\right)^{3/2}\right]\sqrt{\mu}\left(1 - \frac{h}{s}\right)a\Delta\varphi & \text{if } 2L > x_p(\varphi) \end{cases} \tag{17}$$

where $x_p(\varphi)$ is the width of the continental platform [cf. *Crucifix and Berger*, 2002, Figure 1a therein].

II.2.2 Tracer treatment

The ratio *R* of oxygen isotopes ^{18}O and ^{16}O is expressed as the fractional deviation δ^{18}O from the isotopic ratio of the Vienna Standard Mean Ocean Water [V-SMOW, *Gonfiantini*, 1978]:

$$\delta^{18}\mathrm{O} = \left(R / R_{V-SMOW} - 1\right) \times 1000‰ \tag{18}$$

Ice δ^{18}O (δ for short) is introduced in the model as a passive tracer. There is no diffusion for δ and its transport through ice relies on the same advection scheme (first-order upwind) as temperature:

$$\frac{\partial \delta}{\partial t} = -u_y \frac{\partial \delta}{\partial y} - d_\lambda \delta - w \frac{\partial \delta}{\partial z}, \tag{19}$$

Using δ directly rather than mass ratio introduces a negligible conservation error.

We note that by equation (19) the model only computes the two-dimensional distribution of δ along the flow line, as it does for temperature by equation (14). In order to derive the mean isotopic composition of the whole ice sheet (δ_i), knowledge on the isotopic distribution in East-West direction is required. We do not attempt to construct this distribution from the simulated profile at the divide, as ad hoc assumptions would be needed. Instead, we associate to δ_i the mean computed along the flow line. Because snow accumulated at ice divide is isotopically the most depleted, the mean along the flow line (and, hence, the mean for the whole ice sheet) is lighter than derived by any other approach, and the corresponding seawater enrichment is the maximum limit for the NAIS contribution.

II.2.3 Numerical solution

The glacial cycle integration extends from 120 kyr BP to the present. We use an Eulerian-forward scheme for time stepping. The timestep is 1 year, except for periods of intense melting at the ice-sheet base or high ablation at ice surface, when it is reduced to 0.05 year. Staggered grids are employed in both horizontal and vertical directions. The latitudinal-grid resolution is 0.5°. The vertical grid is stretched and has 12 uneven layers, with thicknesses decreasing towards the ice-sheet base.

We use a first-order upwind scheme for advection and a second-order scheme for heat diffusion. Vertical upwinding is done using the relative vertical velocity (*w**), i.e., the difference between the vertical velocity of the ice and that of the grid point [*Payne and Dongelmans*, 1997, Appendix A therein]. At the ice surface $w^*_{sfc} = -M$, and at the base $w^*_{base} = -S$.

II.2.4 Boundary conditions

Flux boundary conditions are applied at the ice-sheet surface and base.
The advective heat fluxes are:

$$F^T_{sfc} = \begin{cases} \rho c M T_a & \text{if } M \geq 0 \\ \rho c M T_{sfc} & \text{if } M < 0 \end{cases} \tag{20}$$

at the ice surface, where T_a is the air temperature at ice surface and T_{sfc} the temperature of the upper ice layer, and

$$F^T_{base} = -\rho c S T_{base} \tag{21}$$

at ice-sheet base.

The advective fluxes for δ^{18}O are:

$$F^{\delta}_{sfc} = \begin{cases} M\delta_{snow} & \text{if } M \geq 0 \\ M\delta_{sfc} & \text{if } M < 0 \end{cases}, \tag{22}$$

and

$$F^{\delta}_{base} = -S\delta_{base}, \tag{23}$$

where δ_s denotes the isotopic composition of snow, δ_{sfc} is the δ^{18}O of the upper ice layer and δ_{base} the δ^{18}O of the bottom layer.

The diffusive heat fluxes are:

$$\begin{cases} Q^T_{sfc} = \rho c \Delta z_{sfc} \left(T_a - T_{sfc} \right) / \tau_{damp} \\ Q^T_{base} = -G \end{cases}, \tag{24}$$

where Δz_{sfc} is the thickness of the uppermost ice layer, τ_{damp} the time scale for restoring the surface temperature T_{sfc} to the prescribed air temperature T_a, and G the geothermal heat flux. The diffusive fluxes for $\delta^{18}O$ are nul.

II.2.5 Climate forcing

The local annual mass balance M on the ice surface is derived using the equilibrium-line concept, as follows [*Oerlemans*, 1982]:

$$M = \min\left[M_{\max}, M_{\max}\left(s - h_{equ}\right)/h_{\max} \right] \text{ m yr}^{-1} \tag{25}$$

where the upper limit for the accumulation rate M_{max} and the parameter h_{max} are similar to those used by [*Pollard*, 1983].
The equilibrium-line elevation h_{equ} is computed as a function of near-surface air temperature T_a and elevation:

$$h_{equ} = s + \left(T_a - T_{equ}\right)/\beta \tag{26}$$

where β is the atmospheric lapse rate, and T_{equ} the equilibrium-line temperature [*Oerlemans*, 1982].

The near-surface air temperature parameterization follows the glacial index method of *Marshall et al.* [2000]:

$$\begin{aligned} T_a(\varphi,t) = {} & T(\varphi,0) + I(t)\left[T(\varphi,21) - T(\varphi,0)\right] \\ & - \beta\left\{s(\varphi,t) - s(\varphi,0) - I(t)\left[s(\varphi,21) - s(\varphi,0)\right]\right\} \end{aligned} \tag{27}$$

where the glacial index $I(t)$ is derived from the NGRIP $\delta^{18}O$ record [*North Greenland Ice Core Project members*, 2004] by assigning climate indices of $I = 0$ to present-day and $I = 1$ to LGM $\delta^{18}O$ values in the ice core and linearly interpolating between these end members. Latitudinal distributions of surface temperature at present day, $T(\varphi,0)$, and at LGM, $T(\varphi,21)$, are computed by zonally averaging the output of the atmospheric general circulation model ECHAM3/T42 [*Romanova et al.*, 2004, Figure 1c therein] over the North-American continent.

The parameterization of the oxygen-isotopic composition of snow combines the relationship between mean annual surface temperature and $\delta^{18}O$ of precipitation derived by *Johnsen and White* [1989] for present-day Greenland, the results of AGCM simulations by *Jouzel et al.* [1994] and the glacial index:

$$\delta_s = -13.7 + \alpha(t) T_a \tag{28}$$

with the slope $\alpha(t)$ computed as:

$$\alpha(t) = \alpha_0 + I(t)\left[\alpha_{LGM} - \alpha_0\right] \tag{29}$$

where α_0 and α_{LGM} are the slopes determined by *Jouzel et al.* [1994] for the NAIS domain for present day and the LGM, respectively.

Table II-1 Parameters of the 2.5-dimensional thermomechanical ice-sheet model

Symbol	Description	Value	Unit
a	radius of the Earth	6371.0×10^3	m
ρ	ice density	910	kg m $^{-3}$
g	gravitational acceleration	9.81	m s $^{-2}$
τ_0	bottom stress for frozen ice base	15,200	Pa
n	ice rheology exponent	3	
A_0	multiplier in Arrhenius relation	3.61×10^{-13} if $T^* <$ -10°C 1.73×10^{-3} if $T^* \geq$ -10°C	s $^{-1}$ Pa $^{-3}$
Q	creep activation energy	6.0×10^4 if $T^* <$ -10°C 13.9×10^4 if $T^* \geq$ -10°C	J mol $^{-1}$
E	flow-enhancement factor	80	
T_0	triple-point temperature of water	273.15	K
Φ	dependence of melting on pressure	9.8×10^{-8}	K Pa $^{-1}$
B	multiplier in sliding law	8.0×10^{-3}	m yr^{-1}Pa^{-1}
k	thermal conductivity of ice	6.62×10^7	J m^{-1} K^{-1} yr^{-1}
c	specific heat capacity of ice	2009	J kg^{-1} K^{-1}
λ	latent heat capacity of ice	3.35×10^5	J kg^{-1}
G	geothermal heat flux	-5.0×10^{-2}	W m^{-2}
τ_{damp}	time scale for restoring T_{sfc} to T_a	1	yr
τ_b	timescale of bedrock relaxation	4000	yr
ρ_b	bedrock density	3300	kg m^{-3}
$h_{eq}(y,t)$	equilibrium bedrock elevation with respect to present-day sea level	500 southward of 70ºN -500 northward of 74ºN linear ramp between 70º-74ºN	m
$d\tau/dt$	rate of change of bottom stress	-0.2 (if $T < T_{pmp}$)	Pa yr^{-1}
M_{max}	upper limit for accumulation rate	0.55	m yr $^{-1}$
h_{max}	parameter in surface mass balance	1500	m
T_{equ}	temperature of equilibrium line	-15.0	°C
β	atmospheric lapse rate	6.5×10^{-3}	°C m $^{-1}$
α_0	slope in snow-δ^{18}O – temperature relationship at present day	0.6	‰ °C $^{-1}$
α_{LGM}	slope in snow-δ^{18}O – temperature relationship at the LGM	0.66	‰ °C $^{-1}$

References

Clark, P.U., and D. Pollard (1998), Origin of the middle Pleistocene transition by ice sheet erosion of regolith, *Paleoceanography, 13* (1), 1-9.

CLIMAP Project members (1981), Seasonal reconstructions of the Earth's surface at the last glacial maximum, Geological Society of America.

Crucifix, M., and A. Berger (2002), Simulation of ocean-ice sheet interactions during the last deglaciation, *Paleoceanography, 17* (4), 1054, 10.1029/2001PA000702.

Gallée, H., J.P. van Ypersele, T. Fichefet, C. Tricot, and A. Berger (1992), Simulation of the last glacial cycle by a coupled, sectorially averaged climate-ice sheet model. Part II: Response to insolation and CO_2 variations, *J. Geophys. Res., 97*, 15713-15740.

Gonfiantini, R. (1978), Standards for stable isotope measurements in natural compounds, *Nature, 271*, 534-536.

Huybrechts, P. (1986), A three dimensional time dependent numerical model for polar ice sheets: Some basic testing with a stable and efficient finite difference scheme, in *Tech. Rep. 86/1*, Vrije Univ. Brussel Geogr. Inst., Brussels.

Huybrechts, P., T. Payne, and EISMINT Intercomparison Group (1996), The EISMINT benchmarks for testing ice-sheet models, *Ann. Glaciol., 23*, 1-12.

Johnsen, S.J., and J. White (1989), The origin of Arctic precipitation under present and glacial conditions, *Tellus, 41B*, 452-468.

Jouzel, J., R.D. Koster, R.J. Suozzo, and G.L. Russell (1994), Stable water isotope behavior during the last glacial maximum: A general circulation model analysis, *J. Geophys. Res., 99* (D12), 25791-25801.

Le Meur, E., and P. Huybrechts (1996), A comparison of different ways of dealing with isostasy: examples from modelling the Antarctic ice sheet during the last glacial cycle, *Annal. Glaciol., 23*, 309-317.

Marshall, S.J., L. Tarasov, G.K.C. Clarke, and W.R. Peltier (2000), Glaciological reconstruction of the Laurentide Ice Sheet: physical processes and modelling challenges, *Can. J. Earth Sci., 37*, 769-793.

Milankovitch, M. (1930), Mathematische Klimalehre und astronomische Theorie der Klimaschwankungen, in *Handbuch der Klimatologie*, edited by W. Köppen, and R. Geiger, pp. A1-A176, Verlag v. Gebr. Borntraeger, Berlin.

Mix, A.C., and W.F. Ruddiman (1984), Oxygen-isotope analyses and Pleistocene ice volumes, *Quat. Res., 21*, 1-20.

North Greenland Ice Core Project members (2004), High-resolution record of Northern Hemisphere climate extending into the last interglacial period, *Nature*, *431*, 147-151.

Oerlemans, J. (1980), Model experiments on the 100 000 year glacial cycle, *Nature*, *287*, 430-432.

Oerlemans, J. (1982), Glacial cycles and ice-sheet modelling, *Clim. Change*, *4*, 353-374.

Paterson, W.S.B. (1994), *The physics of glaciers*, Pergamon, Oxford, 481 pp.

Payne, A.J. (1995), Limit cycles in the basal thermal regime of ice sheets, *J. Geophys. Res.*, *B100*, 4249-4263.

Payne, A.J., and P.W. Dongelmans (1997), Self-organization in the thermomechanical flow of ice sheets, *J. Geophys. Res.*, *B102*, 12219-12233.

Payne, A.J., P. Huybrechts, A. Abe-Ouchi, R. Calov, J.L. Fastook, R. Greve, S.J. Marshall, I. Marsiat, C. Ritz, L. Tarasov, and M.P.A. Thomassen (2000), Results from the EISMINT model intercomparison: the effects of thermomechanical coupling, *J. Glaciol.*, *46* (153), 227-238.

Pollard, D. (1983), Ice-age simulations with a calving ice-sheet model, *Quat. Res.*, *20*, 30-48.

Robin, G. (1955), Ice movement and temperature distribution in glaciers and ice sheets, *J. Glaciol.*, *2*, 523-532.

Romanova, V., M. Prange, and G. Lohmann (2004), Stability of the thermohaline circulation and its dependence on the background hydrological cycle, *Clim. Dyn.*, *22*, 527-538.

Chapter III

MODELING THE OXYGEN-ISOTOPIC COMPOSITION OF THE NORTH AMERICAN ICE SHEET AND ITS EFFECT ON THE ISOTOPIC COMPOSITION OF THE OCEAN DURING THE LAST GLACIAL CYCLE

Adriana Sima[1], André Paul[1], Michael Schulz[1], and Johannes Oerlemans[2]

[1] *Department of Geosciences, Bremen University, D-28334 Bremen, Germany*
[2] *IMAU, Utrecht University, 3508 TA Utrecht, the Netherlands*

Abstract

We used a 2.5-dimensional thermomechanical ice-sheet model including the oxygen-isotope ratio $^{18}O/^{16}O$ of ice as a passive tracer to simulate the isotopic composition ($\delta^{18}O$) of the North American Ice Sheet (NAIS) during the last glacial cycle. This model allowed us to estimate the contribution of the NAIS to the change of mean seawater $\delta^{18}O$ (δ_w) between the Last Glacial Maximum (LGM) and the Holocene and to evaluate the effect of nonequilibrium isotopic composition of the NAIS on the relationship between ice-volume variations and isotopic enrichment of the ocean, assumed well mixed. The enrichment due to the NAIS at the LGM was 0.63‰, corresponding to ~74 m of eustatic sea-level drop and to a mean $\delta^{18}O$ of the NAIS of approximately –31‰. The modeled NAIS volume variations and the induced δ_w changes over the past 120,000 years indicated no significant time lag. The inaccuracy associated with estimating ice-volume variations from changes in δ_w was generally less than 10%.We conclude that the decoupling between ice-volume and mean-δ_w signals due to nonequilibrium isotopic composition of ice sheet is negligible. However, phase differences between ice volume and δ_w at particular locations in the ocean can appear due to ocean circulation.

Invited to be re-submitted to **Geophysical Research Letters**

III.1 Introduction

The oxygen-isotopic composition of seawater (δ_w) is a key parameter in paleoclimate research. It depends on global ice volume (V_g) and the isotopic composition of the ice (δ_i), and, together with seawater temperature, determines the isotopic composition of foraminiferal carbonate (δ_c). Hence, knowledge of past δ_w variations can be used to infer V_g history, or, in conjunction with δ_c records, to reconstruct seawater temperature changes. But, in spite of various methods to estimate past δ_w [*Duplessy et al.*, 2002, and references therein], uncertainty persists in separating the contributions of δ_w and temperature to the total change in δ_c. Also, interpreting δ_w changes as an ice-volume proxy is hampered by possible decoupling of V_g and δ_w signals due to climatically-driven changes in δ_i during the course of a glacial-interglacial cycle.

Ice-sheet models incorporating oxygen-isotope transport represent a valuable tool for addressing these intricacies. Such models were successfully applied to simulate the time-evolving three-dimensional isotopic stratigraphy of Greenland [*Clarke and Marshall*, 2002; *Lhomme*, 2004] and Antarctica [*Lhomme*, 2004] ice sheets. The latest results suggest contributions to the change of δ_w ($\Delta\delta_w$) at the LGM of 0.01‰ for Greenland, 0.13±2‰ for West Antarctica and –0.04‰ for East Antarctica. We used a new numerical model for the North American Ice Sheet (NAIS) to compute the impact of this ice sheet on the ocean isotopic enrichment during the last glacial cycle.

With respect to the relationship between ice-volume variations and $\Delta\delta_w$, *Mix and Ruddiman* [1984] (hereafter *MR*) suggest that, due to changes of the mean δ^{18}O of ice sheets, $\Delta\delta_w$ may misrepresent the amplitude of the ice-volume signal and lag ice volume by 1 to 3 thousand years (kyr). In particular, *Clark and Mix* [2002] make the nonequilibrium isotopic composition of ice sheets partly responsible for the timing differences observed in marine δ^{18}O records between the last isotopic maximum (LIM, centered at ~18 kyr before present (BP)) and LGM (ended at ~19 kyr BP). However, in common paleoceanographic practice the effect of changing isotopic composition of ice is considered small [*Chappell and Shackleton*, 1986] and a constant coefficient of proportionality is assumed in reconstructing sea-level variations from δ_c records [e.g., *Waelbroeck et al.*, 2002]. Our model, more complex than those used by *MR*, allowed us to re-examine the error induced by this assumption.

III.2 Model description

The 2.5-dimensional thermomechanical ice-sheet model [after *Gallée et al.*, 1992; *Payne*, 1995; *Crucifix and Berger*, 2002] simulates the evolution of the NAIS complex, which dominated ice-volume variations during the late Pleistocene [cf. *Peltier*, 1994; 2004]. Computation was done along a north-south flow line, whereas in the zonal direction a perfectly-plastic profile symmetric to the ice-sheet crest was assumed (see supplementary material for a detailed model description).

The integration extended from 120 kyr BP to present. Climate forcing was parameterized by the glacial index method [*Marshall et al.*, 2000], using the output of a comprehensive atmospheric general circulation model (AGCM) [*Romanova et al.*, 2004] and the NGRIP δ^{18}O record [*North Greenland Ice Core Project members*, 2004] for surface temperature, and by the snow-line concept [*Oerlemans*, 1982] for mass balance.

The oxygen-isotope ratio $^{18}O/^{16}O$ of ice was treated as a passive tracer. The parameterization of oxygen-isotopic composition of snow combined a relationship between mean annual surface temperature and precipitation δ^{18}O for present-day Greenland [*Johnsen and White*, 1989] and results of AGCM simulations [*Jouzel et al.*, 1994] for the NAIS domain. We assumed a well-mixed ocean and calculated the changes of δ_w induced by NAIS volume variations as:

$$\Delta\delta_w = -\frac{S_i}{d_o - S_g}\delta_i \qquad (1)$$

where d_o is the present average depth of the ocean, S_i is the NAIS volume-equivalent sea level and S_g the global ice-equivalent sea-level. NAIS volume V_{ice} and S_i are related by $S_i = \rho_i V_{ice}/(\rho_w A_o)$, with A_o the present ocean area and ρ_w and ρ_i the average densities of water and ice ($A_o = 360.5 \times 10^6$ km^2, $d_o = 3800$ m, $\rho_w = 1000$ kg/m^3 and $\rho_i = 910$ kg/m^3). No correction was made for variations in ocean area between the LGM and present. The global sea-level change was computed as $S_g = 1.7 * S_i$, by assuming a ~60% contribution of the NAIS to the total ice-volume variations [*Peltier*, 2004]. To better compare V_{ice} and $\Delta\delta_w$, we computed an "isotopic volume", V_{iso}, using a constant reference value δ_{ref} for the mean δ^{18}O of ice (cf. *MR*):

$$V_{iso} = \frac{\delta_i}{\delta_{ref}} V_{ice}\,. \qquad (2)$$

In order to fit V_{ice} and V_{iso} values at the LGM (21 kyr BP), we chose for δ_{ref} the computed value of δ_i at the LGM. To separate the contributions to changes of V_{iso} we also computed:

$$\frac{dV_{iso}}{dt} = \frac{\delta_i}{\delta_{ref}}\frac{dV_{ice}}{dt} + \frac{V_{ice}}{\delta_{ref}}\frac{d\delta_i}{dt} = \sigma_V + \sigma_O \qquad (3)$$

where σ_V and σ_O denote variations of V_{iso} caused by changes in ice volume and mean-ice δ^{18}O, respectively.

III.3 Results

The simulated history of NAIS volume over the last glacial-interglacial cycle is shown in Figure III-1a. The ice sheet approached its maximum volume at 25 kyr BP and then exhibited only small variations until 19 kyr BP, when the deglaciation started. At the LGM the volume was 29.3×10^{15} m^3, corresponding to ~74 m of eustatic sea-level change. The northern ice margin remained always at 72ºN; the southern margin reached 43.5ºN at the LGM. The maximum ice thickness was ~3500 m, of which ~ 3000 m lay above the present-day sea level. In our simulation the deglaciation was not complete and an ice volume equivalent to 3 m of sea level was still left at present day.

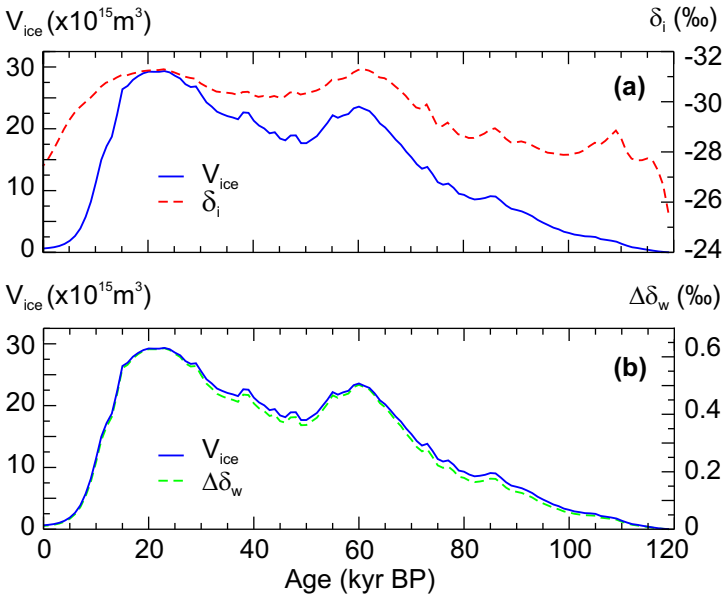

Figure III-1. (a) Simulated volume history (solid) and mean ice δ^{18}O variations (dashed) for NAIS over the last glacial-interglacial cycle. (b) Simulated NAIS volume history (solid) and induced seawater isotopic enrichment $\Delta\delta_w$ (dashed).

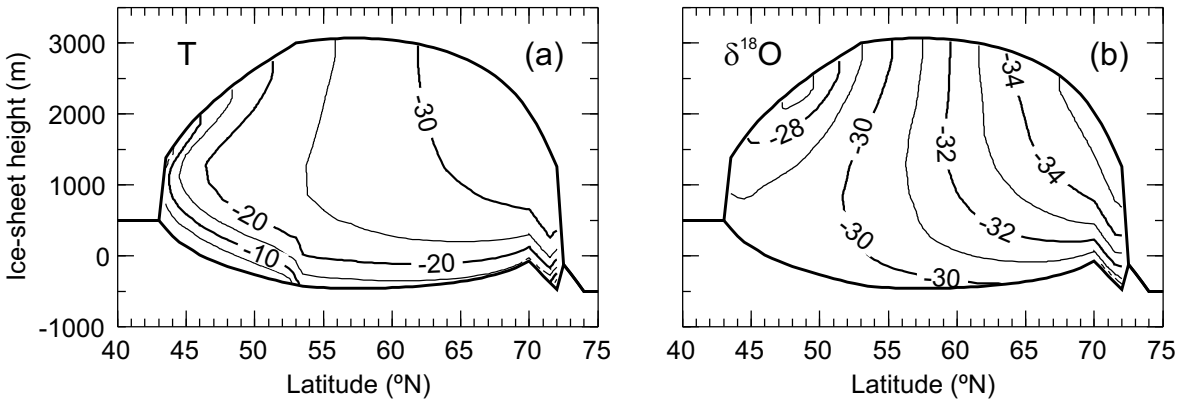

Figure III-2. Distributions of (a) ice temperature and (b) δ^{18}O of the modeled NAIS along the flow line at the LGM.

At the LGM most of the ice had temperatures between –33º and –15º (Figure III-2a). Values above –15ºC were found at the base and at the southern margin of the ice sheet. About one third of the ice-sheet base was at the pressure melting point. The values for ice δ^{18}O ranged approximately between –35 and –27‰ (Figure III-2b). Most of the basal ice had δ^{18}O values close to –30‰.

The time evolution of δ_i (Figure III-1a) showed a rapid decrease during glacial inception (from ~ –24‰ to –29‰ within 10 kyr) and then variations of up to 3‰ in amplitude (approximately between –28‰ and –31‰), modulated by changing ice volume. The lightest values (–31.3‰) were reached at 60 kyr BP and at the LGM, concurrent with maximum values of ice volume. After the LGM, the ice-mean δ^{18}O started to increase, initially rather slowly (by only 0.3‰ until 15 kyr BP), and more rapidly afterwards. The ice left at the end of the simulation had a mean δ^{18}O of ~ –27‰.

Changes of δ_w induced by NAIS-volume variations amounted up to 0.63‰ at the LGM (Figure III-1b). When scaled to fit the maximum and minimum values, $\Delta\delta_w$ and V_{ice} were in very good agreement: there was no time lag[1], and only small differences in magnitude were visible, mainly during ice build-up phases. As a consequence, the modeled ice volume V_{ice} and isotopic volume V_{iso} were also in very good agreement (Figure III-3a). Again there was no obvious time lag and only a slight underestimation of V_{ice} by V_{iso} could be seen, especially during ice-sheet growth intervals. The differences between V_{ice} and V_{iso} (Figure III-3b) were up to 0.8×10^{15} m^3, with the largest values in the intervals 100 to 70 kyr

[1] The phase concept is defined for liniar systems, and, hence, not applicable in a straightforward way to the nonliniar ice sheet-ocean system. Our approach in studying phase differences between the modeled ice-volume variations and the ocean response is to compare the midpoints of transitions in the two signals [cf., e.g., Raymo, 1997], given by local extremes in the first time derivatives (see equation 3 and Figure III-4).

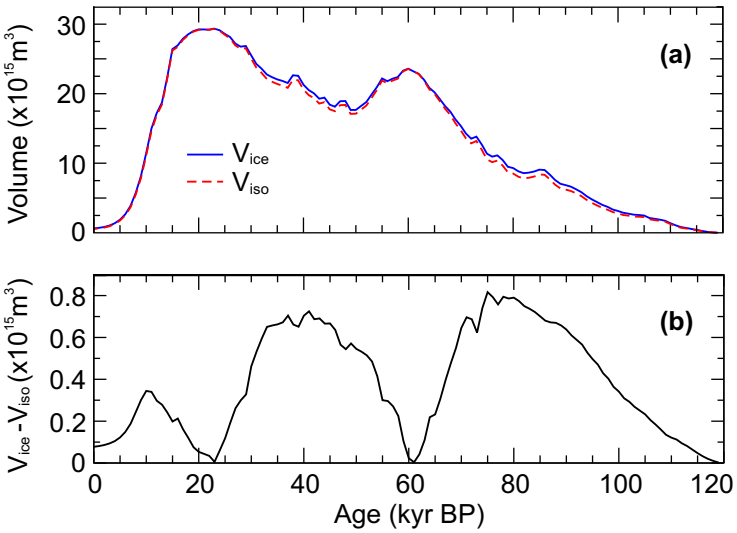

Figure III-3. (a) Modeled ice volume V_{ice} (blue solid) and isotopic volume V_{iso} (red dashed). (b) Difference between V_{ice} and V_{iso}.

BP and 50 to 30 kyr BP. These differences represent generally less than 10% of V_{ice}. Somewhat larger errors, of 10-18%, occurred during the first 10 kyr of the glacial cycle (glacial inception) and in the second part of the deglaciation. When comparing the two terms contributing to the rate of change of V_{iso} (Equation 3 and Figure III-4), the contribution due to variation in V_{ice} (σ_V) was generally at least one order of magnitude larger than the contribution caused by changes in mean-ice δ^{18}O (σ_O). Therefore, V_{ice} variations dominated the temporal evolution of V_{iso}, with regard to both timing and amplitude.

III.4 Discussion

Model parameters were chosen to match the NAIS contribution (S_i = 74 m) to the LGM eustatic sea-level drop (S_g = 126 m) of *Peltier* [2004]. The thickness and southern extent of the NAIS at the LGM, as known from reconstructions [e.g., *Dyke et al.*, 2002], were reasonably simulated. Also, the modeled history of NAIS volume over the last glacial-interglacial cycle (Figure III-1a) closely resembles the simulation with a three-dimensional ice-sheet model by *Marshall et al.* [2002]. The amount of ice left at present day is small compared to glacial-to-interglacial ice-volume change and therefore does not affect our conclusions.

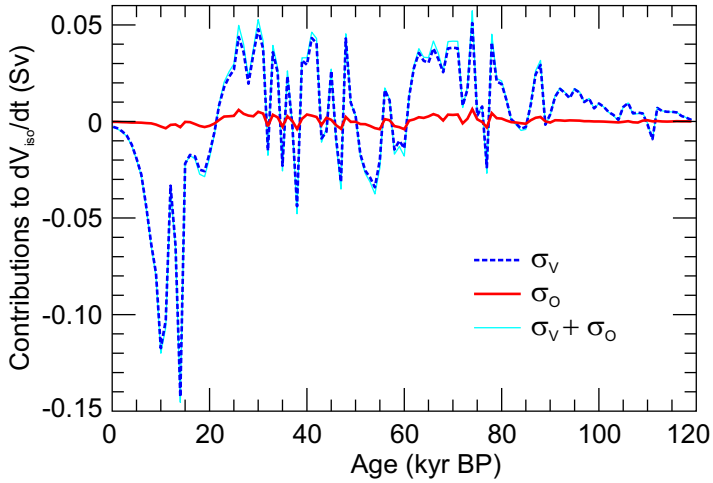

Figure III-4. Rate of change of V_{iso} (thin) and its components: σ_V, denoting variations caused by changes in ice volume (thick dashed) and σ_O, corresponding to variations due to mean-ice δ^{18}O (thick solid).

Due to only diagnostic computation in the zonal direction, no distinction was made between the Laurentide and Cordilleran ice sheets, and presence of ice in Alaska was implied. Since the northern margin of the simulated ice sheet remained at 72°N, the Innuitian ice sheet was not represented. However, as we were mainly interested in the total volume and mean oxygen-isotopic composition of the NAIS, the model served our purpose very well, and its shortcomings were compensated by computational efficiency.

The parameterization of δ^{18}O of precipitation is critical for the results of the present study. Our parameterization resulted in LGM values for δ^{18}O of basal ice (–30‰) and for snow accumulating at the southern ice-sheet margin (–14‰ to –18‰) consistent with the available information on the Laurentide ice from subglacial calcite and early diagenetic concretions from glacio-lacustrine deposits [*Hillaire-Marcel et al.*, 1979; *Hillaire-Marcel and Causse*, 1989]. However, we note that the mean-ice δ^{18}O computed along the flow line does not represent the mean for the entire ice sheet, because for every latitude, accumulated snow is isotopically more depleted at ice divide than at any other point. This may compensate in the $\Delta\delta_w$ calculation (equation 1) for the possible underestimation of S_i at the LGM by choosing the *Peltier* [2004] value of 74 m [e.g., *Marshall et al.*, 2002]. Using a different value for S_g, e.g., 130 m [*Lambeck et al.*, 2002], would change $\Delta\delta_w$ by only 0.001‰. With these considerations, our computed $\Delta\delta_w$ of 0.63‰ is likely a maximum estimation of the NAIS contribution to the seawater isotopic enrichment at the LGM.

The first-order upwind scheme that we used for advection in the ice-sheet model is known to introduce artificial diffusion, which might influence the simulated distributions of temperature and $\delta^{18}O$ in Figure III-2. The few other studies involving oxygen-isotope distribution in ice employ three-dimensional thermomechanical models combined with high-resolution semi-Lagrangian tracer transport schemes, because they aim at a detailed reconstruction of $\delta^{18}O$ distribution of the ice-sheets still present: Greenland [*Tarasov and Peltier*, 2003; *Clarke et al.*, 2005; *Lhomme et al.*, 2005] and Antarctica [*Lhomme*, 2004]. Such models are validated by comparing modeled and observed profiles at ice-coring sites. In contrast, little information is available on the isotopic composition of the NAIS, and the results of our ice-sheet model are in reasonable agreement with it. Moreover, a detailed simulation of the NAIS isotopic distribution is beyond the purpose of the present study, and our main interest is to estimate changes in the mean $\delta^{18}O$ of the ice sheet.

As *MR* have shown using simple zero-dimensional models, the nonequilibrium isotopic composition of the ice sheet has theoretically the potential to decouple real and apparent (isotopic) ice-volume signals. If δ_{ref} is choosen to be equal to the LGM value of δ_i, then V_{iso} fits V_{ice} at the LGM, but underestimates it at any other moment of the glacial cycle. The misrepresentation of V_{ice} by V_{iso} is determined by the departure of δ_i from δ_{ref} (cf. equation 2), which explains why the largest errors (here 10-18%) occurred in the beginning and at the end of the glacial period (cf. Figure III-1a). This results in apparently slower ice build-up and faster decay, in agreement with some of the *MR* simulations. According to equation (3), during periods of constant V_{ice}, when $\sigma_V = 0$, V_{iso} may still change due to $\sigma_O \neq 0$, which leads to phase differences between V_{ice} and V_{iso}. As a consequence, in *MR*'s "best cases" V_{iso} still lags V_{ice} by 500-1000 years and slightly misrepresents V_{ice}. In our simulation these differences were even smaller. Two factors are responsible for this result. One is the higher variability of V_{ice}, induced by the NGRIP forcing and amplified by the thermomechanical coupling. There were no long intervals of nearly constant ice volume, and generally $\sigma_V \gg \sigma_O$, practically synchronizing V_{iso} with V_{ice}. The second reason is our parameterization for the isotopic composition of snow, which resulted in a contrast of only ~10‰ between δ_i at minimum and maximum volume and, therefore, in a smaller underestimation of V_{ice} by V_{iso}. We consider this good agreement, better then suggested by *MR*, as a valid result, because it is based on (a) a realistic ice-volume history instead of prescribed idealised sinusoidal transitions and (b) a parameterization for snow $\delta^{18}O$ consistent with the current knowledge on the isotopic composition of the Laurentide ice sheet.

III.5 Conclusions

Our 2.5-dimensional thermomechanical ice-sheet model provided essential insight in the oxygen-isotopic composition of the North American Ice Sheet (NAIS). It allowed us to make an estimation of the NAIS contribution to the ocean isotopic enrichment between the Last Glacial Maximum (LGM) and the Holocene, and reassess the time-evolving relationship between ice-volume variations and changes in the oxygen-isotope composition of seawater ($\Delta\delta_w$), first investigated by *Mix and Ruddiman* [1984].

The simulated change of seawater isotopic composition due to the NAIS at the LGM was 0.63‰. We consider this result as a reasonable maximum estimate of NAIS contribution to ocean LGM enrichment. A comparison between NAIS-volume variations and the induced changes in the oxygen isotope composition of the well-mixed ocean showed no time lag between the two signals and only small differences in magnitude, mainly during times of ice-sheet growth.

To completely determine the relationship between global ice-volume variations and $\Delta\delta_w$, the major ice sheets must be simulated in concert. Still, as NAIS has been the largest contributor to $\Delta\delta_w$ during the late Pleistocene, we suggest the nonequilibrium isotopic composition of ice sheets induces no significant time lags between global ice volume and oxygen-isotope composition of a well-mixed ocean, and generally less than 10% differences in magnitude. In future work, the assumed well-mixed ocean will be replaced by a more complex ocean model, in order to investigate the possible decoupling of ice volume and benthic foraminiferal $\delta^{18}\mathrm{O}$ by the ocean mixing time.

References

Chappell, J., and N.J. Shackleton (1986), Oxygen isotopes and sea level, *Nature*, *324*, 137-140.

Clark, P.U., and A.C. Mix (2002), Ice sheets and sea level of the Last Glacial Maximum, *Quat. Sci. Rev.*, *21*, 1-7.

Clarke, G.K.C., N. Lhomme, and S.J. Marshall (2005), Tracer transport in the Greenland Ice Sheet: three-dimensional isotopic stratigraphy, *Quat. Sci. Rev.*, *24*, 155-171.

Clarke, G.K.C., and S.J. Marshall (2002), Isotopic balance of the Greenland Ice Sheet: modelled concentrations of water isotopes from 30,000 BP to present, *Quat. Sci. Rev.*, *21*, 419-430.

Crucifix, M., and A. Berger (2002), Simulation of ocean-ice sheet interactions during the last deglaciation, *Paleoceanography*, *17* (4), 1054, 10.1029/2001PA000702.

Duplessy, J.-C., L. Labeyrie, and C. Waelbroeck (2002), Constraints on the ocean oxygen isotopic enrichment between the Last Glacial Maximum and the Holocene: Paleoceanographic implications, *Quat. Sci. Rev.*, *21*, 315-330.

Dyke, A.S., J.T. Andrews, P.U. Clark, J.H. England, G.H. Miller, J. Shaw, and J.J. Veillette (2002), The Laurentide and Innuitian ice sheets during the Last Glacial Maximum, *Quat. Sci. Rev.*, *21*, 9-31.

Gallée, H., J.P. van Ypersele, T. Fichefet, C. Tricot, and A. Berger (1992), Simulation of the last glacial cycle by a coupled, sectorially averaged climate-ice sheet model. Part II: Response to insolation and CO_2 variations, *J. Geophys. Res.*, *97*, 15713-15740.

Hillaire-Marcel, C., and C. Causse (1989), The late Pleistocene Laurentide glacier: Th/U dating of its major fluctuations and $\delta^{18}O$ range of the ice, *Quat. Res.*, *32*, 125-138.

Hillaire-Marcel, C., J.M. Soucy, and A. Cailleux (1979), Analyse isotopique deconcretions sous-glaciaires de l'inlandsis laurentidien en teneur en oxygene-18 de la glace, *Can. J. Earth Sci.*, *16* (7), 1494-1498.

Johnsen, S.J., and J. White (1989), The origin of Arctic precipitation under present and glacial conditions, *Tellus*, *41B*, 452-468.

Jouzel, J., R.D. Koster, R.J. Suozzo, and G.L. Russell (1994), Stable water isotope behavior during the last glacial maximum: A general circulation model analysis, *J. Geophys. Res.*, *99* (D12), 25791-25801.

Lambeck, K., Y. Yokoyama, and A. Purcell (2002), Into and out of the Last Glacial Maximum: sea-level change during Oxygen Isotope Stages 3 and 2, *Quat. Sci. Rev.*, *21*, 343-360.

Lhomme, N. (2004), Modelling water isotopes in polar ice sheets, PhD thesis, Univ. of British Columbia, Vancouver.

Lhomme, N., G.K.C. Clarke, and S.J. Marshall (2005), Tracer transport in the Greenland ice sheet: constraints on ice core and glacial history, *Quat. Sci. Rev.*, *24* (1-2), 173-194.

Marshall, S.J., T.S. James, and G.K.C. Clarke (2002), North American Ice Sheet reconstructions at the Last Glacial Maximum, *Quat. Sci. Rev.*, *21*, 175-192.

Marshall, S.J., L. Tarasov, G.K.C. Clarke, and W.R. Peltier (2000), Glaciological reconstruction of the Laurentide Ice Sheet: physical processes and modelling challenges, *Can. J. Earth Sci.*, *37*, 769-793.

Mix, A.C., and W.F. Ruddiman (1984), Oxygen-isotope analyses and Pleistocene ice volumes, *Quat. Res.*, *21*, 1-20.

North Greenland Ice Core Project members (2004), High-resolution record of Northern Hemisphere climate extending into the last interglacial period, *Nature*, *431*, 147-151.

Oerlemans, J. (1982), Glacial cycles and ice-sheet modelling, *Clim. Change*, *4*, 353-374.

Payne, A.J. (1995), Limit cycles in the basal thermal regime of ice sheets, *J. Geophys. Res.*, *B100*, 4249-4263.

Peltier, W.R. (1994), Ice age paleotopography, *Science*, *265*, 195-201.

Peltier, W.R. (2004), Global glacial isostasy and the surface of the ice-age Earth: the ICE-5G (VM2) model and GRACE, *Ann. Rev. Earth Plan. Sci.*, *32*, 111-149.

Raymo, M.E. (1997), The timing of major climate terminations, *Paleoceanogr.*, *12* (4), 577-585.

Romanova, V., M. Prange, and G. Lohmann (2004), Stability of the thermohaline circulation and its dependence on the background hydrological cycle, *Clim. Dyn.*, *22*, 527-538.

Tarasov, L., and W.R. Peltier (2003), Greenland glacial history, borehole constraints, and Eemian extent, *J. Geophys. Res.*, *108* (B3), Art. No. 2143.

Waelbroeck, C., L. Labeyrie, E. Michel, J.-C. Duplessy, J.F. McManus, K. Lambeck, E. Balbon, and M. Labracherie (2002), Sea-level and deep water temperature changes derived from benthic foraminifera isotopic records, *Quat. Sci. Rev.*, *21*, 295-305.

Chapter IV

PHASE RELATIONSHIP BETWEEN ICE VOLUME AND OXYGEN-ISOTOPE RATIOS IN SEAWATER AND CALCITE DURING THE LAST GLACIAL CYCLE: ROLE OF OCEAN CIRCULATION

Adriana Sima and André Paul

Department of Geosciences, Bremen University, D-28334 Bremen, Germany

Abstract

We used combined ice-sheet and ocean modeling to investigate qualitatively the phase relationship between ice-volume variations and the induced changes in the isotopic composition (δ^{18}O) of seawater (δ_w) and foraminiferal calcite (δ_c) during the last glacial cycle. First, we simulated the mean isotopic composition of the North American Ice Sheet (NAIS) during the past 120,000 years with a 2.5-dimensional thermomechanical ice-sheet model including ice δ^{18}O as a passive tracer. This allowed us to estimate the changes in the magnitude and δ^{18}O of the water flux exchanged between the NAIS and the Atlantic Ocean. Then, the water flux was used to force a zonally-averaged model of the Atlantic Ocean, as part of a coupled climate model of reduced complexity. The resulting changes of mean-ocean δ_w, as well as δ_w and δ_c variations at different locations in the ocean were compared to the modeled NAIS ice volume, in order to investigate the possible phase differences due to ocean circulation. The simulated NAIS volume variations and the induced mean-ocean δ^{18}O changes over the past 120,000 years indicated no significant time lag. However, locally the time lag in the ocean could reach up to 2000 years during glaciation, depending on the rate of deep-water formation. In contrast, the deglaciation signal was found to be practically simultaneous.

To be submitted to **Paleoceanography**

IV.1 Introduction

The oxygen-isotopic composition $\delta^{18}O$ of foraminiferal calcite (δ_c), which mainly reflects variations in ice volume and seawater temperature, represents an important index of global climate change. In particular, based on the work of [*Shackleton*, 1967], δ_c of benthic foraminifera measured in deep-sea sediments has been considered for a long time to faithfully record global ice-volume variations and the equivalent sea-level changes during the last ~1 million years. Hence, for this period, benthic δ_c provided not only climatic, but also stratigraphic information, and formed the basis for the marine isotope stage stratigraphic system [*Imbrie et al.*, 1984; *Martinson et al.*, 1987].

However, while recent estimations of the of ice-volume effect on the seawater isotopic enrichment at the Last Glacial Maximum (LGM) yield approximately 1‰ [e.g., *Adkins et al.*, 2002; *Schrag et al.*, 2002; *Malone et al.*, 2004], an increasing number of benthic δ_c records show variations of up to 2‰ amplitude [e.g., *Shackleton*, 1977; *Duplessy et al.*, 1980; *Labeyrie et al.*, 1987; *McManus et al.*, 1999; *Shackleton et al.*, 2000], thus indicating a significant effect of seawater temperature.

Separating the individual contributions of temperature and ice volume to the total change in foraminiferal $\delta^{18}O$ is an important problem in paleoceanography, which needs to be solved in order to correctly interpret the marine records in terms of past climate change. Also, accurate dating of climatic events is critical in developing and testing theories on mechanisms of past climate change, especially with respect to lead/lag relationships between various key parameters as ice volume, insolation, temperature, CO2 etc.
For the last glacial period, global ice-volume variations can be reconstructed from direct evidence for paleo-sea levels, such as shorelines and coral reefs. When compared to such sea-level estimates [e.g., *Lambeck and Chappell*, 2001; *Lambeck et al.*, 2002], the reconstructions based on foraminiferal $\delta^{18}O$ do not match. This mismatch has been long recognised, and interpreted as mainly due to changes in deep-water temperature [*Chappell and Shackleton*, 1986; *Shackleton*, 1987]. However, when attempting to disentangle the contributions of ice volume and temperature to the total change in δ_c, other factors must be considered as well.

One factor is the nonequilibrium isotopic composition of ice sheets, which can decouple the isotopic response of the ocean from the ice-volume signal. *Mix and Ruddiman* [1984] attempted to quantify this effect, based on experiments with conceptual models simulating the ocean isotopic response to hypothetical transitions of ice growth and ice decay. They

concluded that, as an effect of changing δ_i only, foraminiferal $\delta^{18}O$ might lag the ice volume by 1 to 3 kyr and misrepresent the amplitude of ice-volume variations by up to 30%.

Another factor is the ocean circulation. In reality, the effect of freshwater fluxes associated with ice-volume changes is not instantly transmitted from the source to the entire ocean. Between a change of the freshwater balance and its recording in foraminifera at a specific location in the ocean, there must be a lag depending on the distance to the signal source and the ocean circulation. This lag might contribute to the mismatch between sea-level curves derived from calcite $\delta^{18}O$ and those inferred from direct evidence.

Also, a detailed analysis of benthic records from the deep Atlantic and Pacific Oceans reveal that the benthic δ_c variations are far from being simultaneous, and a ~ 4,000-year lead of the Atlantic over the Pacific Ocean exists across the last deglaciation [*Skinner and Shackleton*, 2005]. Such a large discrepancy is interpreted as mainly resulting from a late increase in deep-water temperature at the Pacific site, but the delay in transmitting from one ocean to the other the $\delta^{18}O$ signal associated to ice-volume variations might also play a role.

To study the isotopic response of the ocean to ice-volume variations, we developed a realistic and yet computationally-efficient ice-sheet model including oxygen-isotope transport and used it to simulate the evolution of the volume and mean isotopic composition of the North American Ice Sheet (NAIS) during the last glacial cycle, i.e., the past 120 thousand years (kyr).

In a first step, we assumed a well-mixed ocean. This allowed a re-examination of the possible phase and amplitude error in reconstructing ice-volume variations from changes in seawater $\delta^{18}O$ by neglecting the effect of changing mean-ice $\delta^{18}O$ (δ_i) and employing a linear relationship (see Chapter III). No significant phase difference was found between the ice-volume signal and the induced mean isotopic enrichment of the ocean, and amplitude misrepresentation was generally less than 10%.

In the present study, we replaced the well-mixed ocean by an ocean model with explicit spatial resolution in the meridional (north-south) and vertical directions. On a qualitative basis, we could thus test the hypothesis of the importance of the ocean circulation for the relationship between ice-volume variations and the changes in the isotopic composition of seawater and calcite induced at different locations and depths in the ocean.

IV.2 Methods

IV.2.1 Ice-sheet model

The 2.5-dimensional thermomechanical ice-sheet model combines the computation along a north-south flow line after *Payne* [1995] with an equilibrium profile in the zonal direction following *Gallée et al.* [1992] and *Crucifix and Berger* [2002]. Our model simulates the North-American Ice Sheet (NAIS), the main contributor to ice-volume variations during the late Pleistocene [cf. *CLIMAP Project members*, 1981; *Peltier*, 1994; 2004]

IV.2.1.1 Model description

The evolution of ice-sheet thickness *H* along the flow line as a function of latitude φ is given by the vertically integrated continuity equation [cf. *Gallée et al.*, 1992, equation 1 therein]:

$$\frac{\partial H}{\partial t} = M - \frac{1}{a\cos\varphi}\frac{\partial}{\partial\varphi}\left(\overline{u_y}H\cos\varphi\right) - D_\lambda - S,$$

where *M* is the local annual mass balance at ice surface, *a* the radius of the Earth, $\bar{u}$ is the vertically-averaged horizontal velocity, D_λ represents the lateral discharge of ice mass and *S* the melt rate at the ice-sheet base (see Section II.2 for a detailed model description).
In the east-west direction a perfectly-plastic profile symmetric to the ice-sheet crest is assumed and the zonal ice-mass discharge is parameterized as [*Gallée et al.*, 1992; *Crucifix and Berger*, 2002]:

$$D_\lambda = -\frac{1}{\left(a\cos\varphi\right)^2} DH\frac{\partial^2 s}{\partial\lambda^2} = DH\frac{s}{L^2}$$

where *s* is the ice-surface elevation above the present-day sea level and $D = 8\bar{A}\frac{(\rho g)^n}{a^2}\left|\frac{\partial s}{\partial\varphi}\right|^{n-1}$, with ρ_i the ice density and *g* the gravitational acceleration. The vertically integrated flow parameter $\bar{A}$ is in our case temperature-dependent. The longitudinal extent of the ice sheet *L* depends on the ice surface elevation as follows: $L = s^2/\mu$, with $\mu = 2\tau_0/\rho_i g$, where τ_0 is the prescribed, constant bottom stress, derived from the *CLIMAP* [1981] reconstruction [*Crucifix and Berger*, 2002]. The lateral discharge is evenly distributed in the vertical: $d_\lambda(z) = D_\lambda / H$.

In the meridional and vertical directions the computation follows *Payne* [1995], with two main differences: (a) an empirical „flow enhancement“ factor *E* is introduced into Glen's flow law to account for the effects of crystal anisotropy and impurities on bulk ice deformation [cf. *Tarasov and Peltier*, 1999] and (b) additional terms corresponding to the zonal ice-mass discharge D_λ are included in the equations for vertical velocity and for ice temperature evolution. The initial topography is taken from *Clark and Pollard* [1998] and bedrock adjustment is computed from a local lithosphere–relaxed asthenosphere model [*Le Meur and Huybrechts*, 1996] with a characteristic time constant of 4 kyr.

The equation for temperature evolution contains vertical diffusion, horizontal and vertical advection and frictional heat generation terms. When the temperature at ice-sheet base reaches the pressure melting point, the melt rate *S* is calculated. Also, in this case, enhanced flow in the zonal direction is simulated by a gradual decrease of the bottom stress τ_0 with a rate of 0.2 Pa/yr, until a minimum value of 10,000 Pa is reached. This parameterization is based on the treatment of Heinrich events by *Crucifix and Berger* [2002] and results in an increase of the lateral discharge [cf. *Crucifix and Berger*, 2002, Appendix B therein].

Ice-volume computation follows *Crucifix and Berger* [2002, Appendix A therein]. The water flux exchanged between ice-sheet and ocean is:

$$F_w = -\frac{\rho_i}{\rho_w}\frac{dV_i}{dt},$$

defined as positive when the ice volume V_i decreases and meltwater flows to the ocean, and negative when water is evaporated from the ocean and accumulated in the ice sheet.

IV.2.1.2 Tracer treatment

The ratio *R* of oxygen isotopes ^{18}O and ^{16}O is expressed as the fractional deviation from the isotopic ratio of the Vienna Standard Mean Ocean Water [V-SMOW, *Gonfiantini*, 1978]:

$$\delta^{18}\mathrm{O} = \left(R / R_{V-SMOW} - 1\right) \times 1000‰$$

Ice-δ^{18}O is introduced in the model as a passive tracer. There is no diffusion for δ^{18}O and its transport through ice relies on the same advection scheme as temperature. Using δ^{18}O directly rather than mass ratio introduces a negligible conservation error.

The model only computes the two-dimensional distribution of δ along the flow line, as it does for temperature. As information about the distribution of δ in the East-West direction is missing in the model, we use for the mean isotopic composition of the whole ice sheet

(δ_i) the mean value computed along the flow line. Because the snow accumulated at ice divide is isotopically the most depleted, the resulted δ_i is lighter than derived by any other approach, and the corresponding seawater enrichment is the maximum limit for the NAIS contribution. The δ^{18}O of the water flux exchanged between the ice sheet and the ocean is given at every moment by the mean δ^{18}O of the ice sheet.

IV.2.1.3 Numerical solution

The glacial cycle integration extends from 120 kyr BP to the present. The timestep is 1 year, except for periods of intense melting at the ice-sheet base or high ablation at ice surface, when it is reduced to 0.05 year. The latitudinal-grid resolution is 0.5°. The vertical grid is stretched and has 12 uneven layers, with thicknesses decreasing towards the ice-sheet base. Flux boundary conditions are applied at the ice-sheet surface and base. We use a first-order upwind scheme for advection and a second-order scheme for heat diffusion.

IV.2.1.4 Climate forcing

The local annual mass balance *M* on the ice surface is derived using the equilibrium-line concept [*Oerlemans*, 1982]:

$$M = \min\left[M_{\max}, M_{\max}\left(s - h_{equ}\right)/h_{\max} \right] \text{ m yr}^{-1}$$

where the equilibrium-line elevation h_{equ} is a function of surface temperature T_a and elevation:

$$h_{equ} = s + \left(T_a - T_{equ}\right)/\beta$$

with $\beta = 0.0065$°C m^{-1} the atmospheric lapse rate and T_{equ} = –15° the equilibrium-line temperature. Parameters M_{max} and h_{max} have similar values to those used by *Pollard* [1983]: 0.55 m yr^{-1} and 1500 m, respectively.

The surface-temperature parameterization follows the glacial index method of *Marshall et al* [2000]. The glacial index *I*(*t*) is computed using the NGRIP δ^{18}O record [*North Greenland Ice Core Project members*, 2004], and the latitudinal distributions of surface temperature at present day and at the LGM are derived by zonally averaging the output of the atmospheric general circulation model ECHAM3/T42 [*Romanova et al.*, 2004, Figure 1c therein] over the North-American continent.

Snow $\delta^{18}O$ is parameterized as a function of mean annual surface temperature, similar to the relationship by *Johnsen and White* [1989] for present-day Greenland:

$$\delta_s = -13.7 + \alpha(t) T_a$$

with the time-dependent slope $\alpha(t)$ computed as:

$$\alpha(t) = \alpha_0 + I(t)\left[\alpha_{LGM} - \alpha_0\right]$$

where $\alpha_0 = 0.6$ and $\alpha_{LGM} = 0.66$ are the slopes determined by *Jouzel et al.* [1994] for the NAIS domain for present day and the LGM, respectively.

IV.2.2 Climate model

The HANSE climate model of reduced complexity consists of three components: atmosphere, sea ice and ocean [*Paul and Schulz*, 2002].

IV.2.2.1 Atmosphere

In the atmospheric component, the atmospheric heat and moisture capacities as well as the land heat capacity are assumed to be zero. The atmospheric zonal heat transport is taken to be infinitely rapid. Thus, the atmospheric heat balance at latitude φ reads:

$$0 = -\left(1 - f_l\right) K \left(T_a - T_s\right) - \left(A + B T_a\right),$$

where f_l is the land fraction of the latitude belt, $F = K\left(T_a - T_s\right)$ is the surface heat flux (positive downward), and

$$A = \mathrm{div}\, H_a - R_a^{SW} + A_0,$$

contains the heat transport divergence div H_a, the shortwave radiation balance R_a^{SW}, and the temperature-insensitive part of the longwave radiation balance A_0. Furthermore, K = 40 W m^{-2} K^{-1} is the air-sea heat exchange coefficient, T_a the atmospheric temperature and T_s the sea-surface temperature.

The atmospheric energy balance can be solved for the atmospheric temperature,

$$T_a = \frac{\left(1 - f_1\right) K T_s - A}{\left(1 - f_1\right) K + B},$$

which in turn can be inserted into the surface heat flux equation:

$$F = \frac{KB}{(1-f_1)K + B}\left(-A/B - T_s\right).$$

The term $KB/\lfloor(1-f_1)K+B\rfloor$ can be thought of as an effective thermal damping, and $-A/B$ as an effective restoring temperature. The effective thermal damping is weak and varies between 5 W m^{-2} K^{-1} in the Northern Hemisphere and 2 W m^{-2} K^{-1} south of 30°S. The land fraction f_l is 1/2 in the Northern Hemisphere, 1/3 between 30°S and the Equator, and 0 south of 30°S. The equilibrium surface freshwater flux corresponds to "shape-2 forcing" by *Winton* [1997], multiplied by a factor of 1.5, and the atmospheric heat transport divergence is fixed [cf. *Paul and Schulz*, 2002, Figure 1A therein]. In computing the shortwave radiation balance R_a^{SW}, the planetary albedo parameterization of *Graves et al.* [1993] is used. The planetary albedo is enhanced by 7% in the presence of sea ice. The zonal component of the zonally averaged global annual mean wind stress is prescribed as a function of latitude accorcing to the NCEP/NCAR re-analysis data [*Kalnay et al.*, 1996].

IV.2.2.2 Sea ice

Any subfreezing water in the uppermost model layer is immediately heated to the local freezing point with a corresponding increase in salinity [*Large et al.*, 1994]. The associated sea ice (more precisely, the negative heat stored in sea ice) Q_{ice} is accumulated locally and advected equatorward. The sea ice advection velocities are based on *Harvey* [1988]. In the Northern Hemisphere, a southward velocity of 0.5 cm s^{-1} is prescribed south of 70°N, with a linear decrease to 0.05 cm s^{-1} at 80°N. Similarly, in the Southern Hemisphere, a northward velocity of 3.0 cm s^{-1} is prescribed north of 60°S, with a linear decrease to 1.0 cm s^{-1} at 70°S. If sufficient heat is supplied, the sea ice is melted, and a corresponding decrease in salinity occurs.

To include the insulating effect of sea ice, the sea-ice surface temperature T_s is calculated from the balance of the conductive heat flux through the ice and the heat flux at the air-sea ice interface:

$$\frac{k_{ice}}{h_{ice}}\left(T_s - T_f\right) = K\left(T_a - T_s\right),$$

where k_{ice} = 2.16 W m^{-1} K^{-1} is the sea-ice conductivity, h_{ice} the sea-ice thickness and T_f the local freezing point. The resulting formula is similar to equation (13) of *Lohmann and Gerdes* [1998]:

$$T_s = \frac{k_{ice} T_f + K h_{ice} T_a}{k_{ice} + K h_{ice}} .$$

The sea-ice thickness h_{ice} is diagnosed from the negative heat stored in sea ice Q_{ice} as follows:

$$h_{ice} = -\frac{Q_{ice}}{\rho_{ice} L_f} ,$$

where ρ_{ice} = 905 kg m^{-3} is the sea-ice density and L_{f} the latent heat of fusion. The surface freshwater flux is directly added to the uppermost model layer and does not influence sea-ice growth.

IV.2.2.3 Ocean

The oceanic component is closely related to the two-dimensional ocean model of *Wright and Stocker* [1992]. Only the Atlantic Ocean is considered, which extends from 80°S to 90°N. The ocean width varies with latitude, and there is an idealized bottom topography with a maximum depth of 5000 m. In the Southern Ocean, between 60° and 50°S, a 2157 m-deep channel is included in which the zonal pressure gradient is set to zero.

A fully nonlinear equation of state is used [*Mellor*, 1991] and a convection scheme that completely stabilizes the water column after every time step [*Rahmstorf*, 1996]. As compared to *Paul and Schulz* [2002], the parameterization of the zonal density gradient (which is required to compute the zonal pressure gradient) is simplifed and based on *Wright and Stocker* [1991]; furthermore, a virtual salt flux boundary condition as opposed to a real freshwater flux boundary condition is used [cf. *Huang*, 1993].

For the transport of temperature, salinity and $\delta^{18}\mathrm{O}$, an explicit (leap-frog) discretization in time is chosen. The time step is 18.25 days. The spatial discretization of the advection terms follows the QUICK scheme, which has low numerical diffusion and dispersion [*Farrow and Stevens*, 1995]. The meridional resolution is 5° and there are 20 layers in the vertical.

IV.2.3 Paleotemperature equation

We compute the changes in the $\delta^{18}\mathrm{O}$ of carbonate (δ_c) using the paleotemperature equation of *Mulitza et al.* [2003]:

$$T = 14.32 - 4.28(\delta_c - \delta_w) + 0.07(\delta_c - \delta_w)^2$$

where δ_c is converted to ‰ SMOW using ‰ SMOW = ‰ PDB + 0.27‰.

IV.2.4 Experimental setup

The ice-sheet model was run for the past 120 kyr and the water-flux (F_w) timeseries was simulated. This flux was used as forcing for a run of the climate model for the same time interval. As in our climate model only the Atlantic Ocean is represented, F_w had to be scaled with the ratio of the Atlantic and the global ocean volumes (0.36). The water flux was either taken from the ocean (as evaporative flux) or added to it (as meltwater input), always in the latitudinal zone between 40° and 50°N. The climate model was initialized with an equilibrium state obtained under unperturbed surface boundary conditions. The initial oxygen-isotope ratio of seawater was set to zero.

IV.3 Results

While the northern margin of the NAIS remained always at 72ºN, the southern margin advanced and retreated in response to the climatic forcing. During glacial inception the ice-surface elevation rose rapidly up to ~1500 m (not shown). In this period the fresh snow became increasingly depleted, mainly due to the isotopic effect of fractionation with altitude. As a result, δ_i decreased from ~ –24‰ in the beginning to ~ –29‰ after the first 10 kyr (Figure IV-1). During the next 10 kyr the ice volume continued to grow, but mainly by ice extending southward. As the ice sheet reached lower latitudes, isotopically-heavier snow was accumulated, resulting in a ~ 1‰ increase of δ_i.

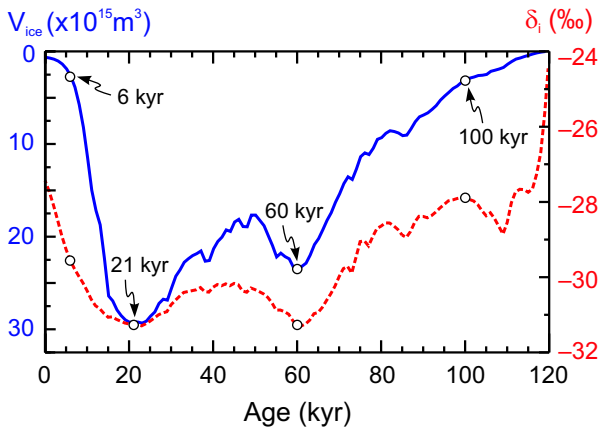

Figure IV-1. Time evolution of the simulated NAIS volume and mean isotopic composition during the last glacial cycle. Details of the ice-sheet profile and distribution along the flow line at the marked moments are presented in Figure IV-2.

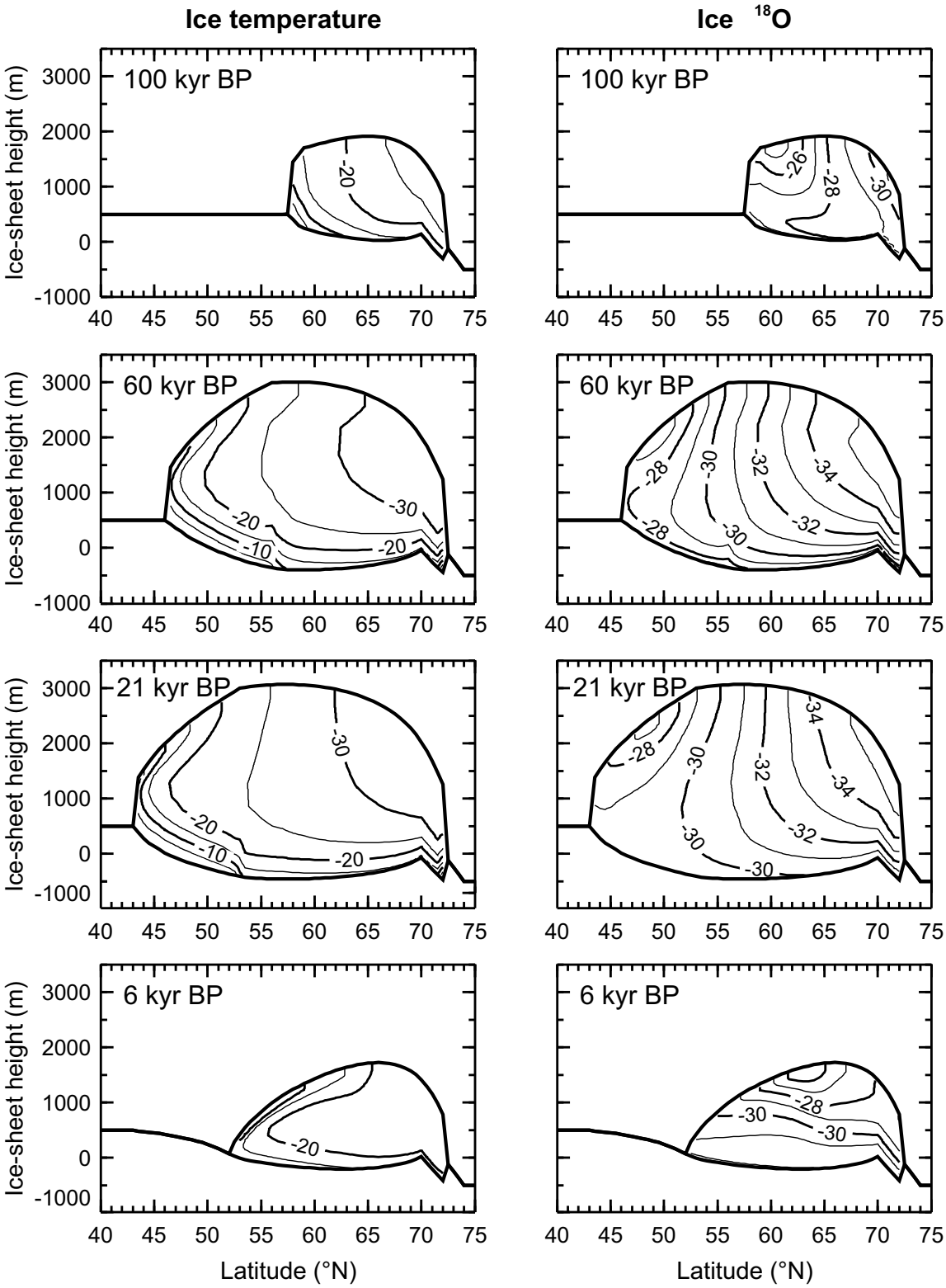

Figure IV-2. Snapshots of the modeled distributions of temperature and $\delta^{18}O$ along the flow line in the NAIS at different moments of the glacial cycle.

The ice-sheet volume kept growing until ~60 kyr BP, then decreased for approximately 10 kyr, then growed again to the LGM value. A similar evolution can be seen for δ_i. At ~ 19 kyr BP the deglaciation began. The warmer and isotopically heavier ice at the southern part of the ice sheet was ablated first, which explains why until ~ 15 kyr BP the decrease in ice volume is associated with only a very small increase (0.3‰) in δ_i. The deglaciation was not quite complete in our simulation, and ice equivalent to ~3 m of eustatic sea level, with a mean isotopic composition of ~ –27‰, was still left at the present day.

The temperature and δ^{18}O distributions along the flow line of the ice sheet experienced a distinct evolution during the glacial cycle (Figure IV-2). At 100 kyr BP, when a local minimum in δ_i occurred, the ice sheet extended to 57ºN and the surface elevation was ~2000 m. The distributions of temperature and δ^{18}O show roughly two regions: the northern half, where ice is cold (between approximately –26 and –20ºC) and isotopically light (–31 to –28‰), and the southern half, warmer (with temperatures up to ~ –5 ºC) and more enriched in ^{18}O (up to –25‰). The ice-sheet base was completely frozen.

At 60 kyr BP, a local maximum in ice volume occurred. In our simulation, the ice-sheet size at this moment differed from that at the LGM by only 3º in latitudinal extent and ~200 m in maximum thickness. The temperature and δ^{18}O distributions at 60 kyr BP and at the LGM were very similar, with most of the values between –33 and –20ºC and between –35 and –30‰ respectively. The warmest (> –20ºC) and isotopically heaviest (–30 to –27‰) ice was concentrated at the southern margin and at the base of the ice-sheet. Approximately one third of the base was at the pressure melting point. At the LGM the NAIS volume was 29.3×10^{15} m^3, equivalent to ~74 m of eustatic sea-level change. The southern ice margin was located at 43ºN, and the maximum thickness was ~3500 m. The mean isotopic composition of the ice sheet was –31.3‰. At 6 kyr BP, close to the (modeled) end of deglaciation, the volume was less than 10% and the maximum thickness was almost half of the LGM values. Strong ablation at the ice surface, especially in the southern part, explains the shape of the ice sheet.

A comparison of the NGRIP δ^{18}O record (Figure IV-3a), used to compute the glacial index employed in the climate forcing, and the water-flux timeseries (Figure IV-3b) reveals that the Dansgaard-Oeschger (DO)-related warmings in the NGRIP record triggerred pulsed freshwater release from the simulated ice sheet. The amplitude of the pulses increased with the amplitude and duration of the transitions in NGRIP and with the ice-sheet volume. In response to the first warming step of the last deglaciation in the Northern-Hemisphere, the Bølling/Allerød, the temperate ice at the southern part of the ice-sheet was ablated first, generating the strong meltwater pulse at ~14 kyr BP. A reduction of the freshwater flux can be seen during the cold Younger-Dryas interval, followed by a second meltwater pulse corresponding to the warm Preboreal.

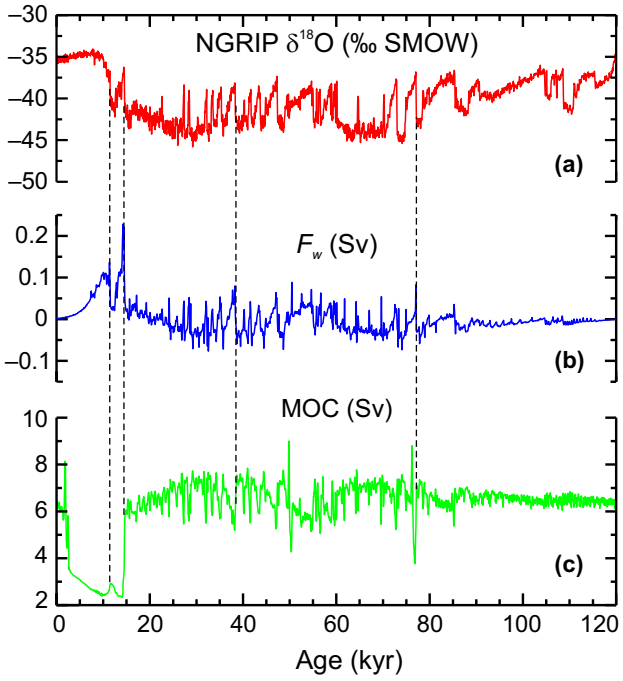

Figure IV-3. (a) The NGRIP $\delta^{18}O$ record [*North Greenland Ice Core Project members*, 2004], used in computing the glacial index employed in the climatic forcing for the ice-sheet model. (b) The timeseries of the water flux F_w exchanged between the NAIS and the Atlantic Ocean, computed by the ice-sheet model. Positive values indicate meltwater flow from the ice sheet to the ocean, and negative values mean water evaporated from the ocean and transfered to the ice sheet. (c) The meridional overturning. Vertical dashed lines help visual correlation of the three timeseria.

In the initial equilibrium state of the ocean model, 6 Sv of North Atlantic Deep Water (NADW) were formed far north of the Greenland-Iceland-Scotland Ridge (GISR, ~60°N), of which 2 Sv were exported across 30°S (Figure IV-4a). The salinity distribution (Figure IV-4b) exhibited the three water masses that are characteristic of the present-day Atlantic Ocean: A tongue of low-salinity Antarctic Intermediate Water (AAIW) that extended from the Southern Ocean to the equator at about 1000 m depth, NADW and Antarctic Bottom Water (AABW). The temperature distribution (Figure IV-4c) was much more homogenous. Below 1000 m, it varied between 1°C for NADW and -1°C for AABW.

With increasing glaciation (120 to 21 kyr BP), the mean salinity (not shown) and seawater $\delta^{18}O$ (Figure IV-5) rose steadily. The maximum of the meridional overturning streamfunction (Figure IV-3c) first increased slightly and then closely followed the imposed freshwater forcing (Figure IV-3b). Peaks of ice-sheet melting (e.g., at 77 and 38 kyr BP) after sudden warmings in the NGRIP record were associated with a slow-down and subsequent recovery of the meridional overturning circulation (MOC).

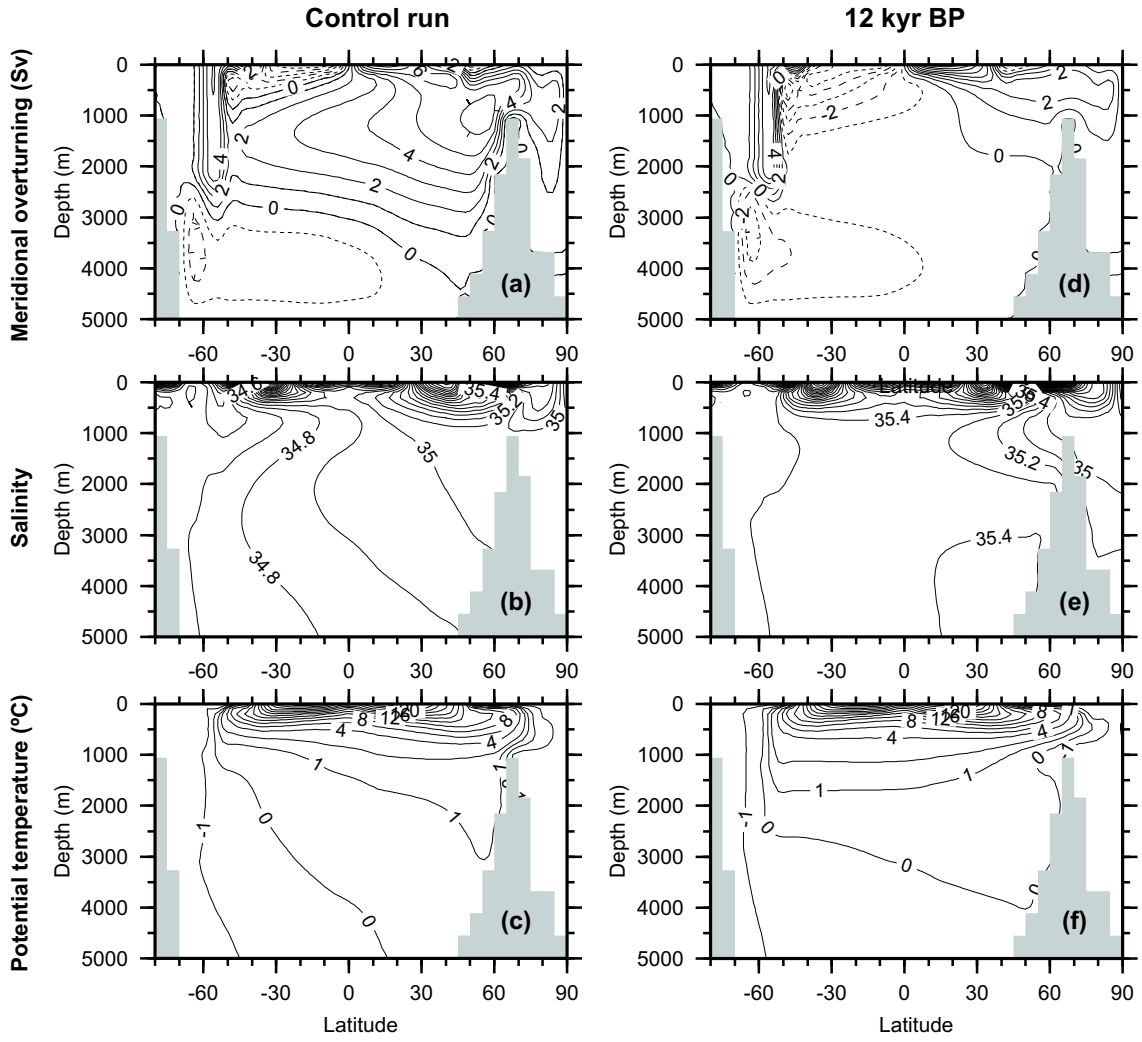

Figure IV-4. Distributions of meridional overturning (upper panels), salinity (middle panels) and potential temperature (lower panels) in the control run (left) and at 12 kyr BP (right).

During the glacial termination (21 kyr BP to present), the mean salinity (not shown) and δ_w (Figure IV-5) decreased rapidly. The overturning (Figure IV-3c) first weakened slightly. At ~14.5 kyr BP, due to the first meltwater pulse, dropped to ~2 Sv and stayed low, recovering only after 3 kyr BP. Hence at 12 kyr BP, no more NADW was formed (Figure IV-4d); it was entirely replaced by AABW. Accordingly, the deep ocean below 2000 m cooled by about 1°C (Figure IV-4f). In the North Atlantic Ocean, there was a shallow overtuning cell that was driven by sea-ice formation and brine relase and left its imprint on the salinity distribution (Figure IV-4e).

The mean seawater $\delta^{18}O$ very closely matched the NAIS volume for the whole glacial cycle (Figure IV-5). The isotopic enrichment induced by the NAIS at the LGM was 0.65‰.

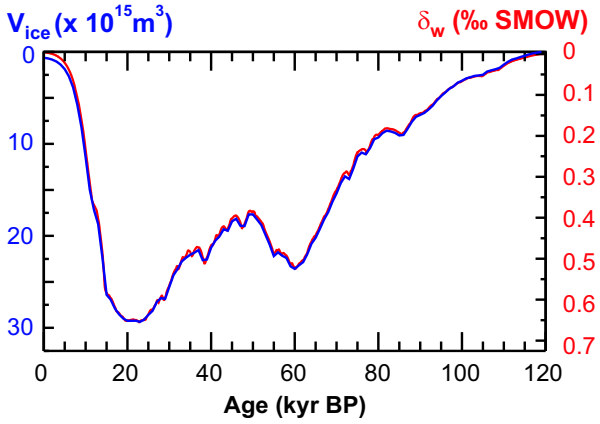

Figure IV-5. Simulated time evolutions of the NAIS volume and the induced changes in the mean-seawater $\delta^{18}O$, scaled to fit the values at the LGM.

The spatial distribution of the δ_w anomaly was rather homogenous most of the time (not shown). Only during the glacial termination, strong gradients occured because the deep ocean was still enriched in ^{18}O but isotopically light meltwater was added at the surface (Figure IV-6a). The δ_c anomaly reflected the cooling of the deep water and the warming of surface and intermediate waters especially in the Southern Hemisphere (Figure IV-6b).

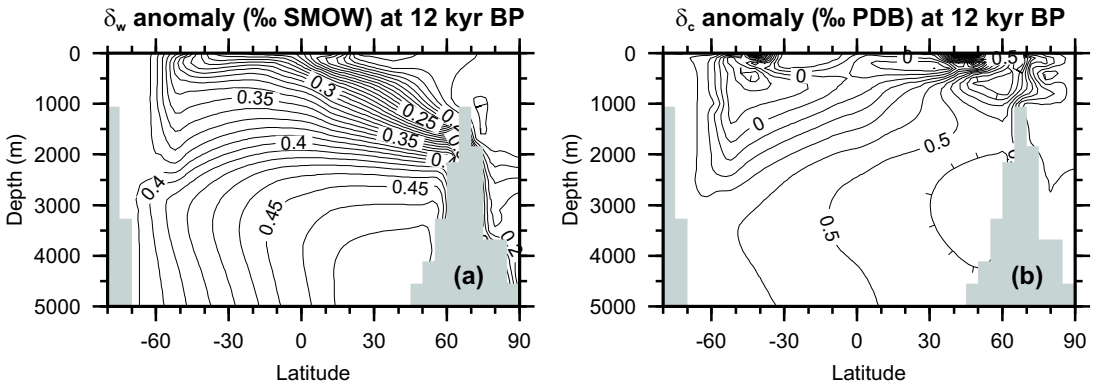

Figure IV-6. Modeled distributions of seawater- and calcite-$\delta^{18}O$ anomalies in the Atlantic Ocean at 12 kyr BP.

In the deep ocean, the North Atlantic δ_w anomaly led the South Atlantic as well as the mean anomaly by again 500-2000 years except for the glacial termination, during which all three signals where largely synchronous (Figure IV-7a). The evolution of the temperature contribution to the δ_c anomaly (Figure IV-7b) during the deglaciation was in two steps, but in opposite direction in the two hemispheres [the bipolar seesaw, an abrupt cooling in the north accompanied by a warming in the south, *Crowley*, 1992; *Stocker*, 1998].

Combining the contributions from δ_w and temperature resulted in an apparent lead of the South Atlantic over the North Atlantic Ocean by several thousand years between 17 and 3 kyr BP (Figure IV-7c).

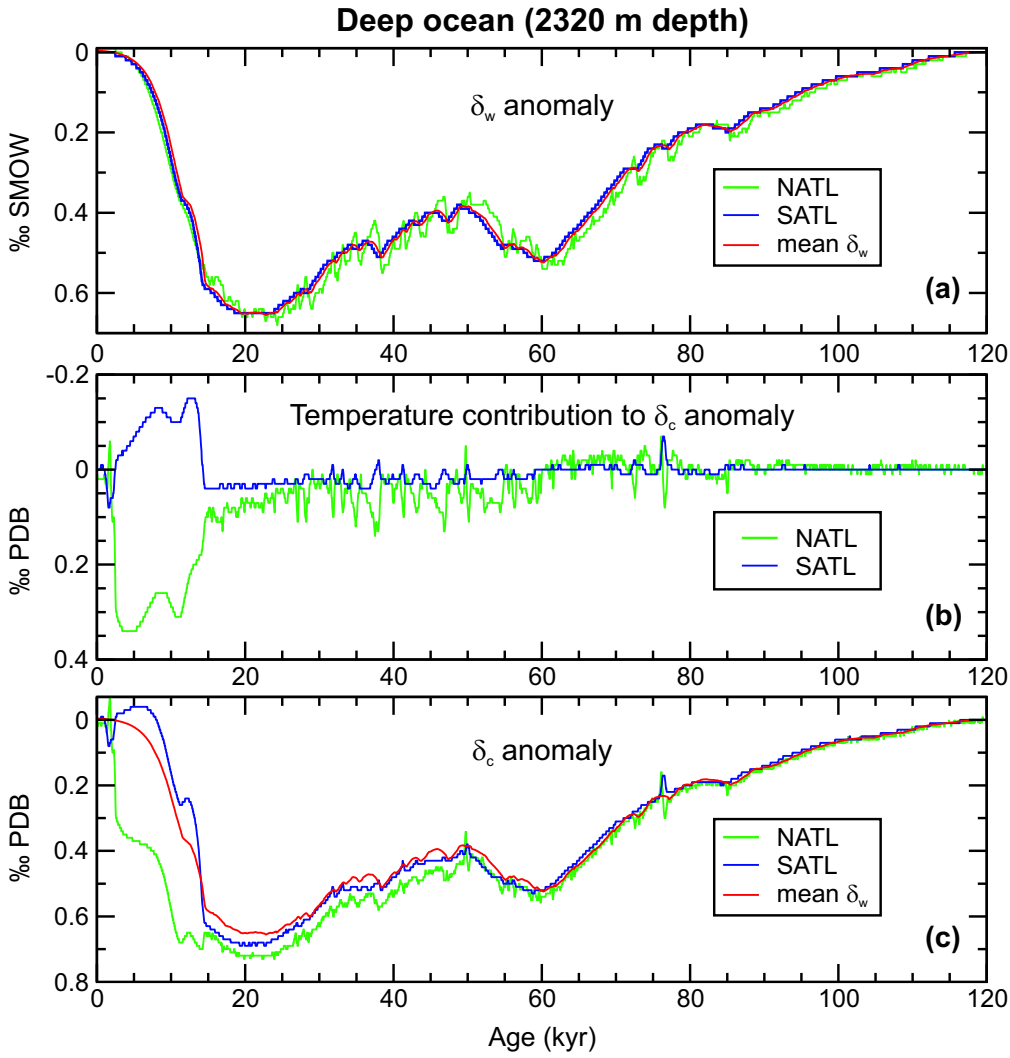

Figure IV-7. (a) Time evolution of mean-seawater δ_w, along with δ_w anomalies at 2320 m depth in the North Atlantic and South Atlantic oceans (averages for the latitudinal band 40°-50° N and 40°-50°S, respectively). (b) Contribution of temperature to the δ_c anomaly (i.e., δ_c computed by assuming no change in δ_w) at the same depth and in the same latitudinal bands. (c) Total δ_c anomaly, computed by taking into account changes in both δ_w and temperature.

At the ocean surface (Figure IV-8), during glacial inception, the δ_w anomaly between 40° and 50° in the South Atlantic Ocean very closely followed that between 50° and 60° in the North Atlantic Ocean (Figure IV-8a). Later, during the build-up of the NAIS until the

LGM, the North Atlantic anomaly led the South Atlantic anomaly by 500-2000 years. Furthermore, it clearly showed the imprint of the millenial-scale fluctuations in the freshwater forcing and the addition of istopically-light meltwater in two steps during the glacial termination. The temperature contribution to the North Atlantic δ_c anomaly reflected permanent sea-ice cover starting 50 kyr BP, while in the South Atlantic Ocean during the glacial termination a large warming (corresponding to ~8°C, not shown) dominated (Figure IV-8b). This Southern Hemisphere warming also shaped the total δ_c anomaly during the glacial termination, but otherwise the δ_c anomaly generally followed the δ_w anomaly (Figure IV-8c).

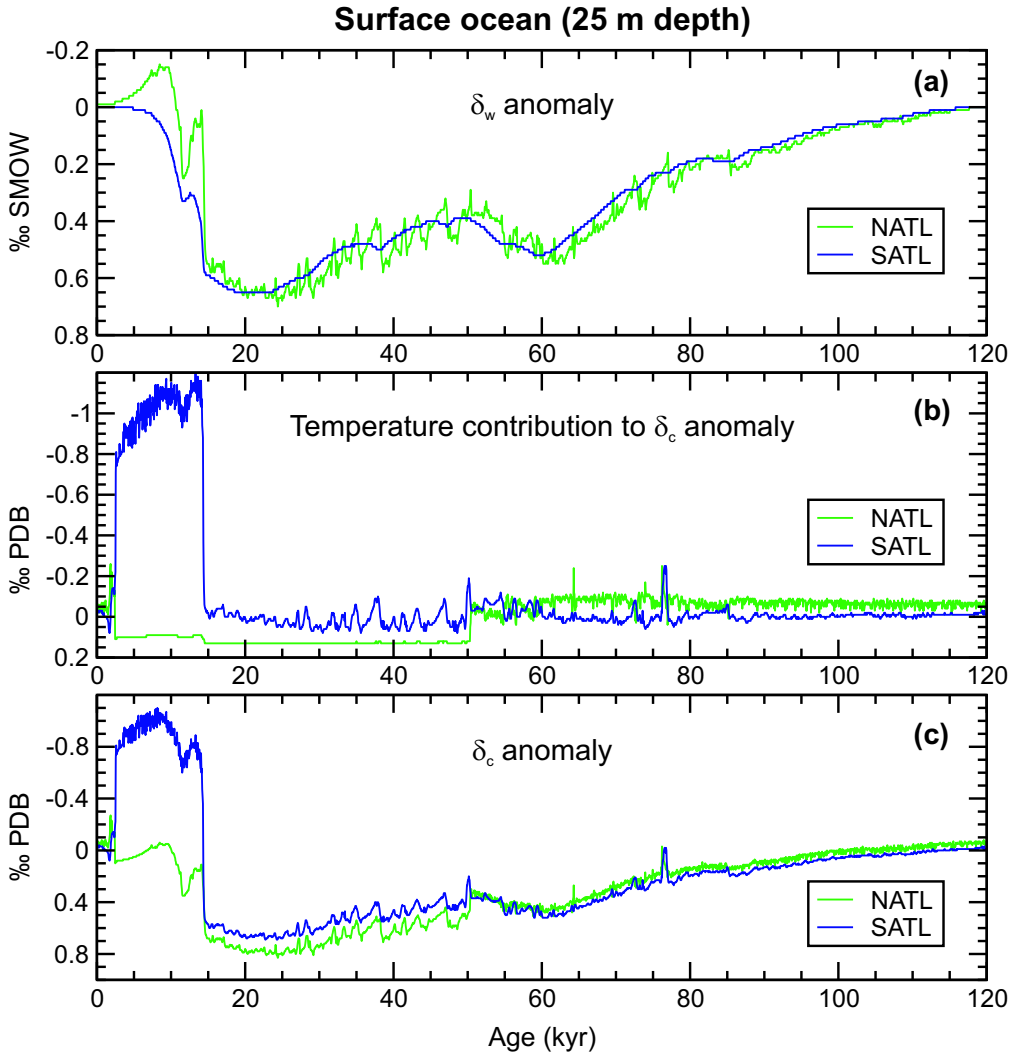

Figure IV-8. (a) Time evolution of δ_w anomalies of the surface water in the North Atlantic and South Atlantic oceans (averages for the latitudinal band 40°-50° N and 40°-50°S, respectively). (b) Contribution of temperature to the δ_c anomaly at the same locations. (c) Total δ_c anomaly.

III.4 Discussion

The ice-sheet model was shown to realistically simulate the time evolution of the NAIS during the last glacial cycle and to provide values for the ice $\delta^{18}O$ consistent with the available direct evidence on the Laurentide ice (see Section III.4). However, too much ice was still left at 6 kyr BP, and the termination was incomplete (Figures IV-1 and IV-2). Furthermore, the fact that certain freshwater pulses were caused by the rapid warming of Greenland air temperature during the course of a DO cycle (Figure IV-3a,b) contradicts the observation by *van Kreveld et al.* [2000, Figure 7 therein] that meltwater injection was preceded by an atmospheric temperature minimum. This may indicate that the ice-sheet model is overly sensitive to the external forcing or misses some internal instability that could lead to massive calving after rapid advances. During the deglaciation, the simulated meltwater curve was qualitatively similar to the reconstruction by *Fairbanks* [1989], with the two characteristic peaks during the deglaciation (Figure IV-3b).

The very good agreement between ice-volume variations and the induced mean-seawater δ_w changes, both in phase and amplitude (Figure IV-5), confirmed the finding that the nonequilibrium isotopic composition of ice sheets has very little effect on the relationship between ice volume and ocean isotopic enrichment (Chapter III). In this work we therefore focussed on the phase relationship between ice-volume changes and the δ_w and δ_c anomalies induced at different locations and depths in the Atlantic Ocean by comparing these anomalies to the mean-seawater $\delta^{18}O$ anomaly (Figure IV-7 a,c).

By analysing planktic and benthic $\delta^{18}O$ records in four deep-sea cores, *Duplessy et al.* [1991] found that the meltwater isotopic signal during the deglaciation pervaded almost instantaneously the whole North Atlantic and in less than a thousand years the deep Pacific and Indian oceans. Based on simple box-model calculations, they explained such a fast propagation as being mainly due to a transitory intensification of the MOC at the beginning of the glacial termination. In our case, the formation of NADW decreased during this time, and even ceased after the first meltwater pulse at ~14 kyr BP (Figure IV-3b). However, the mixing due to the residual circulation in the upper 1500 m as well as near the bottom (Figure IV-4d) apparently sufficed to generate a nearly synchronous evolution of δ_w in the North and South Atlantic Oceans (Figure IV-7a). We note that the collapse of NADW formation during the deglaciation long after the Heinrich 1 event [16.8 - 15.4 kyrs B.P., *Rühlemann et al.*, 2004] is in contrast to the reconstruction by *McManus et al.* [2004]. This

is probably due to the too high sensitivity of our climate model, in which the MOC ceases at lower freshwater input than in reality. In addition to that, the prolonged meltwater flux due to the late deglaciation in the ice-sheet model might also play a role.

One way to improve the results would be to prepare an initial equilibrium state for the ocean-model with a higher rate of the MOC. Another way would be a different treatment of the coupling with the ice model. In our experimental setup the ice-sheet model was coupled off-line to the climate model with no feedback of changes in sea-surface temperature on the temperature and snow accumulation over the ice sheet. The entire water exchange between the NAIS and the Atlantic Ocean occurred in the latitudinal belt between 40º and 50ºN, which is not realistic [e.g., *Licciardi et al.*, 1999]. An improvement would be to follow the approach of *Crucifix and Berger* [2002, section 2.3. therein] in computing meltwater runoff from the NAIS, by taking into account the different drainage basins and the meltwater fractions associated to them.

As indicated by the salinity distribution (Figure IV-4b), the ocean model formed the principal water masses (AAIW, NADW, AABW) known from the present-day Atlantic Ocean. The temperature (Figure IV-4c) was generally too low, with a mean temperature of only 1.4°C as compared to the observed value of ~4°C. As a consequence, the deep ocean that was already close to the freezing point in the initial equilibrium state could not cool by more than 1°C. Combined with the fact that only the NAIS contribution to the total seawater isotopic enrichment was taken into account, the paleotemperature equation yielded a much smaller range in δ_c than reconstructed by, e.g., *Waelbroeck et al.* [2002].

The rate of NADW formation (6 Sv) was also lower than observed [~14 Sv, e.g., *Schmitz*, 1995]. The 2.5-times weaker than observed MOC implies that the time difference of 500-2000 years between the North and South Atlantic Oceans was probably too long by a factor of ~2.5. Time differences of 1000 years and more between the Atlantic and Pacific Oceans [cf. *Skinner and Shackleton*, 2005] could only be expected in simulations with a climate model that explicitly treats both oceans [e.g., *Wright and Stocker*, 1992]. The apparent lead of the South Atlantic over the North Atlantic Ocean by several thousand years during the glacial termination (between 17 and 3 kyr BP) found in our simulation would probably not be affected by these shortcomings. This apparent lead was mainly due to a late warming of the NADW, which artificially prolonged the rise in δ_c [see also *Skinner and Shackleton*, 2005] and highlights the difficulty to base a cause-and-effect relationship on this proxy variable.

Using the water flux simulated by the ice-sheet model instead of an idealized flux as an input for the ocean model is a first step towards a realistic simulation of the changes in the Atlantic Ocean during the last glacial cycle. However, by considering the NAIS alone, the resulted isotopic enrichment of the ocean at the LGM is ~0.65‰, which is by ~0.35‰ smaller than the total anomaly of δ_w at the LGM [~1‰, e.g., *Malone et al.*, 2004]). Taking into account only the NAIS contribution, combined with too low values simulated for temperature in the ocean, results (via the paleotemperature equation) in too low values for the modeled δ_c anomalies, compared with observations. These two aspects should be addressed in order to allow a more quantitative comparison to the proxy data.

III.5 Conclusions

According to our model results, between the North and South Atlantic Oceans time differences of the order of the "flushing time scale" (given by the ratio of the volume and the meridional overturning rate) may occur. This does not come as a surprise, however, the combined effects from δ_w and temperature may cause an apparent lead in δ_c of the South Atlantic over the North Atlantic Ocean of several thousand years during the glacial termination (between 17 and 3 kyr BP). Therefore care is necessary in any attribution of cause-and-effect relationship based on a proxy such as δ_c, which dependes on more than one physical variable.

References

Adkins, J.F., K. Mc Intyre, and D.P. Schrag (2002), The Salinity, Temperature, and $\delta^{18}O$ of the Glacial Deep Ocean, *Science, 298*, 1769-1773.

Chappell, J., and N.J. Shackleton (1986), Oxygen isotopes and sea level, *Nature, 324*, 137-140.

Clark, P.U., and D. Pollard (1998), Origin of the middle Pleistocene transition by ice sheet erosion of regolith, *Paleoceanography, 13* (1), 1-9.

CLIMAP Project members (1981), Seasonal reconstructions of the Earth's surface at the last glacial maximum, Geological Society of America.

Crowley, T.J. (1992), North Atlantic deep water cools the southern hemisphere, *Paleoceanogr., 7*, 489-497.

Crucifix, M., and A. Berger (2002), Simulation of ocean-ice sheet interactions during the last deglaciation, *Paleoceanography, 17* (4), 1054, 10.1029/2001PA000702.

Duplessy, J.C., E. Bard, M. Arnold, N.J. Shackleton, J. Duprat, and L. Labeyrie (1991), How fast did the ocean-atmosphere system run during the last deglaciation?, *Earth Planet. Sci. Lett., 103*, 27-40.

Duplessy, J.C., J. Moyes, and C. Pujol (1980), Deep water formation in the North Atlantic Ocean during the last ice age, *Nature, 286*, 479-482.

Fairbanks, R.G. (1989), A 17,000-year glacio-eustatic sea level record: Influence of glacial melting rates on the Younger Dryas event and deep-ocean circulation, *Nature, 342*, 637-642.

Farrow, D.E., and D.P. Stevens (1995), A new tracer advection scheme for Bryan and Cox type ocean general circulation models, *J. Phys. Oceanogr., 25*, 1731-1741.

Gallée, H., J.P. van Ypersele, T. Fichefet, C. Tricot, and A. Berger (1992), Simulation of the last glacial cycle by a coupled, sectorially averaged climate-ice sheet model. Part II: Response to insolation and CO_2 variations, *J. Geophys. Res., 97*, 15713-15740.

Gonfiantini, R. (1978), Standards for stable isotope measurements in natural compounds, *Nature, 271*, 534-536.

Graves, C.E., W.-H. Lee, and G.R. North (1993), New parameterizations and sensitivities for simple climate models, *J. Geophys. Res., 98* (D3), 5025-5036.

Harvey, L.D.D. (1988), Development of a sea ice model for use in zonally averaged energy balance models, *J. Clim., 1* (C6), 1221-1238.

Huang, R.X. (1993), Real freshwater flux as a natural boundary condition for the salinity balance and thermohaline circulation forced by evaporation and precipitation, *J. Phys. Ocean., 23*, 2428-2447.

Imbrie, J., J.D. Hays, D.G. Martinson, A. McIntyre, A.C. Mix, J.J. Morley, N.G. Pisias, W.L. Prell, and N.J. Shackleton (1984), The orbital theory of Pleistocene climate: Support from a revised chronology of the marine $\delta^{18}O$ record, in *Milankovitch and climate*, edited by A. Berger, J. Imbrie, J. Hays, G. Kukla, and B. Saltzman, pp. 269-305, D. Reidel Publ. Group, Dordrecht.

Johnsen, S.J., and J. White (1989), The origin of Arctic precipitation under present and glacial conditions, *Tellus, 41B*, 452-468.

Jouzel, J., R.D. Koster, R.J. Suozzo, and G.L. Russell (1994), Stable water isotope behavior during the last glacial maximum: A general circulation model analysis, *J. Geophys. Res., 99* (D12), 25791-25801.

Kalnay, E., M. , R. Kanamitsu, W. Kistler, D. Collins, L. Deaven, M. Gandin, S. Iredell, G. Saha, J. White, Y. Woolen, M. Zhu, W. Chelliah, W. Ebisuzaki, J. Higgins, K.C. Janowiak, C. Mo, L.A. Ropelewski, R. Reynolds, and J. R. (1996), The NCEP/NCAR reanalysis project, *Bull. Am. Met. Soc., 77*, 437-471.

Labeyrie, L.D., J.C. Duplessy, and P.L. Blanc (1987), Variations in mode of formation and temperature of oceanic deep waters over the past 125,000 years, *Nature, 327*, 477-482.

Lambeck, K., and J. Chappell (2001), Sea level change through the last glacial cycle, *Science, 292*, 679-686.

Lambeck, K., Y. Yokoyama, and A. Purcell (2002), Into and out of the Last Glacial Maximum: sea-level change during Oxygen Isotope Stages 3 and 2, *Quat. Sci. Rev., 21*, 343-360.

Large, W.G., G. Danabasoglu, S.C. Doney, and J.C. McWilliams (1994), Sensitivity to surface forcing and boundary layer mixing in a global ocean model: Annual-mean climatology, *J. Phys. Ocean., 27*, 2418-2447.

Le Meur, E., and P. Huybrechts (1996), A comparison of different ways of dealing with isostasy: examples from modelling the Antarctic ice sheet during the last glacial cycle, *Annal. Glaciol., 23*, 309-317.

Licciardi, J.M., J.T. Teller, and P.U. Clark (1999), Freshwater routing by the Laurentide Ice Sheet during the last deglaciation. Mechanisms of global climate change at millennial time scales, in *Geophysical Monography 112*, edited by P.U. Clark, R.S. Webb, and L.D. Keigwin, pp. 177-201, American Geophysical Union, Washington D.C.

Lohmann, G., and R. Gerdes (1998), Sea ice effects on the sensitivity of the thermohaline circulation, *J. Climate, 11*, 2789-2803.

Malone, M.J., J.B. Martin, J. Schönfeld, U.S. Ninnemann, D. Nürnburg, and W. T.S. (2004), The oxygen isotopic composition and temperature of Southern Ocean bottom waters during the last glacial maximum, *Earth Plan. Sci. Lett.*, *222* (1), 275-283.

Marshall, S.J., L. Tarasov, G.K.C. Clarke, and W.R. Peltier (2000), Glaciological reconstruction of the Laurentide Ice Sheet: physical processes and modelling challenges, *Can. J. Earth Sci.*, *37*, 769-793.

Martinson, D.G., N.G. Pisias, J.D. Hays, J. Imbrie, T.C. Moore, Jr., and N.J. Shackleton (1987), Age dating and the orbital theory of the icec ages: development of a high-resolution 0 to 300,000-year chronostratigraphy, *Quat. Res.*, *27*, 1-29.

McManus, J.F., R. Francois, J.-M. Gherardi, L.D. Kelgwin, and S. Brown-Leger (2004), Collapse and rapid resumption of Atlantic meridional circulation linked to deglacial climate changes, *428*, 834-837.

McManus, J.F., D.W. Oppo, and J.L. Cullen (1999), A 0.5-million-year record of millennial-scale climate variability in the North Atlantic, *Science*, *283*, 971-975.

Mellor, G.L. (1991), An equation of state for numerical models of oceans and estuaries, *J. Atm. Oc. Tech.*, *8*, 609-611.

Mix, A.C., and W.F. Ruddiman (1984), Oxygen-isotope analyses and Pleistocene ice volumes, *Quat. Res.*, *21*, 1-20.

Mulitza, S., B. Donner, G. Fischer, A. Paul, J. Pätzold, and C. Rühlemann (2003), The South Atlantic oxygen isotope record of planktic foraminifera, in *The South Atlantic in the Late Quaternary: Reconstruction of Material Budgets and Current Systems*, edited by G. Wefer, S. Mulitza, and V. Ratmayer, pp. 121-142, Springer-Verlag Berlin Heidelberg New York Tokyo.

North Greenland Ice Core Project members (2004), High-resolution record of Northern Hemisphere climate extending into the last interglacial period, *Nature*, *431*, 147-151.

Oerlemans, J. (1982), Glacial cycles and ice-sheet modelling, *Clim. Change*, *4*, 353-374.

Paul, A., and M. Schulz (2002), Holocene climate variability on centennial-to-millennial time scales: 2. Internal feedbacks and external forcings as possible causes, in *Climate development and history of the North Atlantic Realm*, edited by G. Wefer, W.H. Berger, K.-E. Behre, and E. Jansen, pp. 55-73, Springer Verlag, Berlin.

Payne, A.J. (1995), Limit cycles in the basal thermal regime of ice sheets, *J. Geophys. Res.*, *B100*, 4249-4263.

Peltier, W.R. (1994), Ice age paleotopography, *Science*, *265*, 195-201.

Peltier, W.R. (2004), Global glacial isostasy and the surface of the ice-age Earth: the ICE-5G (VM2) model and GRACE, *Ann. Rev. Earth Plan. Sci.*, *32*, 111-149.

Pollard, D. (1983), Ice-age simulations with a calving ice-sheet model, *Quat. Res.*, *20*, 30-48.

Rahmstorf, S. (1996), A fast and complete convection scheme for ocean models, in *MOM2. Documentation, User's Guide and Reference Manual, Nr. 3.2*, edited by Pacanowsky, pp. 329, GFDL, Princeton, New Jersey.

Romanova, V., M. Prange, and G. Lohmann (2004), Stability of the thermohaline circulation and its dependence on the background hydrological cycle, *Clim. Dyn.*, *22*, 527-538.

Rühlemann, C., S. Mulitza, G. Lohmann, A. Paul, M. Prange, and W. G. (2004), Intermediate depth warming in the tropical Atlantic related to weakened thermohaline circulation: Combining paleoclimate data and modeling results for the last deglaciation, *Paleoceanogr.*, *19*, PA1025, doi:10.1029/2003PA000948.

Schmitz, W.J. (1995), On the interbasin-scale thermohaline circulation, *Rev. Geophys.*, *33* (2), 151-173.

Schrag, D.P., J.F. Adkins, K. McIntyre, J.L. Alexander, D.A. Hodell, C.D. Charles, and J.F. McManus (2002), The oxygen isotopic composition of seawater during the Last Glacial Maximum, *Quat. Sci. Rev.*, *21*, 331-342.

Shackleton, N.J. (1967), Oxygen isotope analyses and Pleistocene temperatures, re-assessed, *Nature*, *215*, 15-17.

Shackleton, N.J. (1977), The oxygen isotope stratigraphic record of the late Pleistocene, *Phil. Trans. Roy. Soc. London, B 280*, 169-182.

Shackleton, N.J. (1987), Oxygen isotopes, ice volume and sea-level, *Quat. Sci. Rev.*, *6*, 183-190.

Shackleton, N.J., M.A. Hall, and E. Vincent (2000), Phase relationships between millennial-scale events 64,000-24,000 years ago, *Paleoceanography*, *15*, 565-569.

Skinner, L.C., and N.J. Shackleton (2005), An Atlantic lead over Pacific deep-water change across Termination I: implications for the application of the marine isotope stage stratigraphy, *Quat. Sci. Rev.*, *24* (5-6), 571-580.

Stocker, T.F. (1998), Climate change - The seesaw effect, *Science*, *282* (5386), 61-62.

Tarasov, L., and W.R. Peltier (1999), Impact of thermomechanical ice sheet coupling on a model of the 100 kyr ice age cycle, *J. Geophys. Res.*, *D104*, 9517-9545.

van Kreveld, S.A., M. Sarnthein, H. Erlenkeuser, P. Grootes, S. Jung, M.J. Nadeau, U. Pflaumann, and A. Voelker (2000), Potential links between surging ice sheets, circulation changes and the Dansgaard-Oeschger cycles in the Irminger Sea, 60-18 kyr, *Paleoceanogr.*, *15*, 425-442.

Waelbroeck, C., L. Labeyrie, E. Michel, J.-C. Duplessy, J.F. McManus, K. Lambeck, E. Balbon, and M. Labracherie (2002), Sea-level and deep water temperature changes derived from benthic foraminifera isotopic records, *Quat. Sci. Rev.*, *21*, 295-305.

Winton, M. (1997), The effect of cold climate upon North Atlantic Deep Water formation in a simple ocean-atmosphere model, *J. Climate, 10* (1), 37-51.

Wright, D.G., and T.F. Stocker (1991), A zonally averaged model for the thermohaline circulation. Part I: Model Development and flow dynamics, *J. Phys. Oceanogr.*, *21*, 1713-1724.

Wright, D.G., and T.F. Stocker (1992), Sensitivities of a zonally averaged global ocean circulation model, *J. Geophys. Res.*, *C97*, 12707-12730.

Chapter V

THE YOUNGER DRYAS – AN INTRINSIC FEATURE OF LATE PLEISTOCENE CLIMATE CHANGE AT MILLENNIAL TIMESCALES

Adriana Sima, André Paul, and Michael Schulz

Department of Geosciences, University of Bremen, D-28334 Bremen, Germany

Abstract

A box model of the North Atlantic Ocean exhibits self-sustained oscillations of the large-scale ocean circulation, which are reminiscent of Dansgaard-Oeschger (DO)-style oscillations. The freshwater forcing of this ocean model depends on mean climate state, represented by global ice volume. This is computed by a one-dimensional ice-sheet model, subject to changes in high-latitude northern hemisphere summer insolation. At low/large ice volume, the ocean-ice system stays in a permanent interstadial/stadial mode. Millennial scale DO-style oscillations result at intermediate ice-volume values, which thus define a „DO window". During an interglacial-to-glacial transition this DO window is crossed sufficiently slow to allow for sustained DO-style oscillations to develop. In contrast, during a glacial termination the system moves relatively rapid through the DO window, resulting in an intermittent re-appearence of DO-style oscillations, which resemble the sequence of events surrounding the Younger Dryas. When forced with modeled ice-volume evolution over the last 800 thousand years, our model predicts Younger Dryas-type cooling events for each major glacial termination. Accordingly, the Younger Dryas does not appear to be a one-time event.

Earth and Planetary Science Letters 222 (3-4): 741-750 JUN 15 2004

V.1 Introduction

The Younger Dryas (YD) cold spell is one of the most prominent abrupt climate change events in the past and a key feature of the last glacial termination. It is an intermittent, ~1300-yr (year) long return to almost glacial conditions within a general warming trend. At least in the Northern Hemisphere, the last deglaciation appears as a sequence of three main intervals: the Bølling/Allerød warm period (approximately between 14,700 – 12,900 yr BP - years before present), the Younger Dryas cold phase (~12,900 – 11,600 yr BP) and the warm Preboreal (after ~11,600 yr BP) (all dates refer to the Greenland ice core GISP2 chronology; Alley et al., 1993). Although the YD event mainly affected the Northern Hemisphere, it was of global significance (e.g. Alley and Clark, 1999).

Different hypotheses have been suggested to explain the YD (Alley and Clark, 1999 for a summary). The majority of ideas favor the ocean as a crucial element for generating the YD. In this view, differential meltwater input into the North Atlantic is hold responsible for slowing down the Atlantic Ocean meridional overturning circulation, either by re-routing Lake Agassiz water to the St. Lawrence River (Clark et al., 2001) or by a delayed response to the so-called meltwater pulse 1A (MWP-1A; e.g. Fanning and Weaver, 1997; Sakai and Peltier, 1998), which commenced approximately 1800 years prior to the onset of the YD and culminated during the Bølling warm period (Fairbanks et al., 1992; Kienast et al., 2003). Berger and Jansen (1995) proposed a variation on this general theme in that they consider the Bølling/Allerød warm period as an intermittent state, triggered by the wasting of marine-based ice sheets around the North Atlantic Ocean, and the YD as a mere return to glacial conditions.

The rerouting hypothesis (Clark et al., 2001) faces the difficulty that the thermohaline circulation in the North Atlantic prior to the onset of the YD was relatively strong and probably more difficult to destabilize than originally suggested by coarse resolution models (Lohmann and Schulz, 2000). When assuming a meltwater-induced triggering of the YD, the immediate problem is to explain the time lag between MWP-1A and the onset of the YD. Furthermore, the northern hemisphere origin of MWP-1A is still questionable (e.g. Clark et al., 2002), making this meltwater input as trigger for the YD even more unlikely. From experiments with an Earth system model of intermediate complexity, Crucifix and Berger (2002) also concluded that there was probably no direct link between MWP-1A and the initiation of the YD.

Based on the methane record in the Antarctic Vostok ice core for the past 420 kyr (Petit et al., 1999), Broecker (2003) argued that the YD appeared to be a one-time event and not a general feature of glacial terminations. However, the time resolution of the Vostok methane record is on the order of 1,000-2,000 yr before the penultimate interglacial (Petit et al., 1999) and, therefore, prevents any unambiguous detection of YD-type events.

In contrast to the supposition of a one-time event, paleoceanographic reconstructions show some evidence for cold events similar to the YD during five terminations preceeding Termination I (Sarnthein and Tiedemann, 1990). More recently, Lototskaya and Ganssen (1999) identified a „Termination II pause“ which separated the penultimate deglaciation into two steps. Sea-level reconstructions from coral data (Gallup et al., 2002) even suggest a return to colder conditions associated with a regrowth of continental ice during Termination II. Thus the YD may not be a singular event, but an intrinsic feature of glacial terminations.

Here we propose an alternative mechanism to account for the Younger Dryas and similar earlier events, which does not depend on meltwater input into the North Atlantic. We approach the YD from the Northern Hemisphere point of view and elaborate on an idea put forth by Schulz et al. (2002, hereafter SPT). We consider the trigger of the YD to reside in the ocean, and envision the YD cold phase as part of one cycle of a so-called deep-decoupling oscillation of the Atlantic Ocean meridional overturning circulation. Such a cycle may occur during any termination when the mean climate passes through an intermediate state, between glacial maximum and interglacial.

Deep-decoupling oscillations (Harvey, 1992; Winton, 1993; Oka et al., 2001; Paul and Schulz, 2002) can be caused by a continuous freshening of the North Atlantic Ocean, which leads to the developement of a polar halocline and eventually suppresses the formation of North Atlantic Deep Water. During this „deep-decoupled phase“ the meridional circulation and oceanic heat transport are reduced. The subsequent import of heat and salt by advection and diffusion weakens the stratification and finally destroys the polar halocline. The renewal of convection in high latitudes marks the onset of a “deep-coupled phase“, with active deep-water formation and vigorous meridional overturning circulation and heat transport. The reestablishment of the halocline then completes a „deep-decoupling oscillation“. From the abruptness of the transitions, deep-decoupling oscillations are reminiscent of the millennial-scale climate variability documented in the Greenland ice cores (Stuiver and Grootes, 2000). Following Winton (1993), we interpret the deep-decoupled phases as Dansgaard-Oeschger (DO)-stadials and the deep-coupled phases as DO-interstadials.

V.2 Methods

To study deep-decoupling oscillations of the meridional overturning circulation in relation to DO oscillations, we use a combination of ice-sheet and ocean modeling. With the help of a one-dimensional ice-sheet model, we generate a history of glaciation, which, in turn, is used to modulate the low-to-high latitude freshwater forcing in an ocean box model. Finally, we compare the model results to a reconstruction of global sea level and to the oxygen-isotope composition of Greenland ice.

V.2.1 Ice-sheet model

The one-dimensional coupled ice sheet-bedrock model (after Pollard, 1983; Clark and Pollard, 1998) considers only the Laurentide ice sheet, which dominated ice-volume variations during the late Pleistocene (cf. Peltier, 1994). Ice thickness and bedrock elevation are computed as functions of latitude and time along a typical flow line through the ice sheet, such that a north-south profile is approximated.

Ice flow is described by a vertically-integrated continuity equation for ice thickness:

$$\frac{\partial h_i}{\partial t} = -\frac{\partial\left(\overline{U} h_i\right)}{\partial x} + B - C, \tag{1}$$

where h_i is the ice thickness and $\overline{U}$ is the vertically-averaged horizontal velocity (see Table V-1 for symbols and parameter values). The first term on the right-hand side represents internal ice shear or basal sliding at the ice-bed interface. We compute $\overline{U}$ as:

$$\overline{U} = A h_i^{n+1} \left| \frac{\partial\left(h_i + h_b\right)}{\partial x} \right|^{n-1} \frac{\partial\left(h_i + h_b\right)}{\partial x},$$

where h_b is the bedrock elevation above sea level. Net annual mass balance B on the ice surface is derived using the equilibrium-line concept, as follows (Oerlemans, 1980; Pollard, 1983):

$$B = \begin{cases} a\left(h_i + h_b - h_{equ}\right) - b\left(h_i + h_b - h_{equ}\right)^2 & \text{if } h_i + h_b - h_{equ} \le 1{,}500m \\ 0.56 & \text{if } h_i + h_b - h_{equ} > 1{,}500m \end{cases} \text{ m yr}^{-1}$$

Table V-1. Parameters of the one-dimensional ice sheet model

Symbol	Description	Value	Units
x	north-south distance	independent variable	m
t	time	independent variable	yr
$h_i(x,t)$	ice sheet thickness	prognostic variable	m
$h_b(x,t)$	bedrock elevation above sea level	prognostic variable	m
$h_b^{eq}(x,t)$	equilibrium bedrock elevation above sea level	500 southward of 70ºN -500 northward of 74ºN linear ramp between 70º-74ºN	m
h_{equ}^{0}	altitude of equilibrium line at 70ºN	550	m
s_{equ}	slope of equilibrium line	0.001	
k_{ins}	proportionality factor for equilibrium-line elevation	35.1	m W^{-1} m^2
B	mass balance on ice surface	prescribed (see text)	m yr^{-1}
C	calving rate	20 if ‚floating' (see text)	m yr^{-1}
A	ice rheology coefficient	5.77×10^{-4}	m^{-3} yr^{-1}
n	ice rheology exponent	3	
a	coefficient in mass balance	0.81×10^{-3}	yr^{-1}
b	coefficient in mass balance	0.30×10^{-6}	m^{-1} yr^{-1}
τ	timescale of bedrock relaxation	5000	yr
ρ_i	ice density	910	kg m^{-3}
ρ_b	bedrock density	2390	kg m^{-3}

The equilibrium-line elevation is assumed to depend linearly on latitude and to shift with insolation variations:

$$h_{equ} = h_{equ}^{0} + s_{equ}\, x + k_{ins}\, \Delta Q$$

where ΔQ is the difference in the caloric summer insolation at 55°N (Milankovitch, 1930) from that of the present. Fourier coefficients for computing the Earth's orbital elements are taken from Berger (1978). The term C in Eq. (1) represents catastrophic calving. It is set to 20 m yr^{-1} at any grid point of the ice sheet if its base is below sea level ($h_b < 0$) and if the grid point or one of its neighbouring points has floating ice ($\rho_i h_i < -\rho_w h_b$). The calving instability does not introduce ice-age terminations, but amplifies them (Pollard, 1983).

Bedrock adjustment is computed from a „local lithosphere – relaxed asthenosphere“ model (Le Meur and Huybrechts, 1996) with a characteristic time constant τ:

$$\frac{\partial h_b}{\partial t} = \frac{1}{\tau}\left[h_b^{eq} - h_b - \frac{\rho_i h_i}{\rho_b} \right],$$

where h_b is the bedrock elevation above sea level, h_b^{eq} is the equilibrium bedrock elevation above sea level, ρ_i the ice density and ρ_b the bedrock density. In the direction normal to the flow line, no ice-sheet dynamics is computed, but a perfectly-plastic profile symmetric to the ice-sheet crest is assumed (Gallée et al., 1992). This enables us to compute a three-dimensional ice-volume from the two-dimensional cross-sectional area of the ice sheet.

Ice volume is converted to sea level taking into account the total sea surface and the ratio of seawater and ice densities. Thus, we equate 1 m of sea level with 4.091×10^{14} m^3 of ice. The resulting ice equivalent sea-level variations are multiplied by a factor of 1.6 to match the sea level at the Last Glacial Maximum (LGM) (Berger et al., 1996). In this way we account for the continental ice not represented in our model (e.g. the Eurasian ice sheet). In accordance with Peltier (1994), a ~60% contribution of the Laurentide ice sheet to the total sea level at LGM is therefore assumed.

V.2.2 Ocean model

The three-box model of the North Atlantic Ocean (Figure V-1) is based on Winton (1993). We use the same parameters as in SPT. The height of the two surface boxes is h = 100 m and that of the deep box is H = 1000 m. The boundary between low- and high-latitude surface boxes is associated with the subpolar front in the Atlantic Ocean. The northern box represents regions in which deep convection and deep-water formation take place (i.e., the subpolar North Atlantic and Norwegian-Greenland Seas at present). All the boxes have a longitudinal extent of 60°. Temperatures in the surface boxes are constant with T_l = 15°C and T_h = 0°C. The temperature in deep box (T_d) and salinities (S) in all boxes are computed. Mixing M_{ij} between boxes i and j occurs at timescale τ_{ij} such that $M_{ij} = d_{ij} / \tau_{ij}$, where d_{ij} is the exchange-area-weighted distance between box centers ($\tau_{ld} = \tau_{hd}$ = 400 yr and τ_{lh} = 5 yr). Using a quadratic equation of state, M_{hd} is increased by a factor C_h = 10 if the high latitude water column is gravitationally unstable; else C_h = 3 is adopted to account for partial shutdown of multiple convection sites.

As in SPT, we assume a linear relationship between the high-latitude net surface freshwater flux (F_w) and ice-equivalent sea level (Sl): $F_w = a + b \times Sl$, with a = 0.5015 m yr^{-1} and $b = -4.5 \times 10^{-3}$ yr^{-1}. We stress that sea level is envisaged here as a measure of the

mean climate state. Our hypothesis that the high-latitude net surface freshwater flux is enhanced during glacials is based on the following factors:

1. reduction of evaporation,
2. southward shift of the storm track,
3. melting of sea ice,
4. melting of icebergs in regions of seasonal sea-ice cover, and
5. increased runoff from European rivers, which carry meltwater from snow and from the southern margin of the ice sheets.

All these processes are directly or indirectly related to the presence of large ice sheets in the Northern Hemisphere and have been quantified for the LGM. Factors 1 to 3 were made responsible for the increase in freshwater flux in the latitudinal belt between 40º and 60º N during the LGM (Ganopolski and Rahmstorf, 2001). Schmittner et al. (2002) found that it was mainly factor (1) that caused the reduced thermohaline circulation in their simulation of the LGM. Factors 4 and 5 were inferred by Duplessy et al. (1991) from the distribution of oxygen isotopes of planktonic foraminifera in the northern North Atlantic Ocean, especially in the Bay of Biscay and the Nordic Seas. Melting of icebergs and ice sheets (cf. factors 4 and 5) is usually not taken into account in climate models. We assume that the effect of the enhanced high-latitude freshwater flux on the buoyancy flux outweighs the effect of the high-latitude cooling, leading to reduced deep-water formation in the North Atlantic.

Since the focus of this study is on the generation of YD-type events, the parameterization of Heinrich events employed by SPT is not used here.

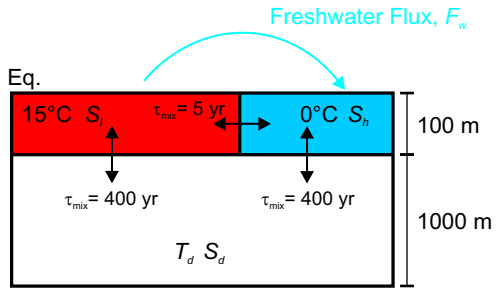

Figure V-1. *Three-box model of the North Atlantic Ocean (after Winton, 1993).* Each box is characterised by temperature (*T*) and salinity (*S*). Subscripts '*l*' and '*h*' denote low and high latitude boxes and '*d*' the deep box. M_{ij} is the mixing between boxes *i* and *j*. F_w is the low-to-high latitude freshwater flux (see text for further details).

V.3 Results

The modeled ice-equivalent sea level is shown in Figure V-2. It exhibits glacial-interglacial cycles of about 100-kyr period, characterized by slow build-up and rapid decay of ice.

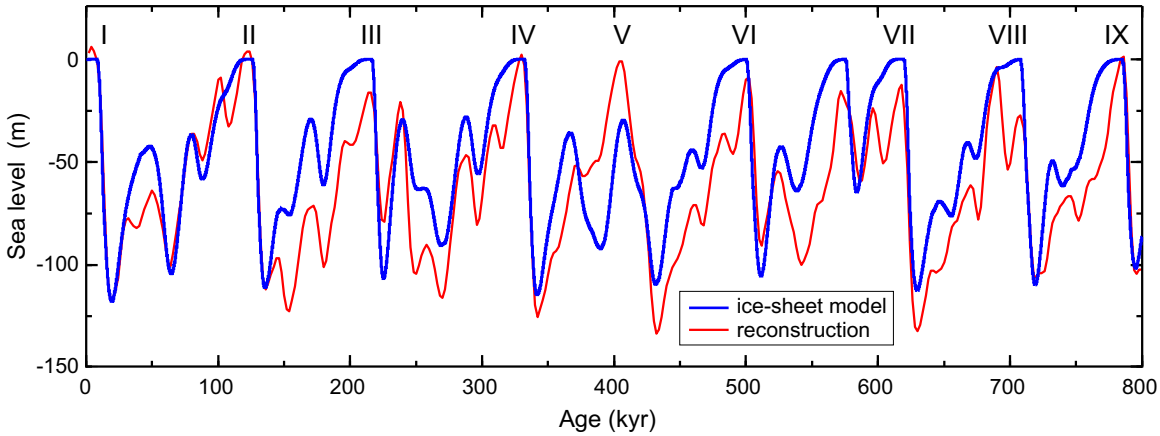

Figure V-2. Modeled ice equivalent sea-level (blue) and Berger et al. (1996) sea-level reconstruction (red). A linear trend was substracted from the reconstructed data to account for a long-term warming trend affecting the underlying oxygen isotope data (Berger et al., 1996). Roman numerals denote terminations.

The state of the ocean box model is determined by the modeled variations of the ice volume via the relationship between *Sl* and F_w. At low values of the freshwater forcing (F_w) the model stays in a permanent interstadial phase, while high values of F_w result in a continuous stadial phase (Figure V-3, see also SPT). For intermediate values of F_w the model exhibits free oscillations which are reminiscent of DO-cycles (Figure V-4). The "strong"-convection phase represents a DO interstadial and the "weak"-convection phase characterizes the DO stadial mode. The latter mode is also considered as surrogate for the LGM state in our model. Although this assumption is in accordance with the common interpretation of paleoceanographic proxy data (summarized in Alley et al., 1999), these data may actually be insufficient to constrain the LGM circulation (Wunsch, 2003). DO-style oscillations occur for F_w values between 0.704 and 0.875 m yr^{-1}. This „DO window" (Fig. 3) corresponds to a sea-level range of –45 m to –83 m, consistent with earlier findings (McManus et al., 1999; Schulz, 2002). Within the DO window, the duration of the stadials increases with rising F_w (SPT).

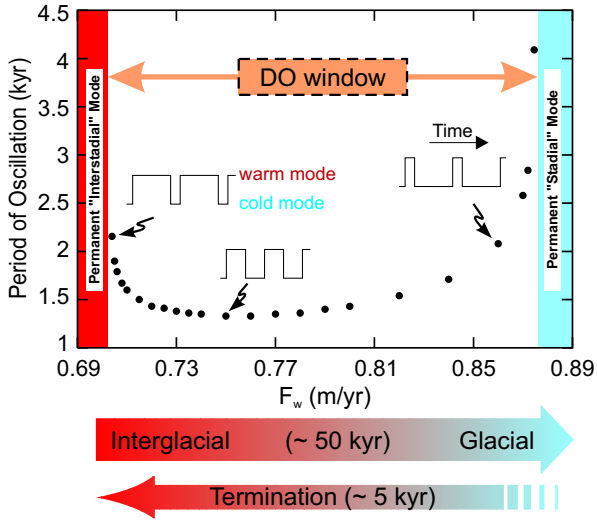

Figure V-3. Period of the oscillations in the ocean model as function of freshwater flux F_w (dots). Ratio between durations of coupled and decoupled phases decreases with increasing F_w, as indicated by square waves (not to scale). The DO window is slowly crossed during the transition from interglacial to glacial conditions, and more rapidly during glacial termination.

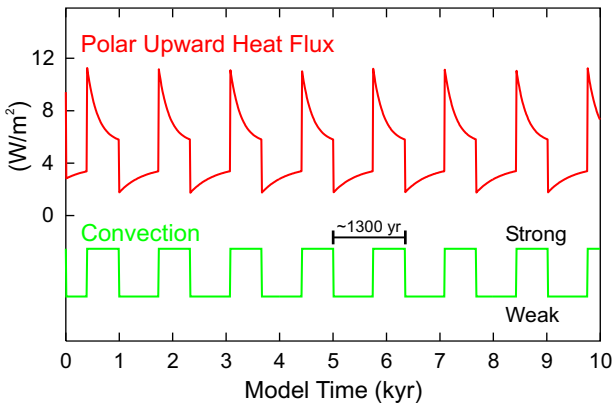

Figure V-4. Free deep-decoupling oscillations in the ocean box model for a constant freshwater flux of 0.75 m/yr.

When forced with the modeled ice-volume evolution, the predicted climate oscillations during the last glacial period show structural similarities with the reconstructed climate fluctuations (Figure V-5). Before ~75 kyr BP the ice-equivalent sea level is above the upper limit of the DO window, so the ice-ocean system stays in the interstadial (warm) mode. Between ~75 and 70 kyr BP, sea level slowly crosses the DO window, giving rise to a sequence of three stadial-interstadial oscillations. Between ~70 and 60 kyr BP, sea level drops below the lower limit of the DO window, so that DO-style oscillations cannot occur anymore and the system enters a permanent stadial state. At about 60 kyr BP, sea level returns into the DO-window and a more than 30 kyr-long oscillation sequence develops, only briefly interrupted around ~48 kyr BP. This interruption gives the impression of a very long interstadial, in close resemblance with the proxy data. After ~27 kyr BP the ice volume becomes again too large to allow DO-style oscillations to develop and the system enters once again the permanent cold state. At ~18 kyr BP the last deglaciation begins. During this glacial termination, the DO window is crossed within ~2,5 kyr, so that a single DO-style oscillation cycle occurs. This results in a succession of events similar to the Bølling/Allerød –YD – Preboreal sequence. At about 12 kyr BP, with the sea level reaching the upper limit of the DO window, the model marks the entering of a permanent warm state, corresponding to the Holocene.

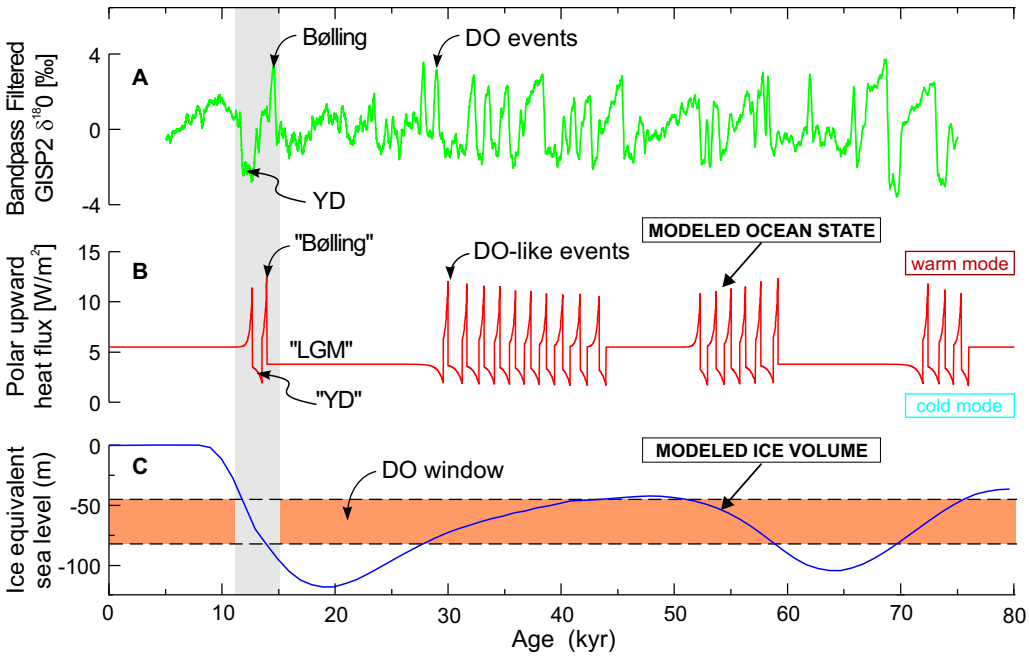

Figure V-5. Modeled climate events during the last glacial period. (a) GISP2 oxygen-isotope record reflecting air-temperature above Greenland [Stuiver and Grootes, 2000], band-pass filtered (SPT). (b) Upward heat flux at high latitudes [W/m^2]. (c) Modeled ice-equivalent sea level [m]. Note that, due the inertia of the climate system, overshoots in heat flux do not necessarily reflect similar anomalies in temperature.

The same model setup, when applied to the entire late Pleistocene, predicts YD-type events during each of the nine major terminations (Figure V-6). If, during a glacial termination, the DO window is crossed within a time interval comparable to the period of the deep-decoupling oscillation, only a single cycle will occur. Accordingly, the deglaciation proceeds in two warming steps, separated by one cold YD-style cooling event. In contrast, if the DO window is crossed within a longer time interval, more than one oscillation can develop.

Our model setup allows for two- and three-step terminations, including one or two YD-style cooling events. Terminations I, II, IV and VII fall in the first category (DO window-crossing time of 1.9 - 2.2 kyr) and Terminations III, VI, VIII and IX in the second (DO window-crossing time of 2.4 – 3.2 kyr) (Fig.6).

An interesting situation arises for Termination V, which is known to be associated with weak orbital forcing (Imbrie and Imbrie, 1980). Correspondingly, the DO window is crossed extremely slow (12.5 kyr in our simulation; Figure V-6), leading to a long sequence of DO-style oscillations. Indeed, a sequence of three benthic $\delta^{13}C$ minima, each indicating a time interval with reduced deep-water production in the North Atlantic Ocean, was found by Poli et al. (2000) during this termination.

V.4 Discussion

Modeled ice-equivalent sea-level variations are in good agreement with the sea-level reconstruction of Berger et al. (1996, Fig.2). In particular, the ice-sheet model realistically simulates the 100-kyr cycles, which dominated the late Pleistocene (cf. Pollard, 1983). We have chosen to compare the ice-model derived sea level to the Berger et al. (1996) reconstruction since it contains only variability at orbital timescales (as does the model) and is sufficiently long to evaluate the model performance over the entire late Pleistocene.
Berger et al. (1996) adopted a value of -117 m for sea level at the LGM in their reconstruction. More recent estimates are slightly lower and amount to about -125 m (e.g. Waelbroeck et al., 2001; Yokoyama et al., 2001). However, choosing a different value for the sea level at LGM would only lead to different scaling parameters in the $F_w - Sl$ relationship, but would not change the essence of our results.

The calving mechanism embodied in Eq. (1) yields the typical sawtooth shape with nine complete deglaciations during the past 800 kyr. During calving episodes, the simulated meltwater discharge reaches values up to 0.2 Sv. Because we aim at generating YD-type events independent of deglaciation meltwater input (see Introduction), this additional freshwater flux is not taken into account in computing F_w.

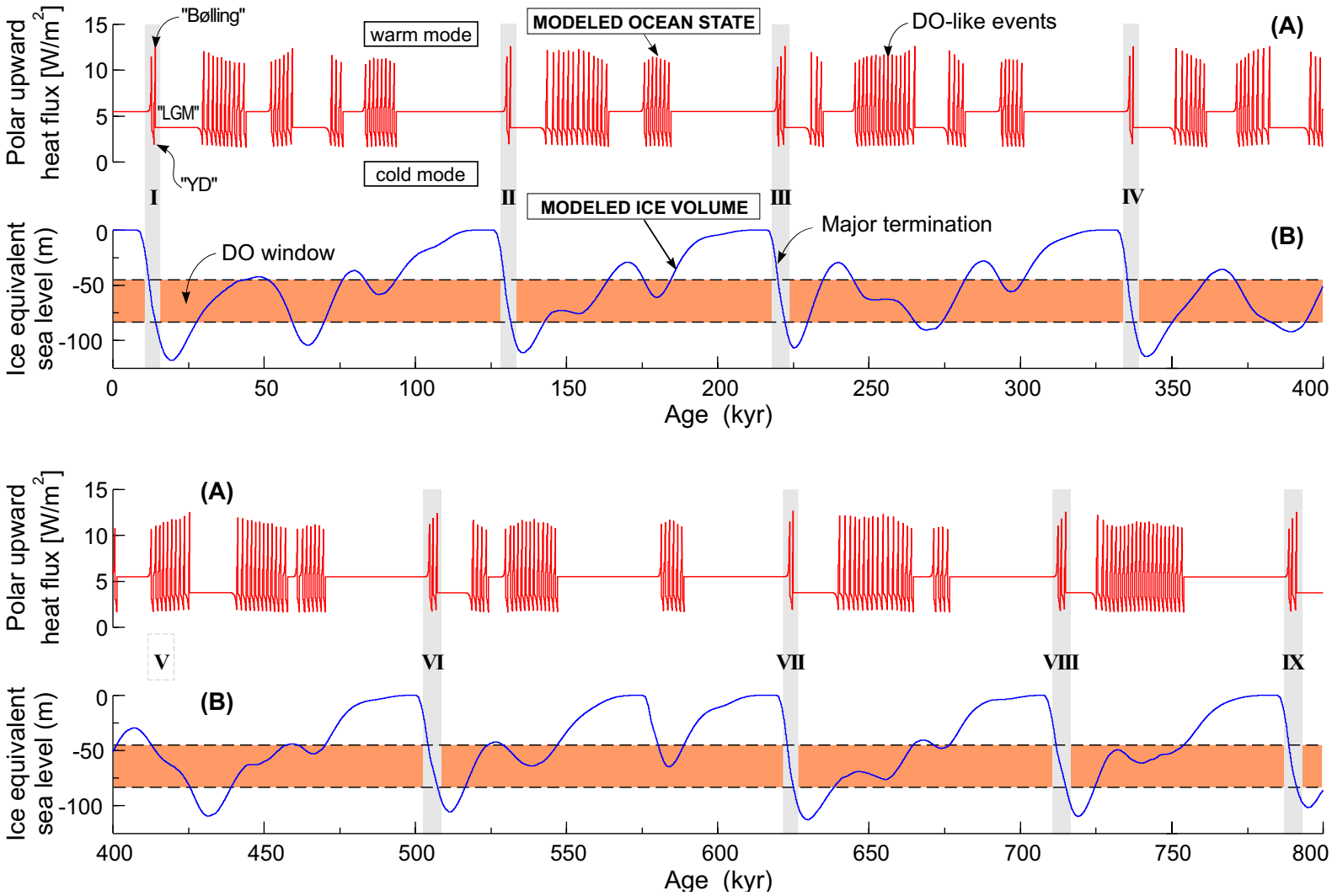

Figure V-6. Modeled climate oscillations during the past 800 kyr. (a) Upward heat flux at high latitudes [W/m^2]; (b) ice-equivalent sea level [m]. Vertical grey bars mark glacial terminations and horizontal orange bar depicts DO window. Younger Dryas-type cooling events occur during all deglaciations.

Compared to the reconstruction, the phasing and relative amplitude of the modeled sea-level is remarkably good over the whole investigated period. An exception is Marine Isotope Stage 11 (423 –362 kyr BP); our model fails to reproduce a full deglaciation in this interval, mainly due to the weakness of the insolation forcing (the „stage 11 problem“, Imbrie and Imbrie, 1980). With the same kind of model, Pollard (1983) succeeded in reproducing a strong transition from isotope stage 11 to 12. In that study a diffusive method was chosen for the asthenospheric treatment. However, there exist serious problems with this approach (e.g. the characteristic response time increases with the size of the load, in contradiction to results from a more sophisticated full-Earth model), hence, we employed the relaxed asthenosphere method, which seems preferable (Le Meur and Huybrechts, 1996).

The appearance of the DO-style climate oscillations depends on the interaction between the period of the free oscillations and the timescale at which the mean climate (as measured by ice-volume equivalent sea level), and hence, F_w, changes. During an interglacial-to-glacial transition the DO window is crossed within ~50 kyr, which is sufficiently slow to allow sustained DO-style oscillations to develop. In contrast, during a glacial termination the system moves relatively rapid (few kyr) through the DO window. This results in an intermittent re-appearence of DO-style oscillations, including one or two YD-type cooling events.A better fit of the timing of modeled oscillations to the proxy data during the last glacial period (Figure V-5) could possibly be achieved by choosing a different relationship between F_w and mean climate state, as measured by *Sl*. However, we consider such fine tuning as unwarranted within our conceptual model framework, which aims at qualitative agreement between simulation and data. The assumed linear relationship between mean climate and high-latitude freshwater flux gave a sequence of events in accordance with the paleoclimate record. We note, however, that deep-decoupling oscillations could also be induced by glacial cooling: Winton (1997) showed that an ocean model can exhibit oscillatory behavior within a certain range of global mean temperature, even if freshwater forcing is held constant. Accordingly, there is possibly a DO window in temperature as well as in freshwater flux, resulting in a two-dimensional region in parameter space . This might influence a particular termination, but would not alter our general finding that the ocean-ice system intermittently oscillates as it rapidly passes through a DO window during glacial terminations.

The proposed mechanism is not mutually exclusive with meltwater related scenarios. In fact, rerouting of meltwater from the Mississippi River drainage to the Hudson or St. Lawrence Rivers (Clark et al., 2001) may amplify the deep-decoupling oscillations during deglaciations.

V.5 Conclusions

Based on an idealized, prescribed ice-volume evolution, Schulz et al. (2002) suggested that the Younger-Dryas event results from an intermittent re-start of self-sustained oscillations of the large-scale oceanic circulation. Instead of prescribed ice-volume variations, we use a modeled ice-volume history generated by a one-dimensional coupled ice sheet-bedrock model, which yields a reasonable representation of the 100-kyr cycles that dominated the late Pleistocene. Considering the major glacial terminations during the past 800 kyr, the Younger-Dryas cold phase appears not as a one-time event or an "accident" of the last termination. On the contrary, Younger Dryas-type events seem to be an intrinsic feature of climate change during glacial-interglacial cycles. They can be conceived as Dansgaard-Oeschger stadials which are part of short Dansgaard-Oeschger oscillation sequences. Such a sequence may occur during any deglaciation, when the mean climate returns to an intermediate state and rapidly crosses the parameter range in which DO-oscillations are possible. Depending on how fast the deglaciation process develops, a glacial termination can occur in two or three steps separated by one or twoYD-type cold phases.

Aknowledgments

We greatly appreciate the thorough and constructive comments by D. Paillard, an anonymous reviewer and the editor. This work was supported by the DFG within the European Graduate College "Proxies in Earth History".

References

R.B. Alley, D.A. Meese, C.A. Shuman, A.J. Gow, K.C. Taylor, P.M. Grootes, J.W.C. White, M. Ram, E.D. Waddington, P.A. Mayewski, G.A. Zielinski, Abrupt accumulation increase at the Younger Dryas termination in the GISP2 ice core, Nature 362 (1993) 527–529.

R.B. Alley, P.U. Clark, The deglaciation of the northern hemisphere: a global perspective, Ann. Rev. Earth Planet. Sci. 27 (1999) 149–182.

R.B. Alley, P.U. Clark, L.D. Keigwin, R.S. Webb, Making sense of millennial-scale climate change, in: P.U. Clark, R.S. Webb, L.D. Keigwin (Eds.), Mechanisms of global climate change at millennial time scales, AGU, Washington, D.C., 1999, pp. 385-394.

A. Berger, Long Term Variations of Daily Insolation and Quaternary Climatic Changes, J. Atm. Sci. 35 (1978) 2362-2367.

W.H. Berger, E. Jansen, Younger Dryas episode: ice collapse and super-fjord heat pump, in: S. R. Troelstra, J. E. van Hinte, G. M. Ganssen (Ed.), The Younger Dryas, R. Netherlands Acad. of Arts and Sci., Amsterdam, 1995, pp. 61–105.

W.H. Berger, T. Bickert, M.K. Yasuda, G. Wefer, Reconstruction of atmospheric CO_2 from the deep-sea record of Ontong Java Plateau: the Milankovitch chron, Geol. Rundsch. 85 (1996) 466–495.

W.S. Broecker, Does the trigger for abrupt climate change reside in the ocean, or in the atmosphere?, Science 300 (2003) 1519–1522.

P.U. Clark, S.J. Marshall, G.K.C. Clarke, S.W. Hostetler, J.M. Licciardi, J.T. Teller, Freshwater forcing of abrupt climate change during the last glaciation, Science 293 (2001) 283–287.

P.U. Clark, J.X. Mitrovica, G.A. Milne, M.E. Tamisiea, Sea-level fingerprinting as a direct test for the source of global meltwater pulse IA, Science 295 (2002) 2438–2441.

P.U. Clark, D. Pollard, Origin of the middle Pleistocene transition by ice sheet erosion of regolith, Paleoceanography 13 (1998) 1-9.

R.G. Fairbanks , C.D. Charles, J.D. Wright, Origin of global meltwater pulses, in: R.E. Taylor, A. Long and R.S. Kra (Eds.), Radiocarbon after four decades, Springer-Verlag, New York, 1992, pp. 473–500.A.F. Fanning, A.J. Weaver, Temporal-geographical meltwater influences on the North Atlantic Conveyor: Implications for the Younger Dryas, Paleoceanography 12 (1997) 307–320.

H. Gallée, J.-P. van Ypersele, T. Fichefet, I. Marsiat, C. Tricot, A. Berger, Simulation of the last glacial cycle by a coupled, sectorially averaged climate-ice-sheet model. II. Response to insolation and CO_2 variation. J. Geophys. Res. 97 (1992) 15713–15740.

C.D. Gallup, H. Cheng, F.W. Taylor, R.L. Edwards, Direct determination of the timing of sea level change during termination II, Science 295 (2002) 310–313.

A. Ganopolski, S. Rahmstorf, Stability and variability of the thermohaline circulation in the past and future: A study with a coupled model of intermediate complexity, in: D. Seidov, M. Maslin, B.J. Haupt (Eds.), Oceans and rapid past and future climate changes: North-South connections, AGU, Washington, DC, 2001, pp. 261–275.

M. Stuiver, P.M. Grootes, GISP2 oxygen isotope ratios, Quat. Res. 53 (2000) 277–284.

L.D.D. Harvey, A Two-Dimensional Ocean Model for Long-Term Climatic Simulations: Stability and Coupling to Atmospheric and Sea Ice Models, J. Geophys. Res. 97 (1992) 9435–9453.

J. Imbrie, J.Z. Imbrie, Modeling the Climatic Response to Orbital Variations, Science 207 (1980) 943–953.

M. Kienast, T. J. J. Hanebuth, C. Pelejero, and S. Steinke, Synchroneity of meltwater pulse 1a and the Bølling warming: New evidence from the South China Sea, Geology 31 (2003) 67–70.

E. Le Meur, P. Huybrechts, Comparison of different ways of dealing with isostasy: examples from modelling the Antarctic ice sheet during the last glacial cycle, Ann. Glaciol. 23 (1996) 309-317.

G. Lohmann, M. Schulz, Reconciling Bølling warmth with peak deglacial meltwater discharge, Paleoceanography 15 (2000) 537-540.

A. Lototskaya, G.M. Ganssen, The structure of Termination II (penultimate deglaciation and Eemian) in the North Atlantic, Quat. Sci. Rev. 18 (1999) 1641–1654.

J.F. McManus, D.W. Oppo, J.L. Cullen, A 0.5-million-year record of millennial-scale climate variability in the North Atlantic, Science 283 (1999) 971– 975.

M. Milankovitch, Mathematische Klimalehre und Astronomische Theorie der Klimaschwankungen, Handbuch der Klimalogie Band 1 Teil A, Borntraeger, Berlin, 1930, 176 pp.

J. Oerlemans, Model experiments on the 100 000 year glacial cycle. Nature 287 (1980) 430–432.

A. Oka, H. Hasumi, N. Suginohara, Stabilization of thermohaline circulation by wind-driven and vertical diffusive salt transport, Clim. Dyn. 18 (2001) 71–83.

A. Paul, M. Schulz, Holocene climate variability on centennial-to-millennial time scales: 2. Internal feedbacks and external forcings as possible causes, in: G. Wefer, W. H. Berger, K.-E. Behre, E. Jansen (Eds.), Climate development and history of the North Atlantic Realm, Springer-Verlag, Berlin, 2002, pp. 55–73.

W.R. Peltier, Ice Age Paleotopography, Science 265 (1994) 195–201.

J.-R. Petit, J. Jouzel, D. Raynaud, N.I. Barkov, J.-M. Barnola, I. Basile, J. Chappellaz, M.E. Davis, G. Delaygue, M. Delmotte, V.M. Kotlyakov, M. Legrand, V.Y. Lipenkov, C. Lorius, L. Pépin, C. Ritz, E. Saltzman, M. Stievenard, Climate and atmospheric history of the past 420,000 years from the Vostok ice core, Antarctica, Nature 399 (1999) 429–436.

M.S. Poli, R.C. Thunell, D. Rio, Millennial-scale changes in North Atlantic Deep Water circulation during marine isotope stages 11 and 12: Linkage to Antarctic climate, Geology 28 (2000) 807–810.

D. Pollard, Ice-age simulations with a calving ice-sheet model, Quat. Res. 20(1983) 30–48.

K, Sakai, W.R. Peltier, Deglaciation-induced climate variability: An explicit model of the glacial-interglacial transition that simulates both the Bolling/Allerod and Younger-Dryas events, J. Met. Soc. Japan 76 (1998) 1029-1044.

M. Sarnthein, R. Tiedemann, Younger Dryas-style cooling events at glacial terminations I-VI at ODP Site 658; associated benthic $\delta^{13}C$ anomalies constrain meltwater hypothesis, Paleoceanography 5 (1990) 1041–1055.

M. Schulz, The tempo of climate change during Dansgaard-Oeschger interstadials and its potential to affect the manifestation of the 1470-year climate cycle, Geophys. Res. Lett. 29 (2002) 10.1029/2001GL013277.

M. Schulz, A. Paul, A. Timmermann, Relaxation oscillators in concert: A framework for climate change at millennial timescales during the late Pleistocene, Geophys. Res. Lett. 29(24) (2002) 10.1029/2002GL016144.

M. Stuiver, P.M. Grootes, GISP2 oxygen isotope ratios, Quat. Res. 53 (2000) 277– 284.

B. Waelbroeck, L. Labeyrie, E. Michel, J.C. Duplessy, J.F. McManus, K. Lambeck, E. Balbon, M. Labracherie, Sea-level and deep water temperature changes derived from benthic foraminifera isotopic records, Quat. Sci. Rev. 21 (2002) 295 –305.

M. Winton, Deep decoupling oscillations of the oceanic thermohaline circulation, in: W. R. Peltier (Ed.), Ice in the climate system, Springer Verlag, Berlin, 1993, pp. 417–432.

M. Winton The effect of cold climate upon North Atlantic deep water formation in a simple ocean-atmosphere model, J. Clim. 8 (1997) 37-51.

C. Wunsch, Determining paleoceanographic circulations, with emphasis on the Last Glacial Maximum, Quat. Sci. Rev. 22 (2003) 371-385.

Y. Yokoyama, P. De Deckker, K. Lambeck, P. Johnston, L.K. Fifield, Sea-level at the last glacial maximum: evidence from northwestern Australia to constrain ice volumes for oxygen isotope stage 2, Palaeogeography Palaeoclimatology Palaeoecology 165 (2001) 281 –297.

Chapter VI

DISCUSSION

The ice-sheet model described Section II.2 is a new and valuable tool for paleoclimate studies. This model is unique from two points of view: it is, to our knowledge, the only 2.5-dimensional model including thermomechanical coupling, and the first model of the North-American Ice Sheet (NAIS) including oxygen-isotope transport. One one hand, its computational efficiency is much higher compared to 3-dimensional models, and, on the other hand, it has a higher level of complexity than 2-dimensional models, allowing a more realistic treatment of the NAIS with respect to the profile in the East-West direction and the natural boundaries imposed by the shape of the North-American continent. Such a level of complexity was (the minimum) required to successfully approach the objectives of the present study.

In the absence of explicit computation of ice dynamics and isotope transport in the East-West direction, only distributions along the flow line in the ice sheet could be modeled for temperature and $\delta^{18}\mathrm{O}$. As noted in Section III.4, by assigning in our simulations the mean $\delta^{18}\mathrm{O}$ computed along the flow line for the mean isotopic composition of the entire ice sheet, a maximum estimation of the effect of the NAIS on the ocean enrichment is obtained. Better estimations for the ocean response could come only from a 3-dimensional model.

An important issue which needs to be discussed is the climatic forcing for the ice-sheet model (described in Section II.2.5). In order to include the effect of temperature on ice flow (i.e., the thermomechanical coupling), the model had to be provided with information on heat exchange between ice and atmosphere. The solution chosen was to restore (with a characteristic damping time) the temperature of the surface layer of the ice sheet to the near-surface air temperature, which was computed which was computed from ECHAM 3/T42 atmospheric general circulation model output [*Romanova et al.*, 2004, Figure 1c therein] using the glacial-index method of *Marshall et al.* [2000]. One important advantage of this method is that it provides a simple and computationally-efficient parameterization for the near-surface air temperature. As a matter of fact, the need for a realistic parameterization for air temperature, which affected not only ice flow, but also the values

inferred for snow $\delta^{18}O$ (cf. equation (28)), was the main reason for changing the forcing in the 2.5-dimensional thermomechanically-coupled model from insolation (used in the previous 2-dimensional version, see Section II.1.2.1) to the NGRIP-based glacial index method. Furthermore, by using this method, the effect of orbital and millennial timescale climate variations is "built-in", as it can be seen in the simulated ice-volume history (e.g., Figure IV-1) and in the timeseries of the water flux exchanged between the ice-sheet and the ocean (Figure IV-3b). In our case this fact is another advantage, because it helps to obtain a realistic ice-volume evolution, which is one of the elements with critical implications on the results of this study. The glacial-index method has also a disadvantage: as it relies on existent Greenland ice-core records, its applicability is restricted to the time interval covered by these records (123 kyr in NGRIP case), which, in turn, is limited by the age of the oldest Greenland ice. An alternative approach would be to compute air temperature and heat fluxes at ice surface using an atmospheric model driven by insolation. This would offer the possibility to integrate the ice-sheet model for time spans longer than the last glacial cycle, but, obviously, on the expense of the computational efficiency.

Another critical element for the results presented in this study is the parameterization of $\delta^{18}O$ of precipitation. Obviously, most of the research effort has been focused on the areas still covered by ice sheets today: Greenland and Antarctica. For these areas, newer calibrations of the relationship between mean annual surface temperature and snow $\delta^{18}O$ (even though not always in agreement with each other) were establised during the last decade, from observations as well as from numerical modeling (see Appendix A). But for other regions than the polar ones, considerably less information is published, and the work by *Jouzel et al.* [1994] is the only one to systematize results from an atmospheric general circulation model in a way we could use them, i.e., as specific calibrations at present day and the LGM for different geographical areas, including the North-American continent and, even more specifically, for the area once occupied by the Laurentide ice sheet. Hence, the parameterization employed in the present work is the best choice with respect to the data at our disposal, and can be improved only when new information becomes available.

An issue which also deserves few more comments is the numerical treatment of advection in the ice-sheet model. A comparison between the first-order upwind sheme we employ and a more accurate, second-order sheme shows differences in the computed ice thickness of 10 to 100 m, resulting in approximately 5% underestimation of ice volume in the former case [*Payne and Dongelmans*, 1997]. But in our case this does not affect the simulated ice volume, as the model parameters are chosen to fit the NAIS volume at the LGM from the reconstruction of *Peltier* [2004]. The numerical diffusion of the employed advection scheme can influence to some extent the modeled distribution of $\delta^{18}O$ in the ice sheet. However, as emphasized in Section IV.4, we do not aim at a detailed simulation of this distribution, as there are no ice-cores to use as a reference. We are mainly interested in the

mean $\delta^{18}O$ of the ice sheet and, based on partial validation procedures reported in Section II.1, we believe that our results are reasonably accurate. Moreover, an improvement can be achieved just by increasing the vertical resolution of the model (see Figure II-3), which allows to still take advantage of the superior numerical stability of the first-order upwind scheme and of the fact that it is positive definite.

In studying the ocean isotopic response to ice-volume variations, an important limitation comes from the fact that our ice-sheet model only represents the NAIS. The choice to simulate this particular ice sheet was justified by the fact, generally recognised, that the NAIS has been the main contributor to ice-volume variations, and, hence, to the isotopic enrichment of the ocean during the past glacial cycles. It is likely that the other large ice sheets have also had a significant influence during certain time intervals. For example, it is argued [*Clark et al.*, 2002] that the main freshwater pulse during the last deglaciation [*Fairbanks*, 1989] was due to the Antarctic ice sheet. However, the mathematical analysis of the relative importance of ice-volume variations vs. changes in the mean-ice δ_i in Section III.4 is probably true for each large ice sheet separately, so our conclusion about the little effect of changing δ_i, based on the NAIS only, is likely to be generally valid. Furthermore, in the particular case of the last glacial termination, our results (Section IV.3) as well as previous work [*Duplessy et al.*, 1991] show that the deglaciation signal was practically simultaneously transmitted throughout the Atlantic Ocean, so that the results related to lead/lag relationships in the ocean are not affected by the limitation to the NAIS.

Based on results from the NAIS only, the amplitude error which may arise by linearly inferring ice-volume variations from δ_w changes was estimated to be generally less then 10% (Section III.3). This error is given at each moment by the departure of δ_i from the reference value (i.e., the δ_i value at the LGM). The Greenland and Antarctic ice sheets have not change much in isotopic composition during the last glacial cycle [*Lhomme*, 2004]. Large uncertainty exist with respect to the isotopic composition of the Eurasian ice sheet [*Duplessy et al.*, 2002], but, as it is a temperate ice sheet, as the NAIS, one can assume that the range of δ_i variations would not by too different. Thus, it is likely that the result we obtained using a model for the NAIS only would not be considerably changed when considering all ice sheets.

Previous estimations of the NAIS contribution to the ocean isotopic enrichment at the LGM, based on glacial reconstructions and direct information on the Laurentide ice, range between 0.56 and 0.86‰ [*Duplessy et al.*, 2002, Table 2]. Our model results reduce the quite large uncertainty and suggest that the maximum limit is 0.65‰. The remaining ~0.35‰ up to the ~1‰ anomaly of δ_w at the LGM [e.g., *Malone et al.*, 2004] must come from the other ice sheets.

Table VII-1. Mean isotopic composition ($\delta^{18}O$) of the North American ice sheet at the Last Glacial Maximum.

	Global ice-equiv. sea level S_g (m)	NAIS equiv. sea level S_i (m)	Ice $\delta^{18}O$ δ_i (‰)		Ocean $\delta^{18}O$ δ_w (‰)	
			minimum estimate [c]	maximum estimate [c]	minimum estimate	maximum estimate
CLIMAP min [a]	127.5	77	–28	–34	0.59	0.71
CLIMAP max [a]	163	92			0.71	0.86
Peltier ICE-5G [b]	126	74			0.56	0.68
This study	126	74	–31.3		0.63	

[a] [*CLIMAP Project members*, 1981]

[b] [*Peltier*, 2004]

[c] [*Duplessy et al.*, 2002]

The ice-sheet model used in Chapter V (described in Section V.2.1) is a simpler version of the model used in Chapters III and IV. This 1-dimensional version was sufficient in that study because only a realistic time evolution of the ice-volume was needed. As (i) no thermomechanical coupling was included (which required a realistic parameterization for air temperature), and (ii) only variations at orbital timescale were needed to be captured, the insolation forcing [*Milankovitch*, 1930] could be used to drive the model, allowing to perform integrations not only over the last glacial cycle, but over the entire late Pleistocene (the past 800 kyr). We argue that the trigger of the millennial-timescale events of the last glacial cycle, revealed by Greenland ice cores, the Younger Dryas and the Dansgaard-Oeschger oscillations, resided in the ocean, and recent modeling work follows our point of view [*Olsen et al.*, 2005]. Furthermore, we suggest that the Younger Dryas is not a one-time event, but Younger Dryas-type events may occur during any deglaciation. New evidence seem to support our modeling results: the "pause" found by *Lototskaia and Gansen* [1999] in a benthic foraminiferal $\delta^{18}O$ record from the North Atlantic Ocean during the Termination II was also identified by *Gouzy et al.* [2004] in another core, taken off the Iberian Margin.

References

Clark, P.U., J.X. Mitrovica, G.A. Milne, and M.E. Tamisiea (2002), Sea-level fingerprinting as a direct test for the source of global meltwater pulse IA, *Science, 295*, 2438-2441.

CLIMAP Project members (1981), Seasonal reconstructions of the Earth's surface at the last glacial maximum, Geological Society of America.

Duplessy, J.C., E. Bard, M. Arnold, N.J. Shackleton, J. Duprat, and L. Labeyrie (1991), How fast did the ocean-atmosphere system run during the last deglaciation?, *Earth Planet. Sci. Lett., 103*, 27-40.

Duplessy, J.-C., L. Labeyrie, and C. Waelbroeck (2002), Constraints on the ocean oxygen isotopic enrichment between the Last Glacial Maximum and the Holocene: Paleoceanographic implications, *Quat. Sci. Rev., 21*, 315-330.

Fairbanks, R.G. (1989), A 17,000-year glacio-eustatic sea level record: Influence of glacial melting rates on the Younger Dryas event and deep-ocean circulation, *Nature, 342*, 637-642.

Gouzy, A., B. Malaizé, C. Pujol, and K. Charlier (2004), Climatic "pause" during Termination II identified in shallow and intermediate waters off the Iberian margin, *Quat. Sci. Rev., 23* (14-15), 1523-1528.

Jouzel, J., R.D. Koster, R.J. Suozzo, and G.L. Russell (1994), Stable water isotope behavior during the last glacial maximum: A general circulation model analysis, *J. Geophys. Res., 99* (D12), 25791-25801.

Lhomme, N. (2004), Modelling water isotopes in polar ice sheets, PhD thesis, Univ. of British Columbia, Vancouver.

Lototskaya, A., and G.M. Ganssen (1999), The structure of Termination II (penultimate deglaciation and Eemian) in the North Atlantic, *Quat. Sci. Rev., 18*, 1641-1654.

Malone, M.J., J.B. Martin, J. Schönfeld, U.S. Ninnemann, D. Nürnburg, and W. T.S. (2004), The oxygen isotopic composition and temperature of Southern Ocean bottom waters during the last glacial maximum, *Earth Plan. Sci. Lett., 222* (1), 275-283.

Marshall, S.J., L. Tarasov, G.K.C. Clarke, and W.R. Peltier (2000), Glaciological reconstruction of the Laurentide Ice Sheet: physical processes and modelling challenges, *Can. J. Earth Sci., 37*, 769-793.

Milankovitch, M. (1930), Mathematische Klimalehre und astronomische Theorie der Klimaschwankungen, in *Handbuch der Klimatologie*, edited by W. Köppen, and R. Geiger, pp. A1-A176, Verlag v. Gebr. Borntraeger, Berlin.

Olsen, S.M., G. Shaffer, and C. Bjerrum (2005), Ocean oxygen isotope constraints on mechanisms for millennial-scale climate variability, *Paleoceanogr., 20*

Payne, A.J., and P.W. Dongelmans (1997), Self-organization in the thermomechanical flow of ice sheets, *J. Geophys. Res., B102*, 12219-12233.

Peltier, W.R. (2004), Global glacial isostasy and the surface of the ice-age Earth: the ICE-5G (VM2) model and GRACE, *Ann. Rev. Earth Plan. Sci., 32*, 111-149.

Romanova, V., M. Prange, and G. Lohmann (2004), Stability of the thermohaline circulation and its dependence on the background hydrological cycle, *Clim. Dyn., 22*, 527-538.

Chapter VII

CONCLUSIONS

This study proved that a 2.5-dimensional thermomechanical ice-sheet model including oxygen-isotope transport is a valuable tool for paleoclimate studies focusing on the glacial-interglacial variability of the late Pleistocene.

Using this model, the effect of changing isotopic composition of ice on the relationship between ice-volume variations and the oxygen-isotopic enrichment of the ocean was investigated at glacial-interglacial timescale. The phase difference found between the ice-volume signal and the induced mean isotopic enrichment of seawater was negligible and the amplitude difference was generally less than 10 %. Therefore, it was concluded that the effect of mean-ice $\delta^{18}O$ variations can be neglected in reconstructing ice volume from marine $\delta^{18}O$ records.

Furthermore, the effect of the ocean circulation on the relationship between ice-volume variations and the ocean isotopic response was investigated qualitatively, by coupling the ice-sheet model to a climate model of reduced complexity. The North-Atlantic deep-water $\delta^{18}O$ variations were found to lead those in the South Atlantic Ocean, whereas the calcite-$\delta^{18}O$ anomalies showed an apparent lead of the South Atlantic over the North Atlantic Ocean during the deglaciation. It was concluded that (i) the ocean circulation is an important element to be taken into account in the climatic and stratigraphic interpretation of benthic $\delta^{18}O$ records and (ii) leads/lags inferred on the basis of proxies depending on more than one physical variable, such as benthic calcite-$\delta^{18}O$, can be misleading in interpreting causal relationships.

Finally, using a simplified (1-dimensional) version of the ice-sheet model combined with a box-model of the North Atlantic Ocean, it was found that YD-type events can occur during any deglaciation of the past 800 kyr, which means that YD is not a one-time event, but an intrinsic feature of the climate change at millennial timescales.

Appendix A: Ice δ^{18}O as a proxy for air temperature

The ratio R of oxygen isotopes ^{16}O and ^{18}O is commonly expressed as the fractional deviation $\delta^{18}\mathrm{O}$ in parts per thousand (‰) from a standard R_{std} :

$$\delta^{18}\mathrm{O}(‰) = (R / R_{std} - 1) \times 1000$$

For water in all phases (liquid, vapour, solid), the Standard Mean Ocean Water (SMOW) is used. The value for Vienna-SMOW [*Gonfiantini*, 1978] is $R_{std} = R_{V-SMOW} = 2005.2 \times 10^{-6}$.

Ice-δ^{18}O reflects the isotopic composition of snow accumulated at the ice-sheet surface, which, in turn, depends largely on the local air temperature.
Based on observations of modern precipitation, the relationship between mean annual snow $\delta^{18}\mathrm{O}$ (‰) and mean annual surface temperature T_s (ºC) was found to be linear:

$$\delta_s = aT_s + b \qquad \text{(A)}$$

There is no unique calibration of the snow $\delta^{18}\mathrm{O}$ dependence on temperature for modern precipitation in Greenland [*Dansgaard et al.*, 1973; *Johnsen and White*, 1989; *Cuffey and Clow*, 1997], but the relationship of *Johnsen and White* [1989], with the spatial slope a = 0.67‰/ºC and the coefficient b = –13.7‰, confirmed by applying an inverse Monte-Carlo method [*Dahl-Jensen et al.*, 1998], seems to be the most reliable.

Equation (A) has been used to infer paleotemperatures from ice-core $\delta^{18}\mathrm{O}$ records, by assuming that the present-day spatial relation does not change with time in the specific region it was calibrated for; that is, the spatial and temporal slopes are similar (the “modern analogue method”). However, in reality, coefficients derived for present day do not hold for past times, as other factors influencing δ_s are subject to change: the seasonal balance of precipitation [*Werner et al.*, 2000], the sources of moisture and the trajectories of air masses carying moisture to high latitudes [*Werner et al.*, 2001]. Again, calibrations of the temporal slopes based on GISP2 [*Cuffey and Clow*, 1997] and GRIP [*Johnsen et al.*, 2001] differ, probably because past variations of seawater-$\delta^{18}\mathrm{O}$ are ignored in the GISP2 study.

Comprehensive climate models including water-isotope transport, as NASA/GISS model [e.g., *Joussaume et al.*, 1984] and ECHAM [e.g., *Hoffmann et al.*, 1998] help to estimate changes in the dependence of δ_s on temperature in the past compared to present day [e.g., *Jouzel et al.*, 1994; 2000]. In spite of the apparent disagreement of different calibrations of spatial and temporal slopes, these studies support the use of oxygen isotopes as a paleothermometer. Also, they allow extending the applicability of equation (A) to the now-vanished middle-latitude North-American and the Eurasian ice sheets.

Appendix B: Foraminiferal $\delta^{18}O$ as a proxy for global ice volume

The oxygen-isotope ratio $^{18}O/^{16}O$ in the calcite ($CaCO_3$) of foraminifer shells is usually expressed versus the Pee Dee Belemnite (PDB) standard. The Vienna-PDB [*Coplen*, 1996] is related to $R_{V\text{-}SMOW}$ by: ‰V-PDB = ‰V-SMOW – 0.27‰ [*Hut*, 1987].

The paleotemperature equation relates the $\delta^{18}O$ of carbonate (δ_c) to the temperature (T) and the oxygen-isotopic composition of seawater (δ_w):

$$T = a + b(\delta_c - \delta_w) + c(\delta_c - \delta_w)^2 .$$

Different calibrations for the coefficients *a*, *b* and *c* are summarised in *Mix* [1987] and revised in *Bemis et al.* [1998]. Newer calibrations are also available [e.g., *Mulitza et al.*, 2003]. Among them, the formula proposed by [*Shackleton*, 1967] for foraminifera at temperatures below 16°C reads:

$$T = 16.9 - 4.0(\delta_c - \delta_w),$$

which can be re-written in terms of departures from present-day values as follows:

$$\Delta\delta_c = \Delta\delta_w - \Delta T / 4.0$$

This equation can be used in two ways. Records of foraminiferal δ_c combined with independent estimations of δ_w variations allow to determine local changes in seawater temperature. Vice versa, when aiming at reconstructing ice volume, constraints on temperature changes are used to extract the δ_w signal out of δ_c records.
Furthermore, δ_w depends on the total amount of water stored in ice sheets as well as on the mean oxygen-isotopic composition of the ice (δ_i). Using assumptions on δ_i, global ice-volume (V_g) variations can be reconstructed from $\Delta\delta_w$. As a common practice, a constant value is assumed for δ_i (generally between –30‰ and –35‰), implying a linear relationship between $\Delta\delta_w$ and V_g (this assumption is verified in Chapter III).

References

Bemis, B.E., H.J. Spero, J. Bijma, and D.W. Lea (1998), Reevaluation of the oxygen isotopic composition of planktonic foraminifera: Experimental results and revised paleotemperature equations, *Paleoceanography*, *13* (2), 150-160.

Coplen, T.B. (1996), Editorial: More uncertainty than necessary, *Paleoceanography*, *11*, 369-370.

Cuffey, K.M., and G.D. Clow (1997), Temperature, accumulation, and ice sheet elevation in central Greenland through the last deglacial transition, *Journal of Geophysical Research - Oceans*, *102* (C12), 26383-26396.

Dahl-Jensen, D., K. Mosegaard, N. Gundestrup, G.D. Clow, S.J. Johnsen, A.W. Hansen, and N. Balling (1998), Past temperatures directly from the Greenland ice sheet, *Science*, *282*, 268-271.

Dansgaard, W., S.J. Johnsen, H.B. Clausen, and N.S. Gundestrup (1973), Stable isotope glaciology, *Medd. om Grønland*, *197* (2), 1-53.

Gonfiantini, R. (1978), Standards for stable isotope measurements in natural compounds, *Nature*, *271*, 534-536.

Hoffmann, G., M. Werner, and M. Heimann (1998), Water isotope module of the ECHAM atmospheric general circulation model: A study on timescales from days to several years, *J. Geophys. Res.*, *103* (D14), 16871-16896.

Hut, G. (1987), Consultants group meeting on stable isotope reference samples for geochemical and hydrological investigations, pp. 42, Int At Energy Agency, Vienna.

Johnsen, S.J., D. Dahl-Jensen, N. Gundestrup, J.P. Steffensen, H.B. Clausen, H. Miller, V. Masson-Delmotte, A.E. Sveinbjörnsdottir, and J. White (2001), Oxygen isotope and palaeotemperature records from six Greenland ice-core stations: Camp Century, Dye-3, GRIP, GISP2, Renland and NorthGRIP, *J. Quat. Sci.*, *16*, 299-307.

Johnsen, S.J., and J. White (1989), The origin of Arctic precipitation under present and glacial conditions, *Tellus*, *41B*, 452-468.

Joussaume, S., R. Sadourny, and J. Jouzel (1984), A general circulation of water isotope cycles in the atmosphere, *Nature*, *311* (D2), 24-29.

Jouzel, J., G. Hoffmann, R.D. Koster, and V. Masson (2000), Water isotopes in precipitation: data/model comparison for present-day and past climates, *Quat. Sci. Rev.*, *19* (1-5), 363-379.

Jouzel, J., R.D. Koster, R.J. Suozzo, and G.L. Russell (1994), Stable water isotope behavior during the last glacial maximum: A general circulation model analysis, *J. Geophys. Res.*, *99* (D12), 25791-25801.

Mix, A.C. (1987), The oxygen-isotope record of glaciation, in *North America and adjacent oceans during the last deglaciation*, edited by W.F. Ruddiman, and H.E. Wright, Jr., pp. 111-135, Boulder, Geol. Soc. America.

Mulitza, S., D. Boltovskoy, B. Donner, H. Meggers, A. Paul, and G. Wefer (2003), Temperature: $\delta^{18}O$ relationships of planktonic foraminifera collected from surface waters, *202* (1-2), 143-152.

Shackleton, N.J. (1967), Oxygen isotope analyses and Pleistocene temperatures, re-assessed, *Nature*, *215*, 15-17.

Werner, M., M. Heimann, and G. Hoffmann (2001), Isotopic composition and origin of polar precipitation in present and glacial climate simulations, *Tellus*, *53B*, 53-71.

Werner, M., U. Mikolajewicz, M. Heimann, and G. Hoffmann (2000), Borehole versus isotope temperatures on Greenland: Seasonality does matter, *Geophys. Res. Lett.*, *27* (5), 723-726.